NASA TN D-363

TECHNICAL NOTE
D-363

INVESTIGATION OF THE AERODYNAMIC CHARACTERISTICS OF A COMBINATION JET-FLAP AND DEFLECTED-SLIPSTREAM CONFIGURATION AT ZERO AND LOW FORWARD SPEEDS

By Kenneth P. Spreemann and Edwin E. Davenport

Langley Research Center
Langley Field, Va.

NATIONAL AERONAUTICS AND SPACE ADMINISTRATION

WASHINGTON

May 1960

NATIONAL AERONAUTICS AND SPACE ADMINISTRATION

TECHNICAL NOTE D-363

INVESTIGATION OF THE AERODYNAMIC CHARACTERISTICS OF A COMBINATION JET-FLAP AND DEFLECTED-SLIPSTREAM CONFIGURATION AT ZERO AND LOW FORWARD SPEEDS

By Kenneth P. Spreemann and Edwin E. Davenport

SUMMARY

An investigation of the aerodynamic characteristics of a semispan wing equipped with a 38.5-percent-chord sliding flap partially immersed in the slipstream of two propellers has been conducted in the 17-foot test section of the Langley 300-MPH 7- by 10-foot tunnel. The wing had an aspect ratio of 7.0, taper ratio 1.0, and an NACA 63A412 airfoil section. The propellers were one wing chord in diameter. A jet of air was ejected over the knee of the flap through a momentum-coefficient range from zero to about 1.0.

The data are presented without analysis; however, a few significant results have been noted. Large losses in lift were encountered at low forward speeds for values obtained within ground proximity compared with values obtained out of ground proximity.

INTRODUCTION

Recent investigations have shown that jet-flap—wing configurations at low forward speeds have provided very high lift coefficients. (For example, see ref. 1.) Also, tests at low forward speeds have indicated that the propeller slipstream deflected by large chord flaps can give very high lift coefficients (ref. 2). Both the jet-flap and the deflected-slipstream principles produce significant lift augmentation over and above the sum of the power-off lift and the vertical component of the thrust. The present investigation was undertaken to provide data that may be useful in analyzing the manner in which these augmentations combine at low forward speeds and the effect of ground proximity.

The model employed in this investigation was an unswept, untapered wing with two propellers mounted in two inboard positions on the wing. Incorporated in the wing was a full-span blowing nozzle that ejected

air over the knee of the sliding flap at 61.5 percent of the wing chord. The data were obtained at zero and low forward speeds in and out of ground proximity.

COEFFICIENTS AND SYMBOLS

The force and moment coefficients used in this paper are based on the dynamic pressure in the slipstream. This system is employed because, when a wing is located in a propeller slipstream, large forces and moments can be produced even though the free-stream velocity decreases to zero. For this condition, coefficients based on the free-stream dynamic pressure approach infinity and hence become meaningless. Therefore, it appears appropriate to base the coefficients on the slipstream dynamic pressure. The coefficients based on this dynamic pressure are indicated by the use of the subscript s in this paper. The relations between the thrust and dynamic pressure in the slipstream have been derived in reference 3. The more familiar coefficient forms based on the free-stream dynamic pressure can be found by dividing by $(1 - C_{T,s})$; that is, $C_L = \frac{C_{L,s}}{1 - C_{T,s}}$. The positive senses of forces, moments, and angles are indicated in figure 1(a) for the static tests and in figure 1(b) for the wind-tunnel tests. The pitching moments are referred to the wing quarter-chord point.

C_L lift coefficient

$C_{L,s}$ lift coefficient based on slipstream dynamic pressure, $\frac{L}{q_s S}$

$C_{X,s}$ longitudinal-force coefficient, $\frac{F_X}{q_s S}$

$C_{m,s}$ pitching-moment coefficient, $\frac{M_Y}{q_s S c}$

C_T thrust coefficient, $\frac{T_P}{\rho_\infty n^2 D^4}$

$C_{T,s}$ thrust coefficient based on slipstream dynamic pressure, $\frac{T_P}{q_s \frac{\pi}{4} D^2}$

C_P	power coefficient, $\frac{2\pi Qn}{\rho_\infty n^3 D^5}$
C_p	pressure coefficient, $\frac{p - p_\infty}{q_s}$
$C_{\mu,s}$	momentum coefficient, $\frac{Q_j \rho_j V_j}{q_s S}$
F'	resultant force from static tests, lb
F	resultant force from tunnel tests, lb
L'	lift from static tests, lb
L	lift from tunnel tests, lb
F_X'	longitudinal force from static tests (Thrust - Drag), lb
F_X	longitudinal force from tunnel tests (Thrust - Drag), lb
M_Y'	pitching moment from static tests, ft-lb
M_Y	pitching moment from tunnel tests, ft-lb
T_j	measured jet thrust from wing-flap configuration, lb
T_P	propeller thrust, lb
Q	propeller shaft torque, ft-lb
Q_j	rate of airflow out of the jet expanded to free-stream static pressure, cu ft/sec
V_j	jet exit velocity (assuming isentropic expansion from plenum chamber to free-stream static pressure), ft/sec
V_∞	free-stream velocity, ft/sec
p_∞	free-stream static pressure, lb/sq ft
p	local static pressure, lb/sq ft
q_∞	free-stream dynamic pressure, $\frac{1}{2}\rho_\infty V_\infty^2$

q_s	slipstream dynamic pressure, $q_\infty + \frac{T_P}{\pi \frac{D^2}{4}}$, lb/sq ft
ρ_∞	mass density of air in free stream, slug/cu ft
ρ_j	mass density of air in jet, slugs/cu ft
b/2	span of semispan wing, ft
c	wing chord, ft
D	propeller diameter, ft
h	height of wing quarter chord above ground, ft
S	semispan wing area, sq ft
x	wing chord station measured from leading edge, ft
y	wing spanwise station measured from root chord, ft
n	propeller rotational speed, rps
α	angle of attack of wing chord plane, deg
i_w	wing incidence, deg
θ	turning angle (inclination of resultant-force vector measured from longitudinal-force axis), $\tan^{-1} \frac{L'}{F_{X'}}$, deg
δ_f	flap deflection relative to wing chord plane, deg
$\delta_{T.E.}$	deflection of trailing-edge extension relative to flap chord plane, deg
β	propeller blade element angle, deg
c_b	propeller blade element chord, ft
r	radius to propeller blade element, ft
R	propeller tip radius, ft
t	propeller blade element thickness, ft

MODEL AND APPARATUS

A drawing and the pertinent dimensions of the model are presented in figure 2. The geometric characteristics of the model are given in the following table:

Wing:	
Area (semispan), sq ft	6.22
Span (semispan), ft	4.67
Chord, ft	1.33
Aspect ratio	7.00
Taper ratio	1.00
Airfoil section	NACA 63A412
Propeller:	
Diameter, ft	1.33
Nacelle diameter, ft	0.33
Airfoil section	Clark Y
Solidity	0.134
Number of blades	3

The model consisted of a semispan wing with two 1.33-foot-diameter propellers located at $\frac{y}{b/2}$ equal to 0.25 and 0.554. A sliding flap was employed on the model with a full-span blowing nozzle ejecting air over the knee of the flap at 0.615 wing chord station. The flap rotated about a line at 0.615 wing chord station and 0.2 inch below the wing chord plane. The approximate shape of the full-span plenum chamber and nozzle is shown in figure 2. The nozzle had a gap of 0.025 inch. Details of the trailing-edge extension used in this investigation are also shown in figure 2. Location of the pressure orifices in the wing behind the inboard propeller are shown in figure 3. Photographs of the model and groundboard installed in the 17-foot test section of the Langley 300-MPH 7- by 10-foot tunnel are shown in figure 4.

The speed of each propeller was determined from stroboscope-type indicators to which were fed output frequencies of small alternators connected to the shaft of each motor. Since the two motors were variable-frequency synchronous motors operated from a common power source, their rotational speeds were matched within 10 rpm. The propeller blade angles were adjusted to give the same thrust at the same rpm. The propeller rotated so that the slipstream twist was in opposition to the wing-tip vortex. The blade characteristics are given in figure 5.

The motors were mounted inside nacelles with strain-gage balances so that thrust and torque could be measured. The total model lift,

longitudinal force, and pitching moment were measured on a strain-gage balance below the tunnel floor.

TESTS AND CORRECTIONS

The tests were conducted in the 17-foot test section of the Langley 300-MPH 7- by 10-foot tunnel. The investigations reported in references 3 and 4 indicated that an increased ratio of tunnel size to model size is necessary for models of the type described herein in order to avoid largely unknown tunnel-wall effects. As a result, the 17-foot test section was constructed in the large end of the Langley 300-MPH 7- by 10-foot tunnel, upstream of the regular test section. The arrangement and calibration of this section are given in the appendix of reference 2.

The tests were run at various free-stream dynamic pressures and propeller thrusts so selected as to maintain a dynamic pressure of 8.0 lb/sq ft in the slipstream. The tests with the propeller off were also made at a free-stream dynamic pressure of 8.0 lb/sq ft. The thrust of the propellers was held constant throughout the angle-of-attack range.

Corrections to the free-stream velocity due to blockage and slipstream contraction were estimated and found to be negligible. The jet-boundary corrections applied to the angle of attack and the longitudinal force were estimated for a square test section by a method similar to that of reference 5. Inasmuch as these corrections depend on the circulation about the wing, it was necessary to subtract the direct thrust contribution of the propeller and jet to the lift before applying them.

The following relations were used:

$$\alpha = \alpha_{measured} + 0.13\Delta C_L$$

$$C_{X,s} = C_{X,s_{measured}} - \left[0.0023(\Delta C_L)^2(1 - C_{T,s})\right]$$

where ΔC_L is the increment of lift coefficient approximately proportional to the circulation and is obtained by subtracting the direct thrust contribution as follows:

$$\Delta C_L = \frac{C_{L,s} - C_{T,s}\left(\frac{2\pi\,\frac{D^2}{4}}{S}\right)\frac{F_p}{T_p}\sin\left(\theta_s + \alpha_{measured}\right) - C_{\mu,s}\,\frac{F_j}{T_j}\sin\left(\theta_j + \alpha_{measured}\right)}{1 - C_{T,s}}$$

where $\frac{F_p}{T_p}$ and θ_s are the thrust recovery factor and turning angle obtained with propeller thrust at zero forward speed and θ_j and $\frac{F_j}{T_j}$ are the turning angle and thrust recovery factor with the blowing nozzle at zero forward speed.

PRESENTATION OF RESULTS

Forces, moments, and turning angles at various flap angles are presented for the static condition out of ground proximity in figure 6. Force and moment coefficients for the various configurations tested in the tunnel in and out of ground proximity are presented in figures 7 and 8 and the (a) parts of figures 9, 10, 12, and 13. Propeller coefficients are given in the (b) parts of figures 9, 10, 12, and 13. Pressure coefficients over the wing leading edge are given in figure 6(e) for the static condition and in parts (c) of figures 9 and 12 at low forward speeds for a limited number of configurations and momentum coefficients.

The results of the investigation are presented in the following detailed listing of the data figures:

DISCUSSION

In all figures in which the longitudinal-force coefficients appear, $C_{X,s} = 0$ indicates steady level flight, negative values of $C_{X,s}$ indicate decelerating or gliding flight, and positive values of $C_{X,s}$ indicate accelerating or climbing flight. The data are presented herein without analysis; however, a few significant results of the investigation should be noted.

A comparison of the lift for steady level flight ($C_{L,s}$ at $C_{X,s} = 0$) out of ground proximity (figs. 9 and 11) with that obtained within ground proximity (figs. 12 and 13) is presented in figures 14 and 15. From these figures it is seen that for values obtained within ground proximity, compared with values obtained out of ground proximity, large losses in lift were encountered at low forward speeds. However, in the higher speed range $C_{T,s} = 0.6$ only small losses were observed at the low momentum coefficients, $C_{\mu,s} < 0.1$. Similar ground effects at low forward speeds on a plain jet-flap model (i.e., without propellers) have been reported in reference 6.

One concept of a jet-flap configuration involves mounting a large number of jet engines in the wing with their inlets at the wing leading edge. Pressure distributions around the wing leading edge were taken in order to provide some information on the airflow within which such inlets may have to operate. From this investigation it is shown that for the range of variables tested (i.e., angle of attack, momentum coefficient, and spanwise location behind the propeller), there was considerable variation in the location of the wing leading-edge stagnation point and peak pressure coefficients.

Langley Research Center,
National Aeronautics and Space Administration,
Langley Field, Va., January 19, 1960.

REFERENCES

1. Lockwood, Vernard E., Turner, Thomas R., and Riebe, John M.: Wind-Tunnel Investigation of Jet-Augmented Flaps on a Rectangular Wing to High Momentum Coefficients. NACA TN 3865, 1956.

2. Kuhn, Richard E., and Hayes, William C., Jr.: Wind-Tunnel Investigation of Longitudinal Aerodynamic Characteristics of Three Propeller-Driven VTOL Configurations in the Transition Speed Range, Including Effects of Ground Proximity. NASA TN D-55, 1960.

3. Kuhn, Richard E., and Draper, John W.: Investigation of the Aerodynamic Characteristics of a Model Wing-Propeller Combination and of the Wing and Propeller Separately at Angles of Attack up to 90°. NACA Rep. 1263, 1956. (Supersedes NACA TN 3304 by Draper and Kuhn.)

4. Kuhn, Richard E., and Hayes, William C., Jr.: Wind-Tunnel Investigation of Effect of Propeller Slipstreams on Aerodynamic Characteristics of a Wing Equipped With a 50-Percent-Chord Sliding Flap and a 30-Percent-Chord Slotted Flap. NACA TN 3918, 1957.

5. Gillis, Clarence L., Polhamus, Edward C., and Gray, Joseph L., Jr.: Charts for Determining Jet-Boundary Corrections for Complete Models in 7- by 10-Foot Closed Rectangular Wind Tunnels. NACA WR L-123, 1945. (Formerly NACA ARR L5G31.)

6. Vogler, Raymond D., and Turner, Thomas R.: Wind-Tunnel Investigation at Low Speeds To Determine Flow-Field Characteristics and Ground Influence on a Model With Jet-Augmented Flaps. NACA TN 4116, 1957.

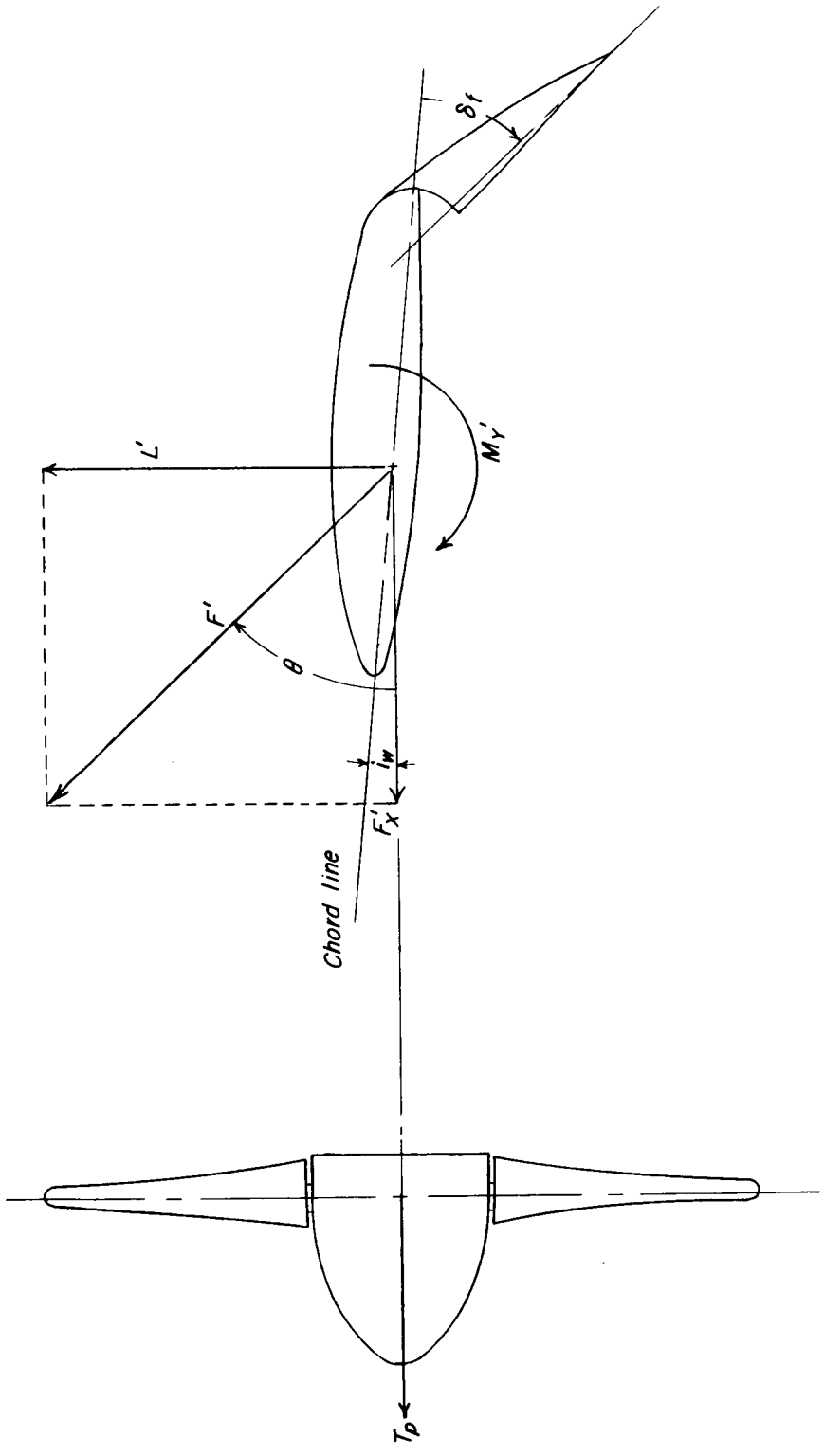

(a) Static tests.

Figure 1.- Conventions used to define positive sense of forces, moments, and angles.

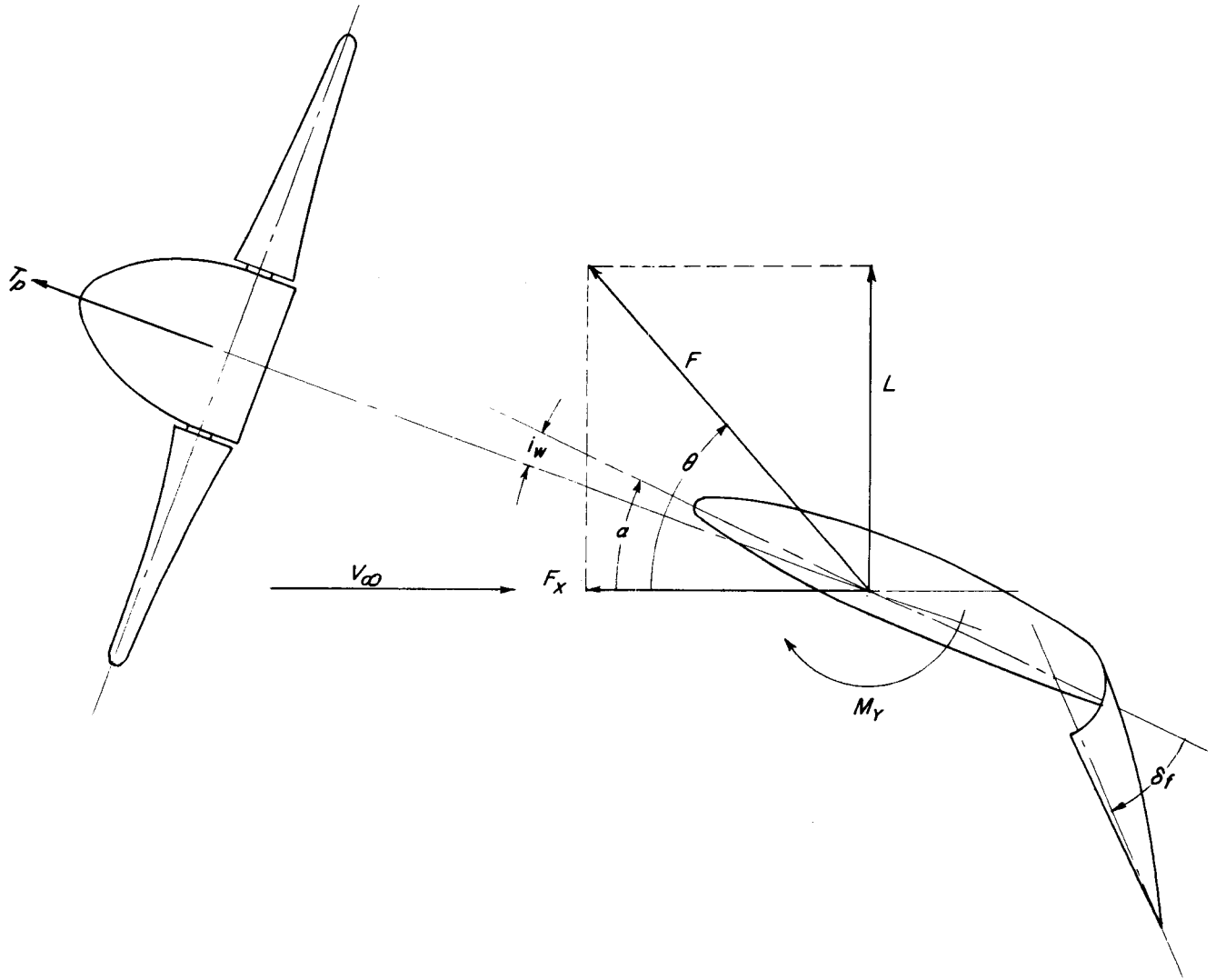

(b) Tunnel tests.

Figure 1.- Concluded.

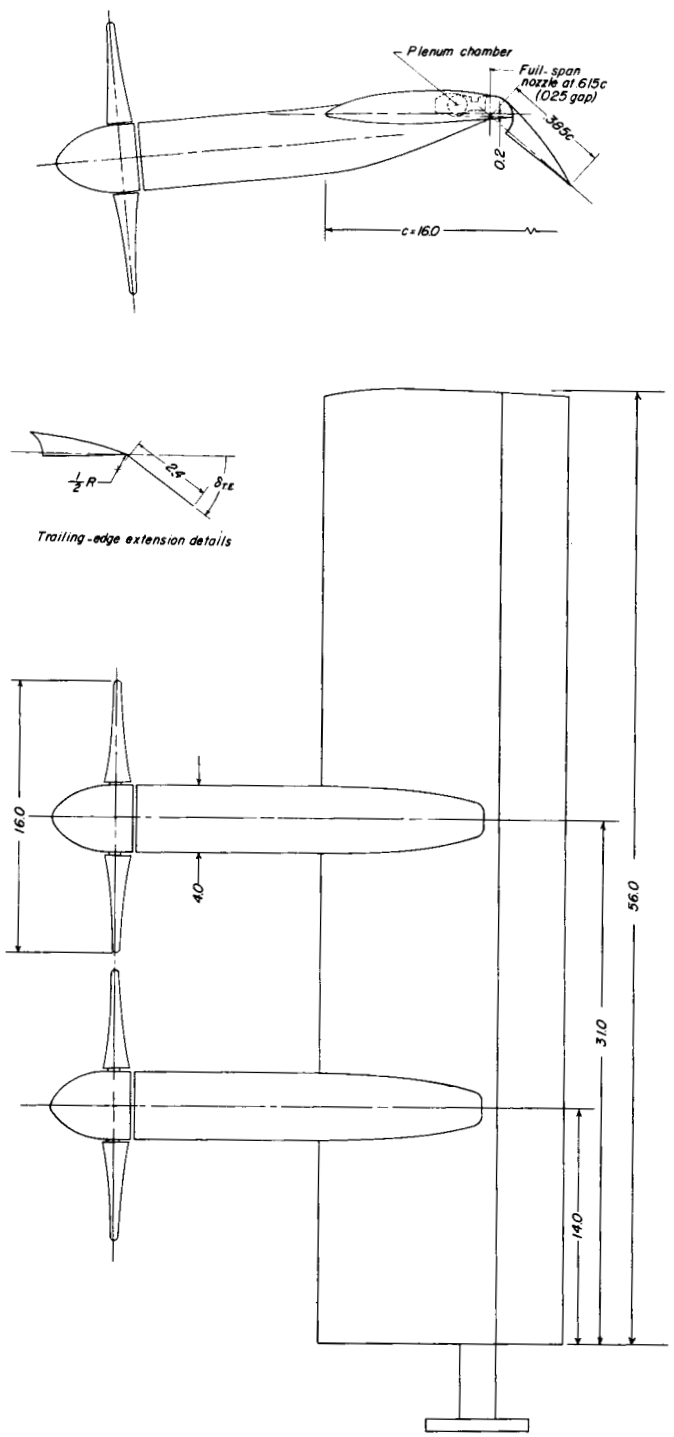

Figure 2.- Drawing of model. (All dimensions in inches.)

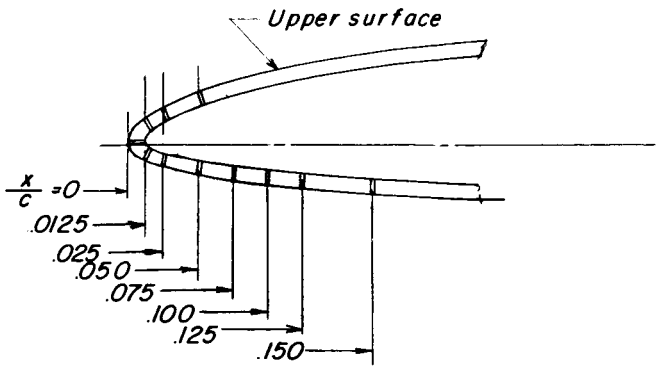

Typical cross section with chordwise locations.

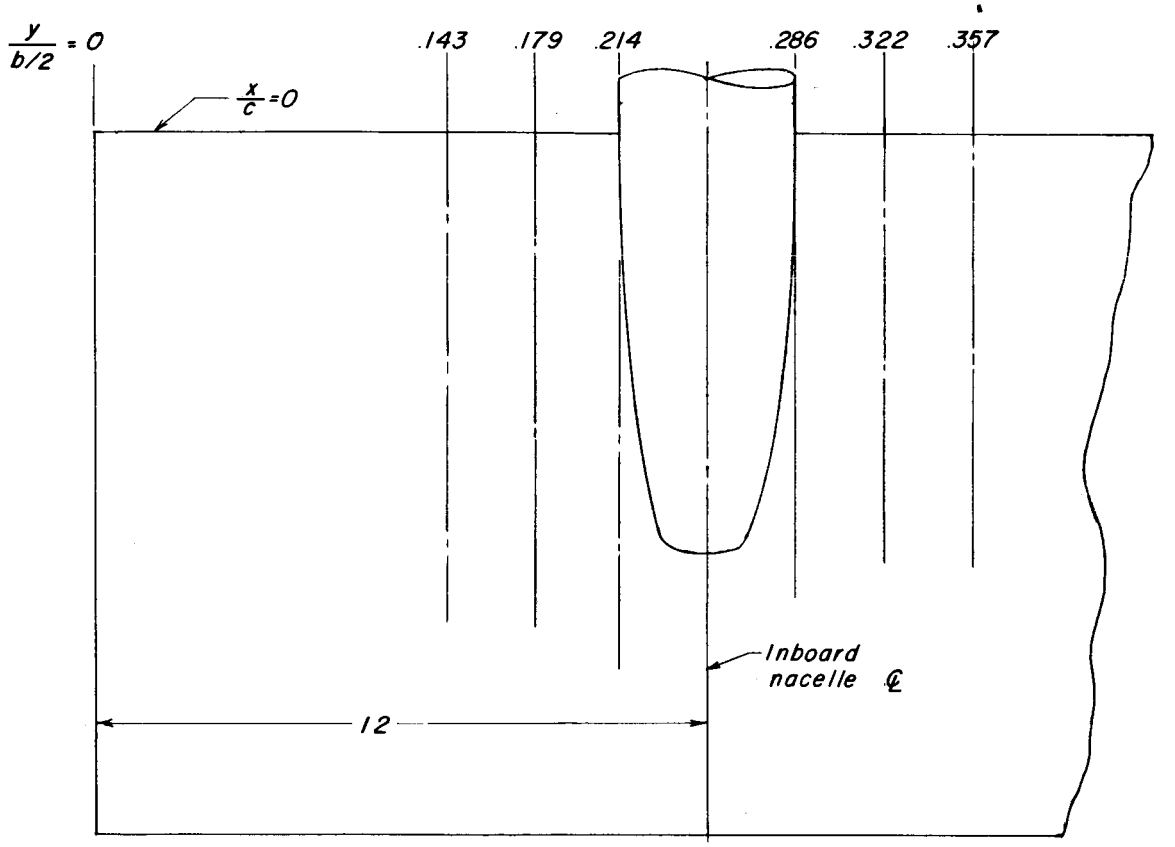

Spanwise stations

Figure 3.- Location of pressure orifices. (All dimensions in inches.)

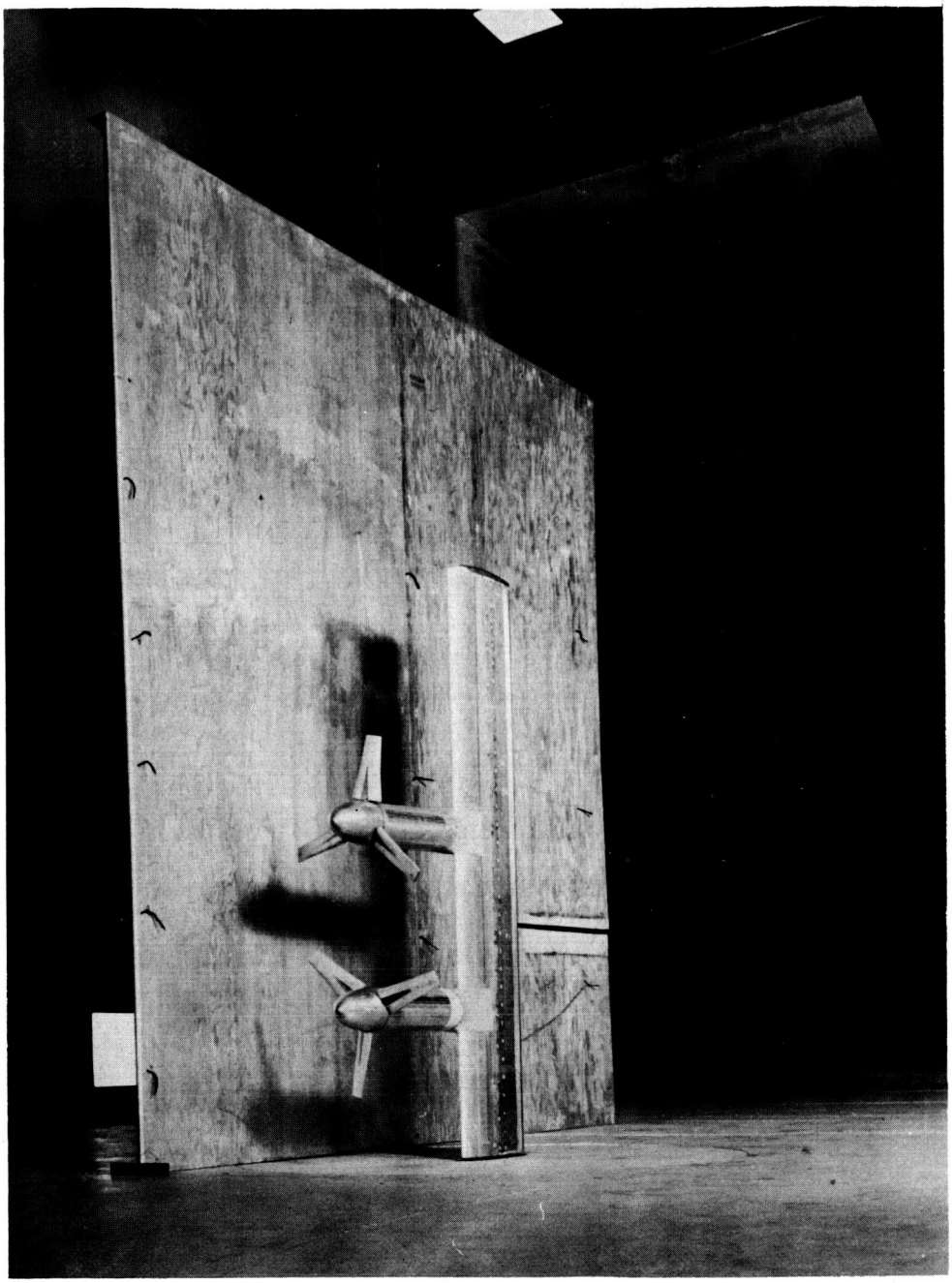

(a) Three-quarter front view. L-57-2826

Figure 4.- Photograph of model in tunnel with ground board installed. $\delta_f = 40^\circ$; $\delta_{T.E.} = 60^\circ$.

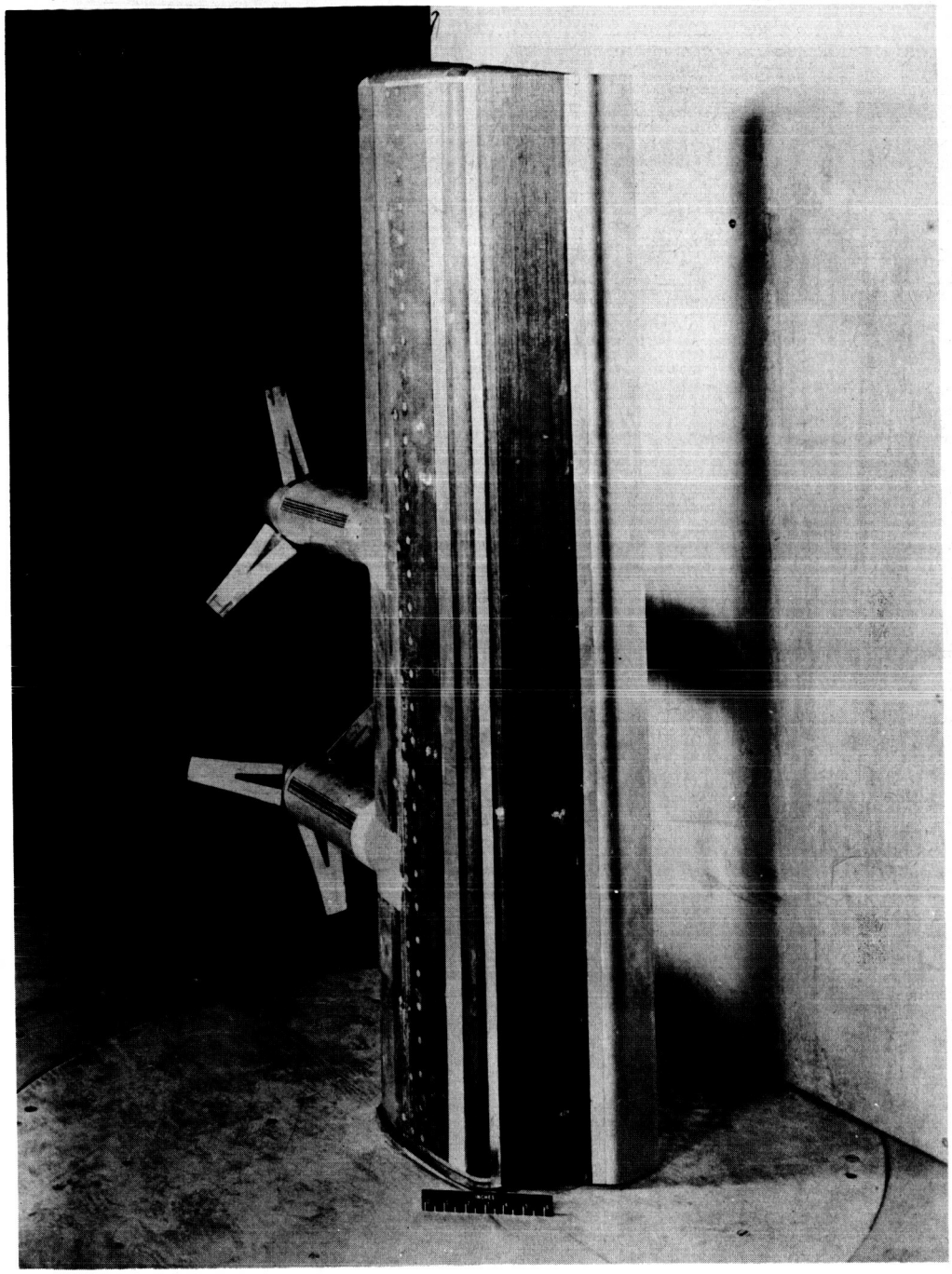

(b) Three-quarter rear view. L-57-2827

Figure 4.- Concluded.

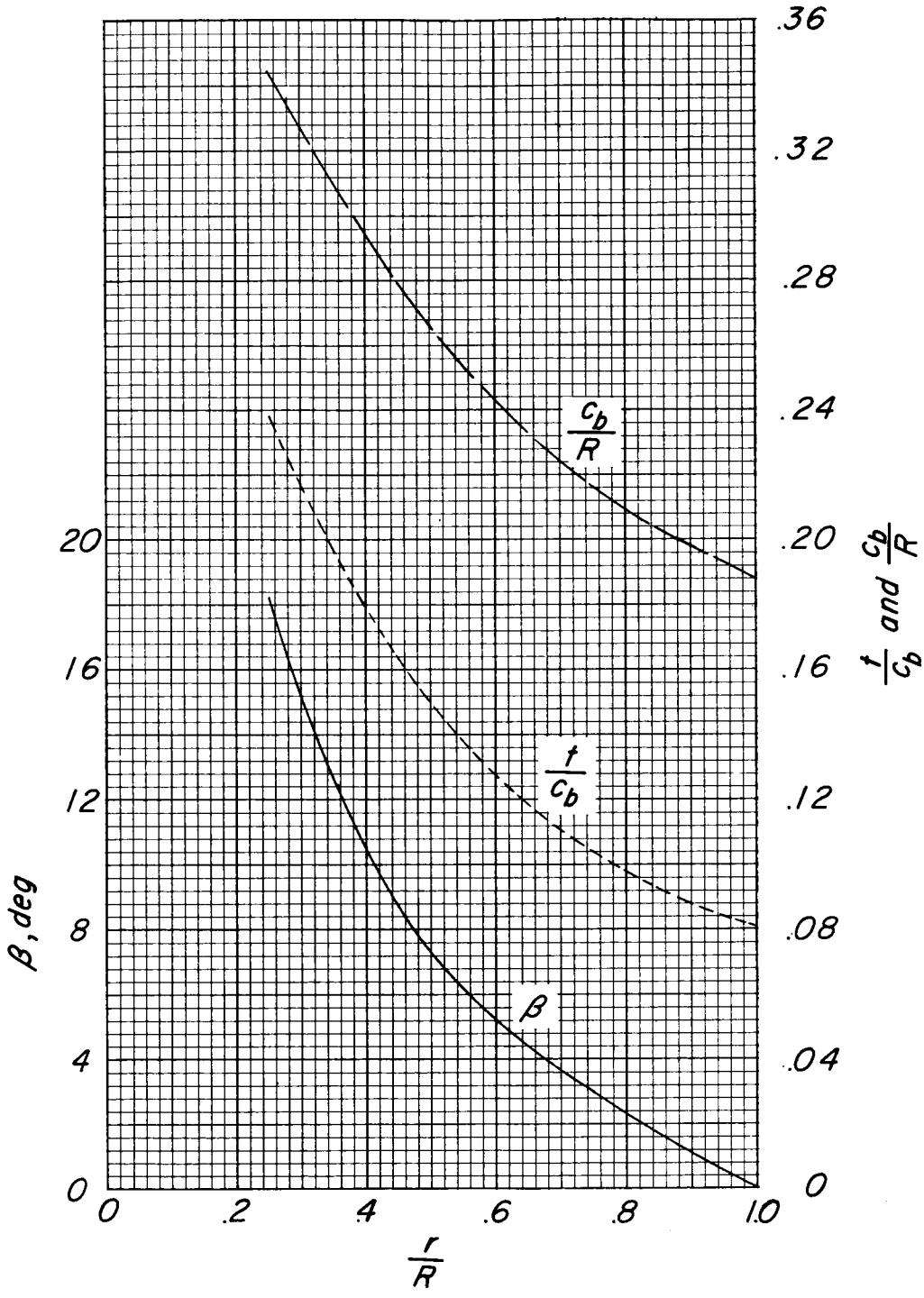

Figure 5.- Physical characteristics of 1.33-foot-diameter propeller employing Clark Y airfoil section.

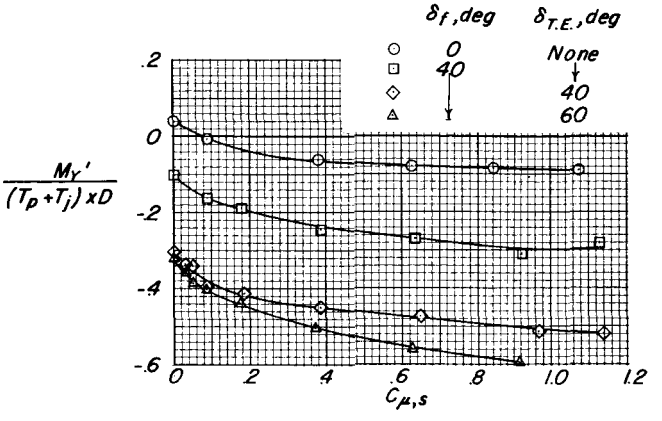

(a) Pitching moment.

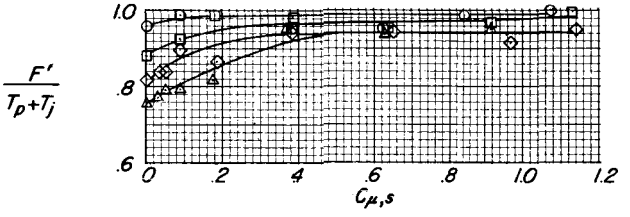

(b) Ratio of resultant force to thrust.

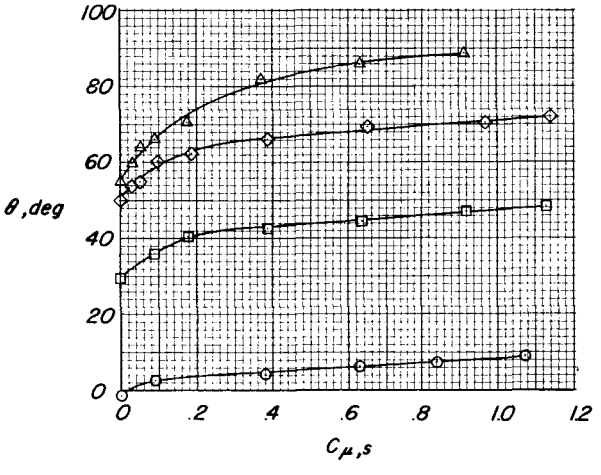

(c) Turning angle.

Figure 6.- Effects of variations in momentum coefficient on the aerodynamic characteristics out of ground proximity with and without trailing-edge extensions. $C_{T,s} = 1.0$; $q_\infty = 0$.

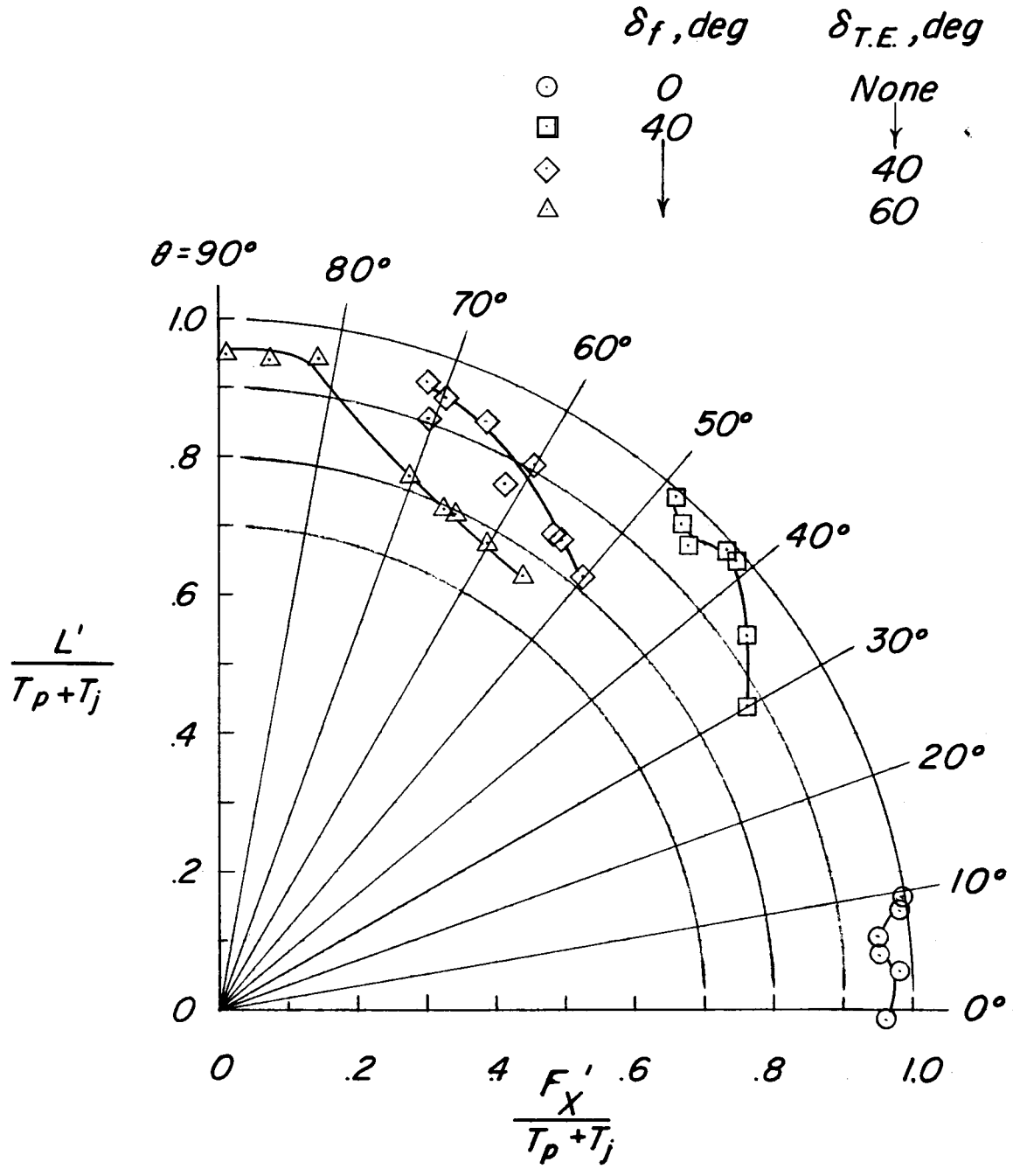

(d) Summary of turning effectiveness.

Figure 6.- Continued.

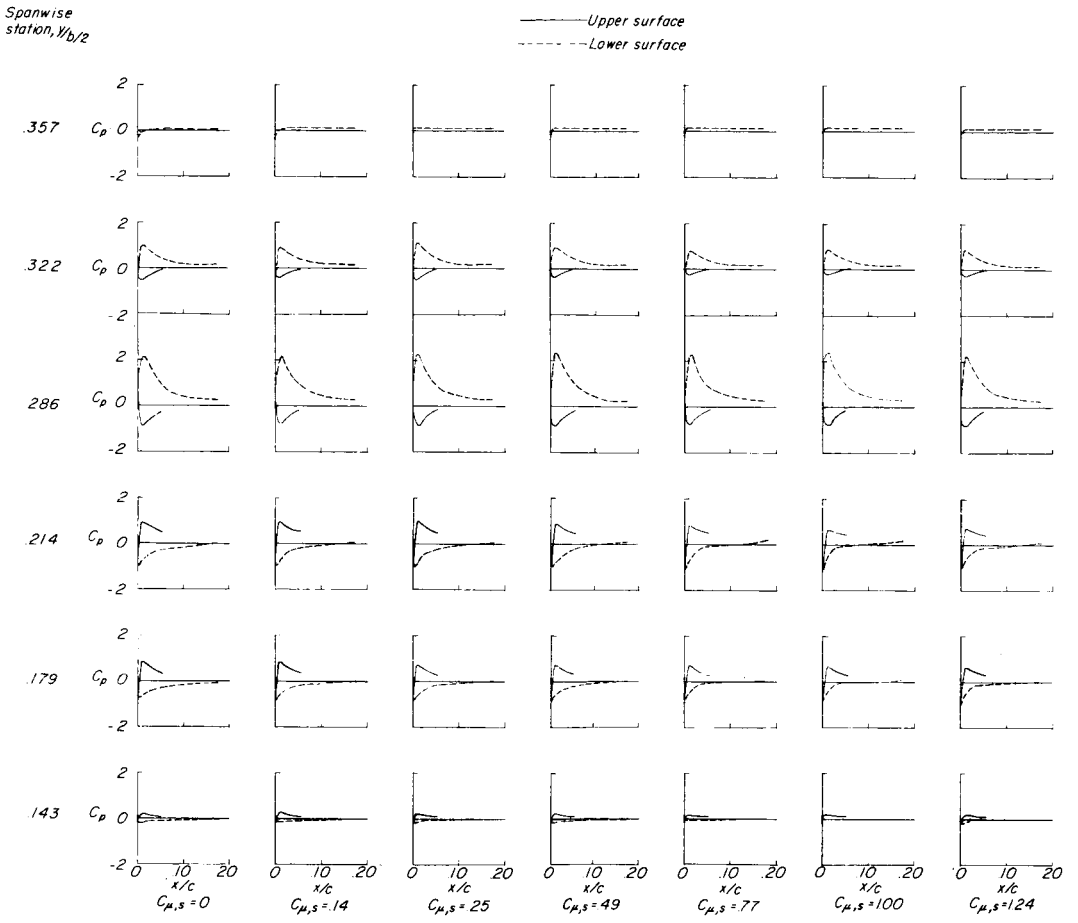

$\delta_f = 0^\circ$

(e) Pressure coefficients.

Figure 6.- Continued.

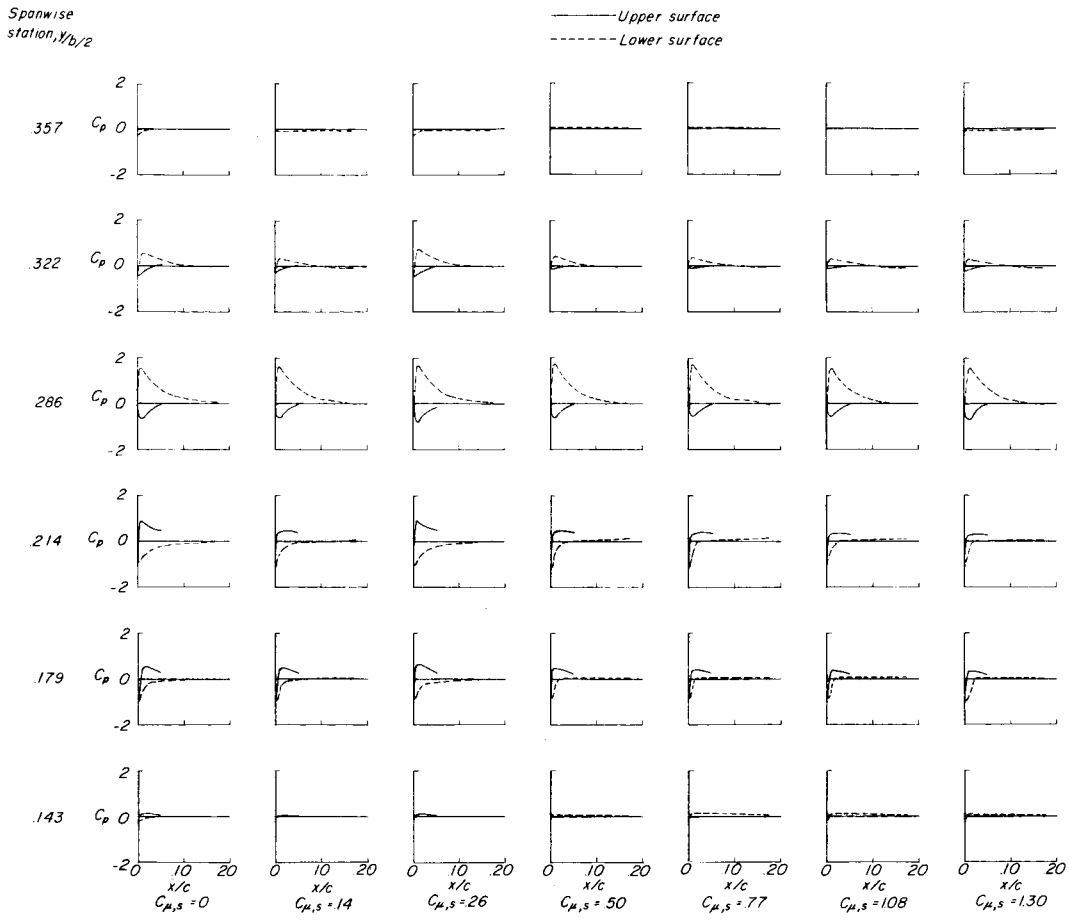

$\delta_f = 40^\circ$

(e) Continued.

Figure 6.- Continued.

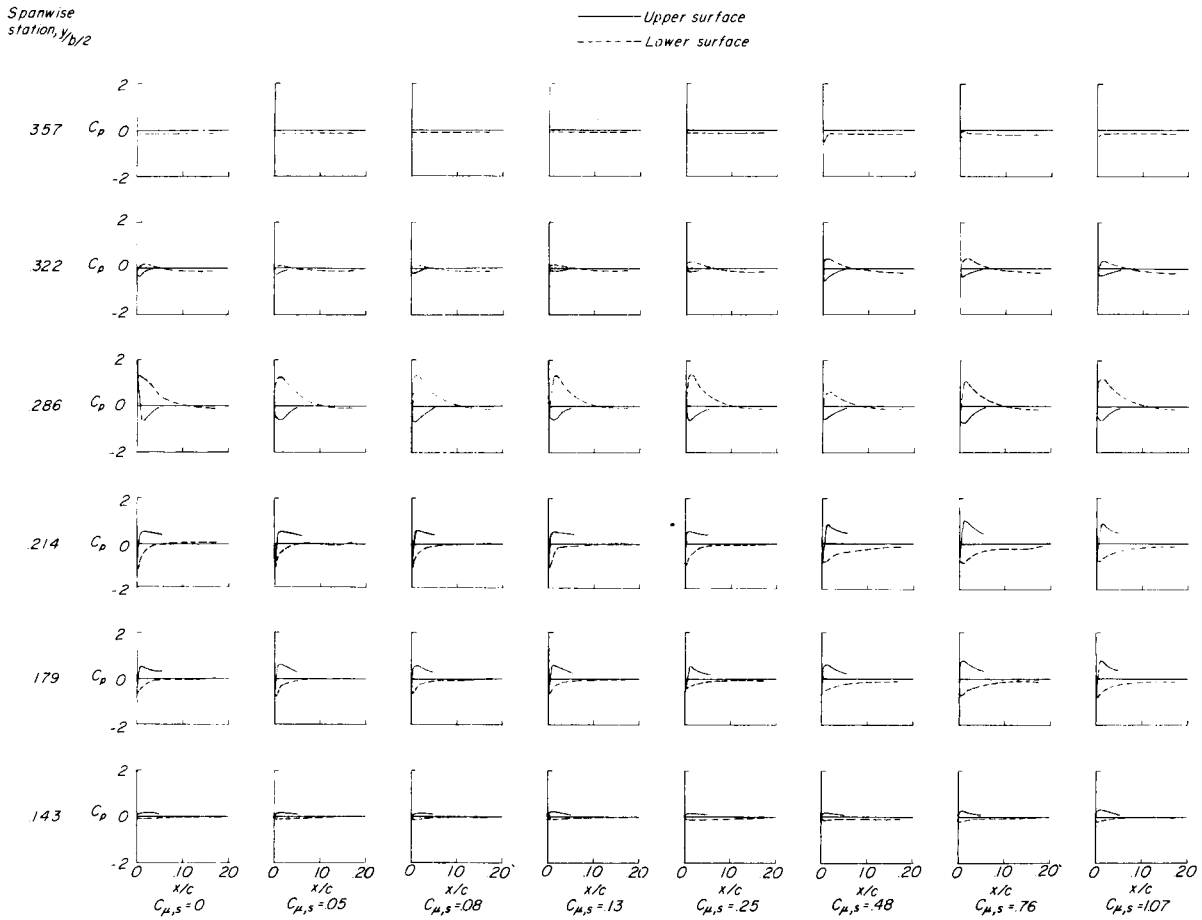

$\delta_f = 40^\circ$; $\delta_{T.E.} = 60^\circ$

(e) Concluded.

Figure 6.- Concluded.

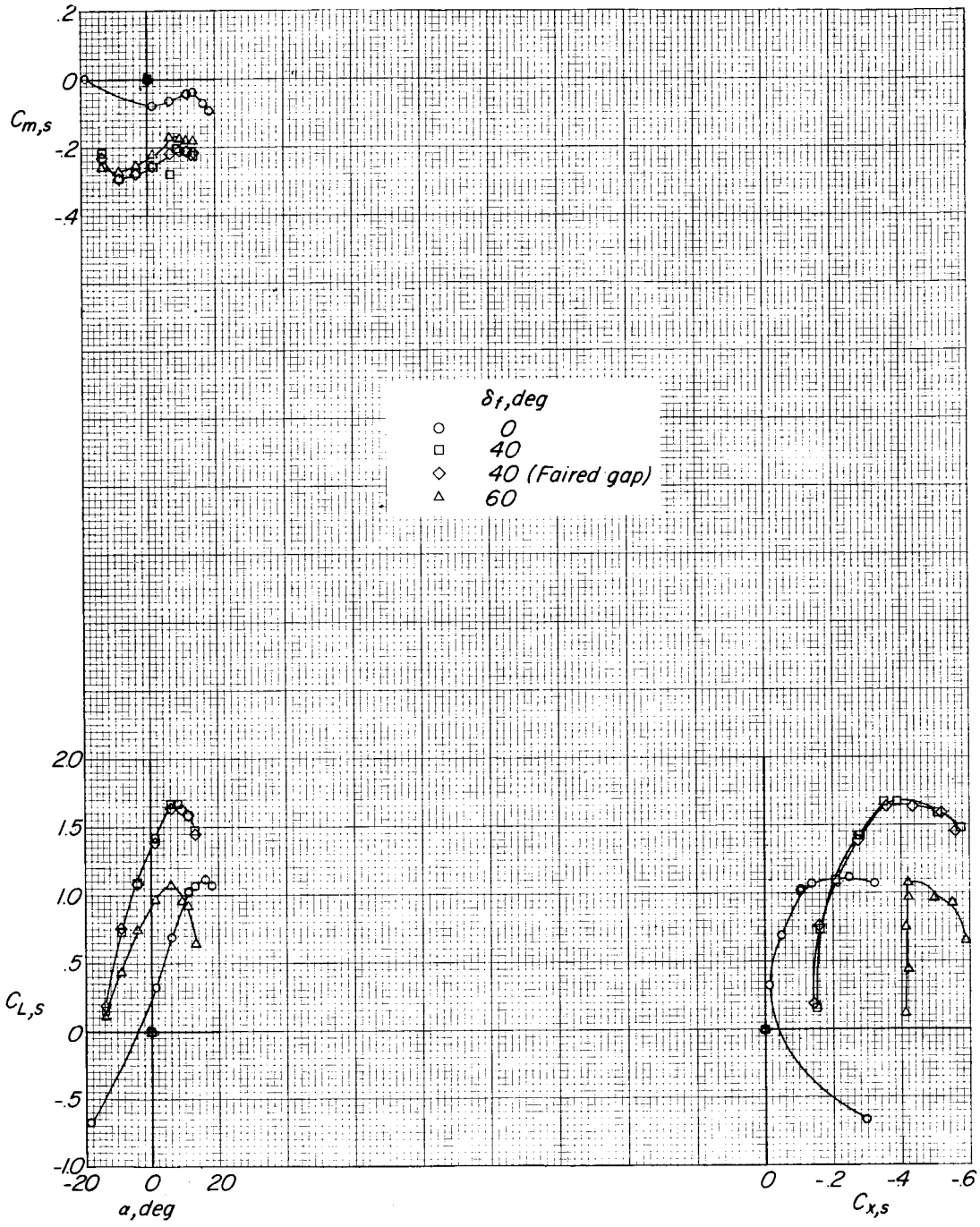

Figure 7.- Effects of flap deflection and faired lower surface gap on aerodynamic characteristics of model, both propellers off. $C_{T,s} = 0$; $C_{\mu,s} = 0$.

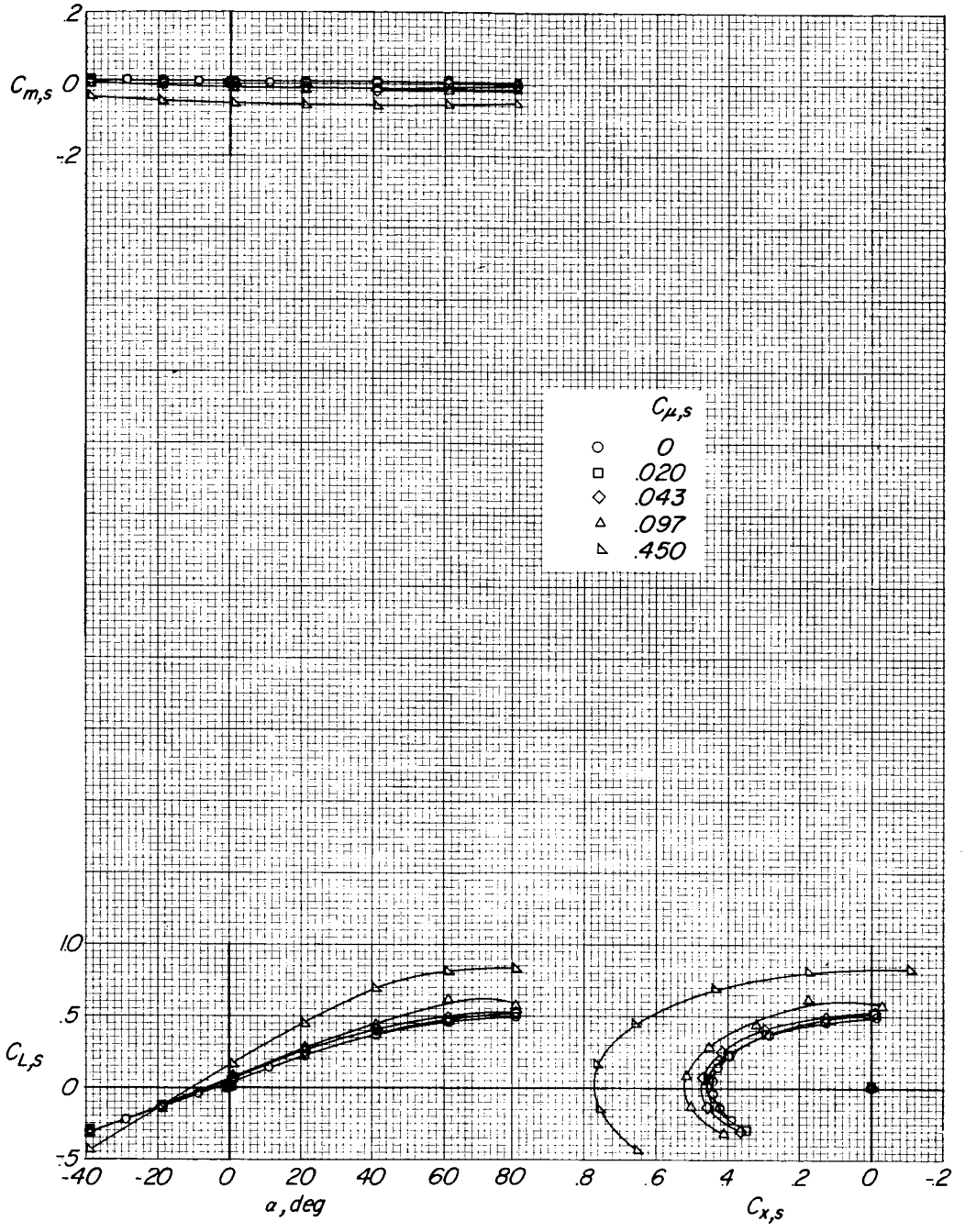

(a) $C_{T,s} = 1.0$.

Figure 8.- Effect of variations in thrust and momentum coefficients on the aerodynamic characteristics of model out of ground proximity; $\delta_f = 0^\circ$.

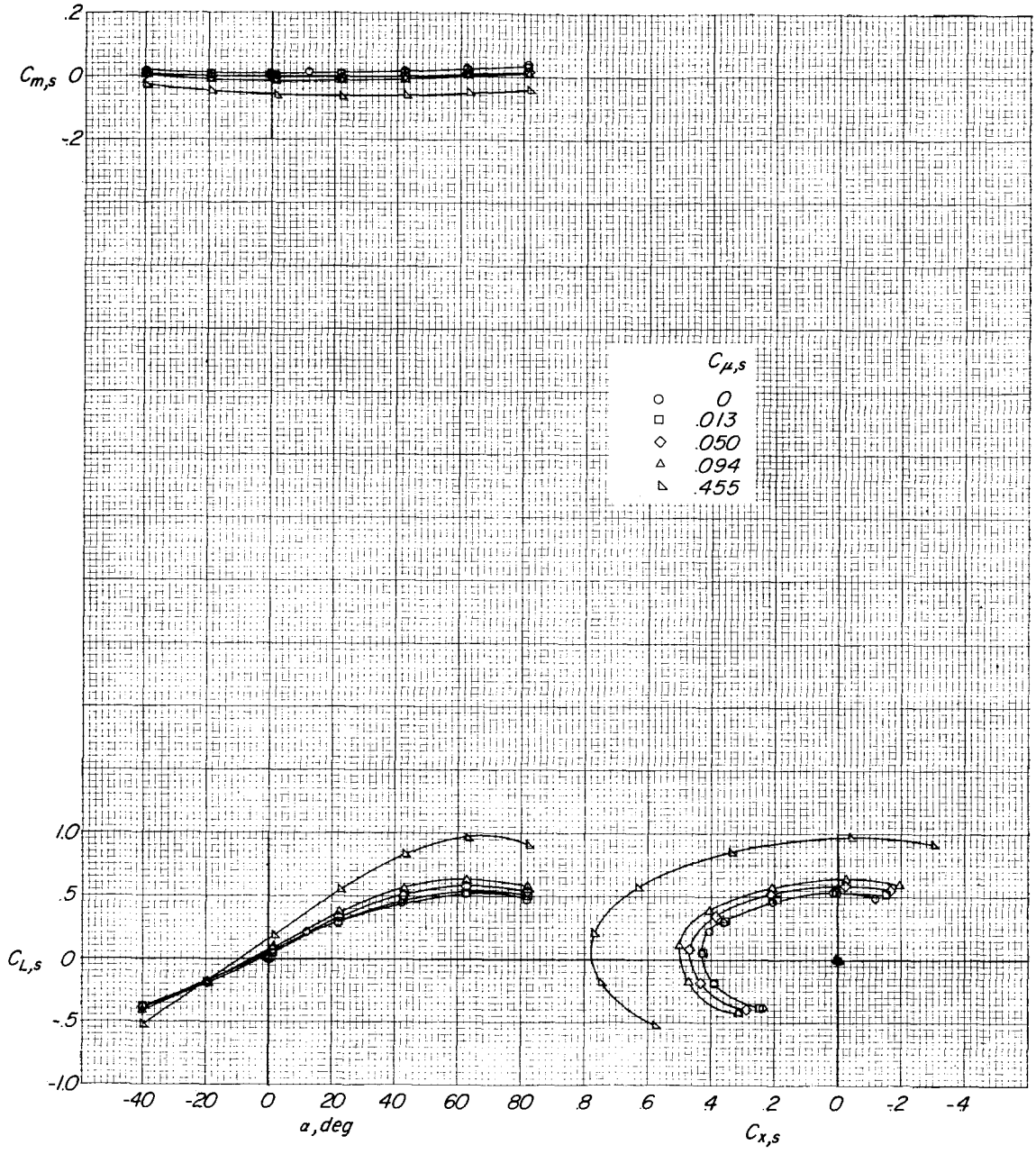

(b) $C_{T,s} = 0.98$.

Figure 8.- Continued.

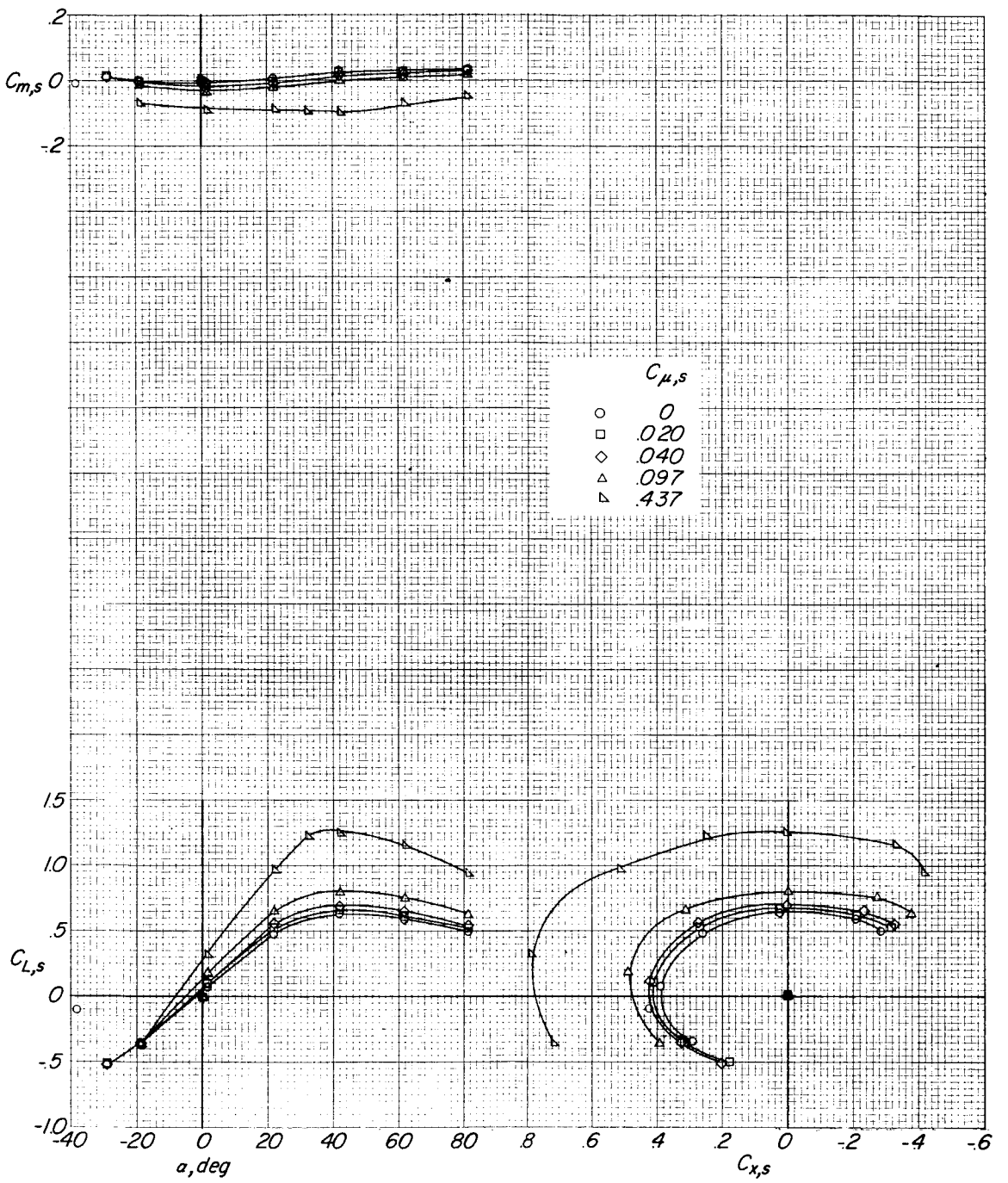

(c) $C_{T,s} = 0.90$.

Figure 8.- Continued.

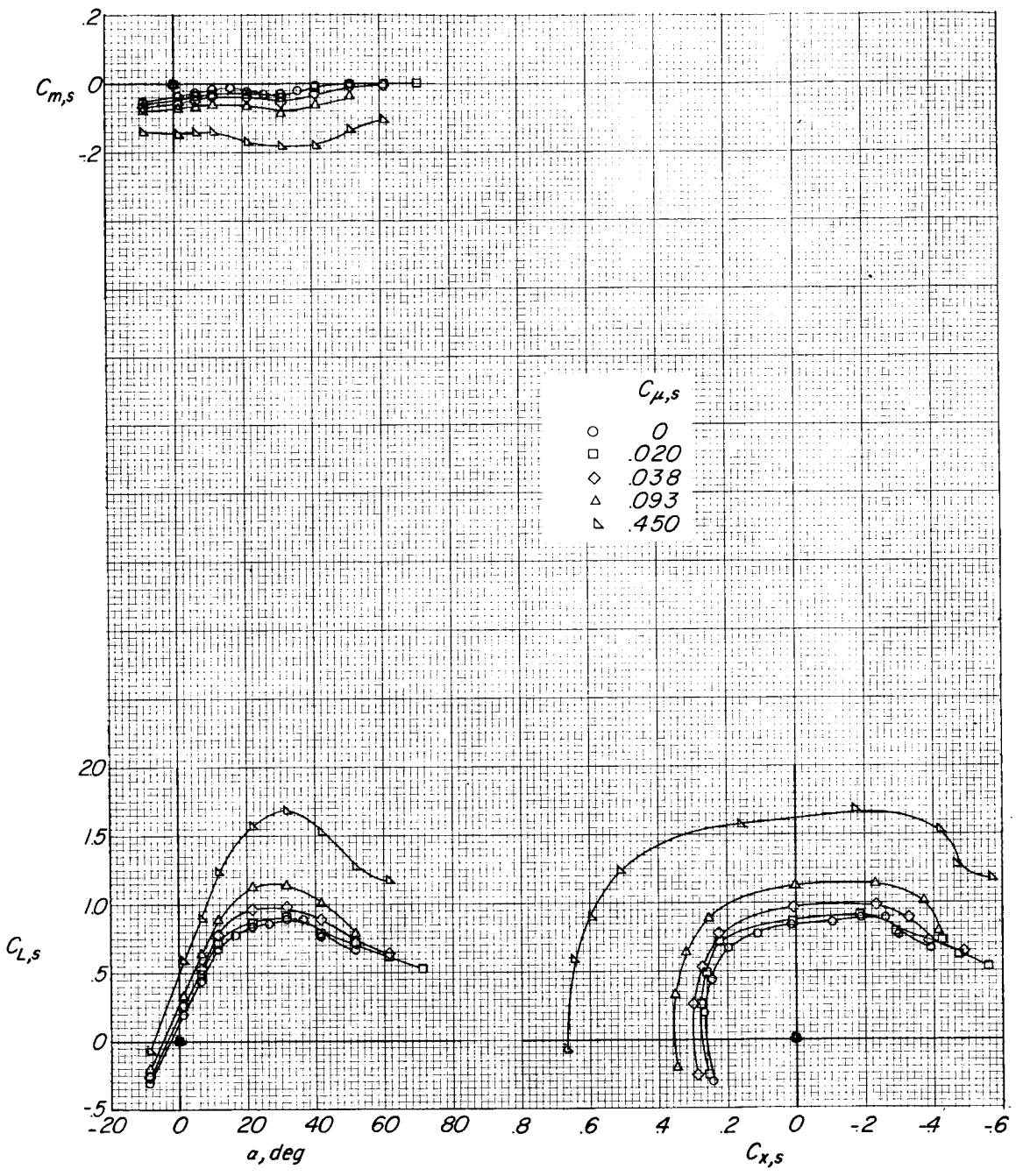

(d) $C_{T,s} = 0.60$.

Figure 8.- Continued.

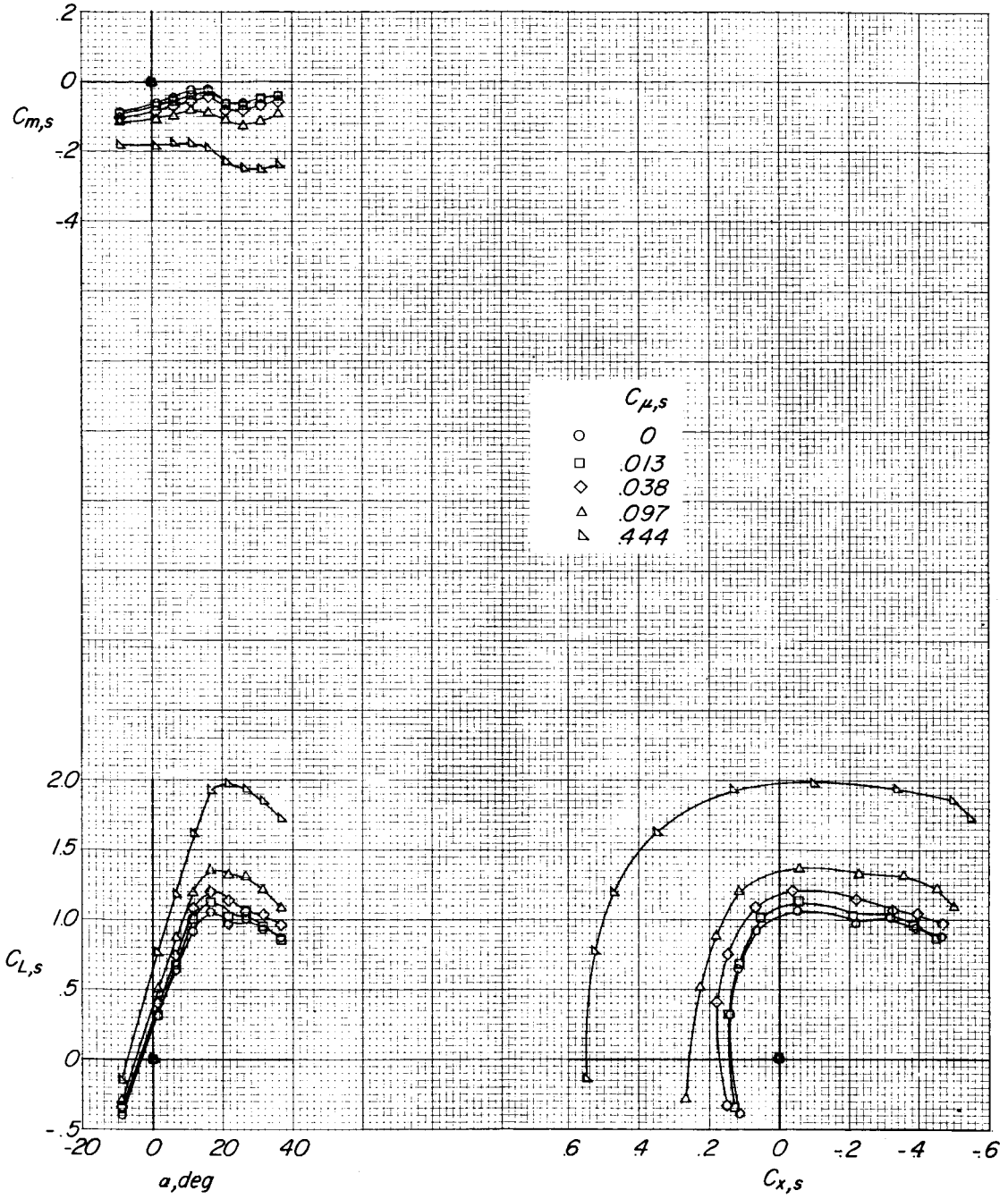

(e) $C_{T,s} = 0.30$.

Figure 8.- Continued.

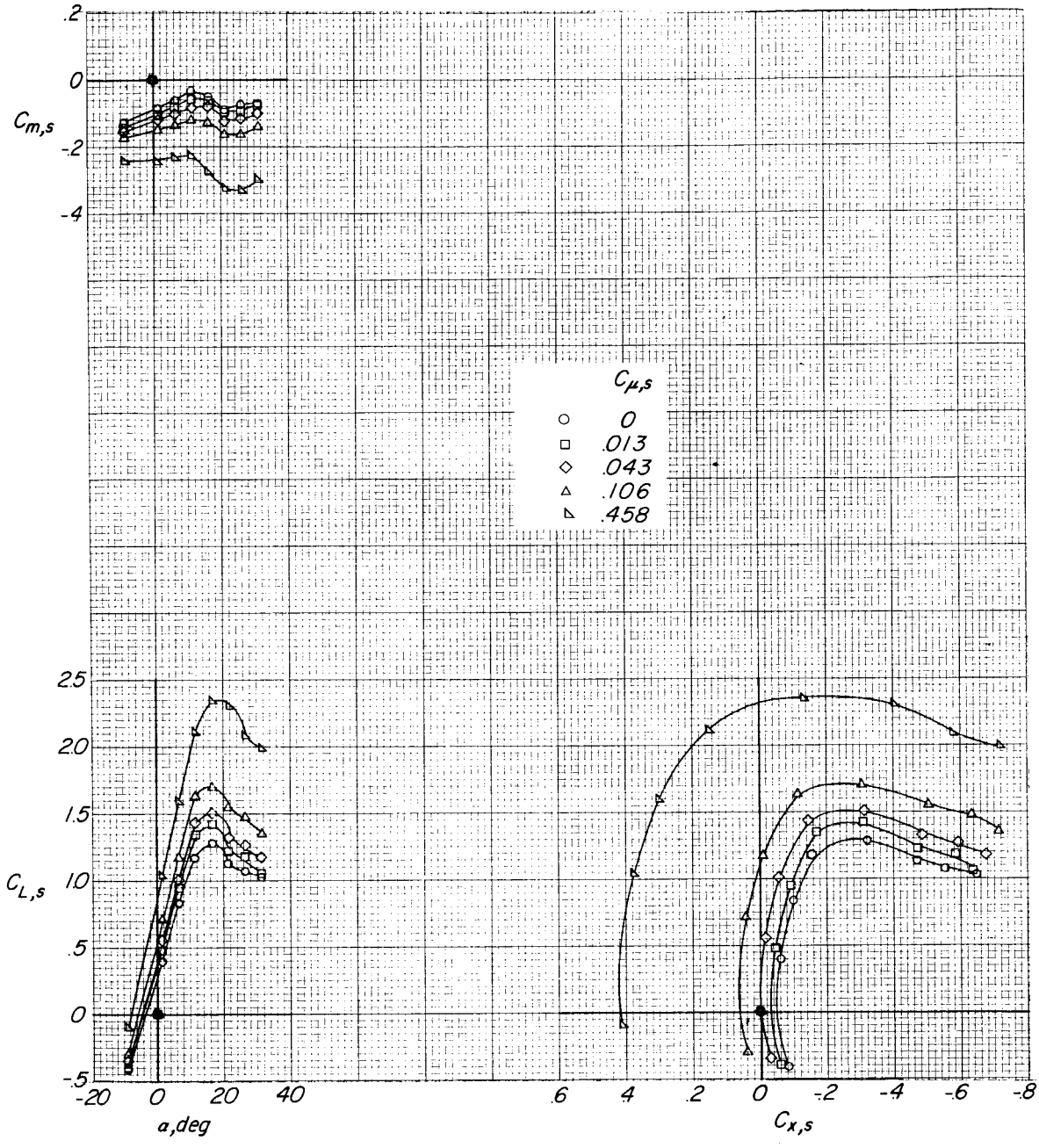

(f) $C_{T,s} = 0.$

Figure 8.- Concluded.

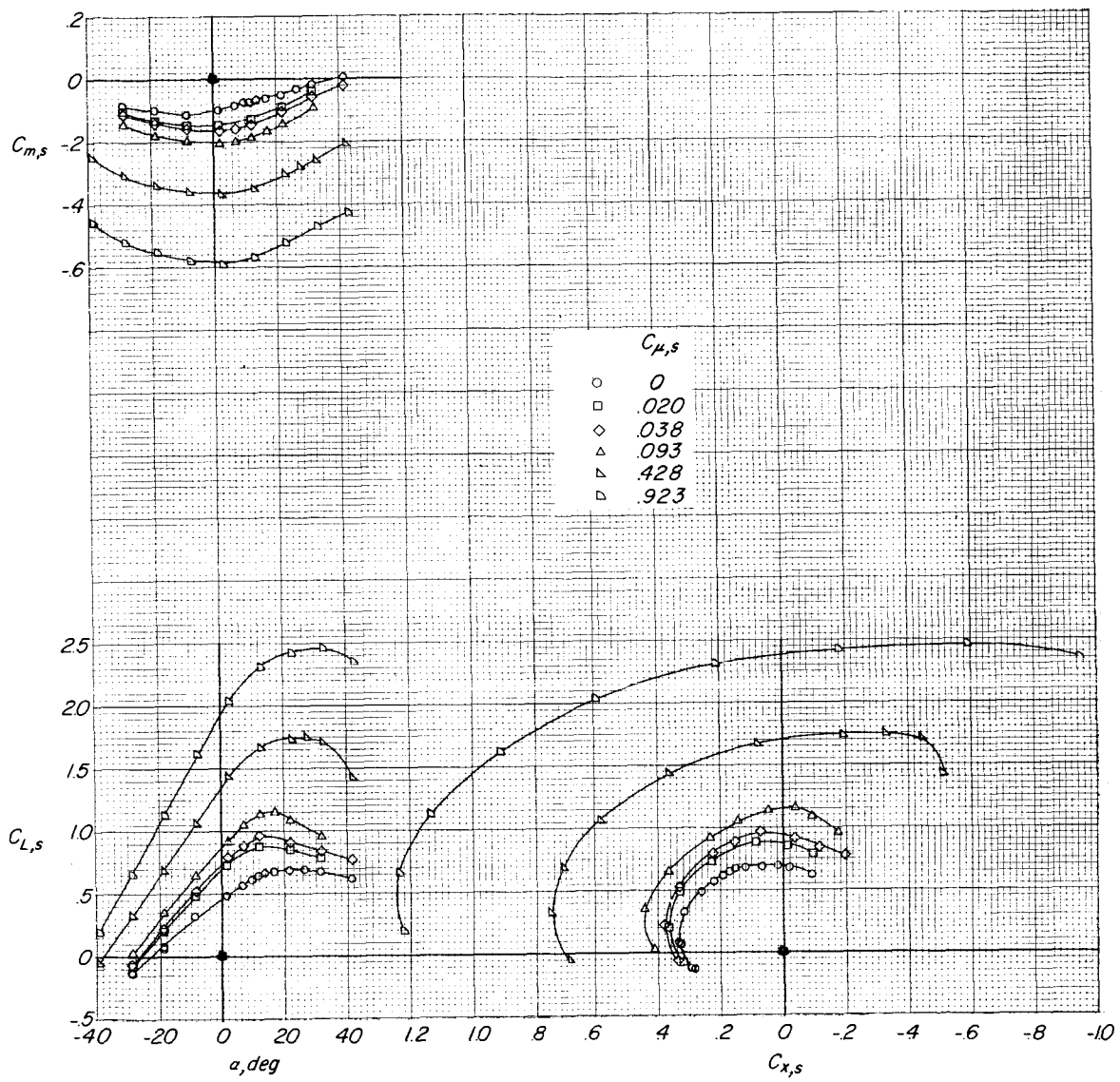

$C_{T,s} = 0.90$

(a) Longitudinal characteristics.

Figure 9.- Effect of variations in thrust and momentum coefficients on aerodynamic characteristics of the model out of ground proximity; $\delta_f = 40^\circ$.

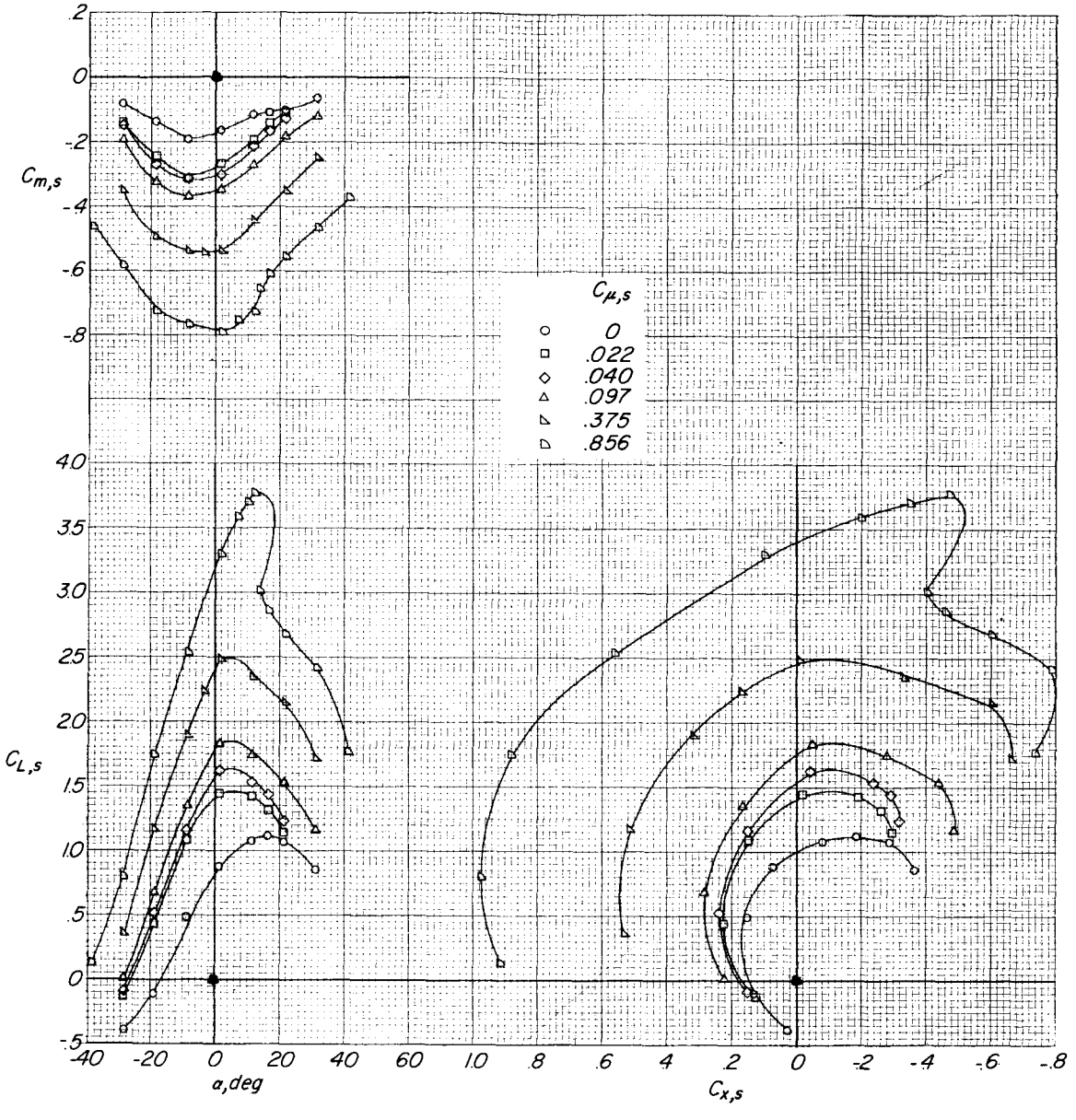

$C_{T,s} = 0.60$

(a) Continued.

Figure 9.- Continued.

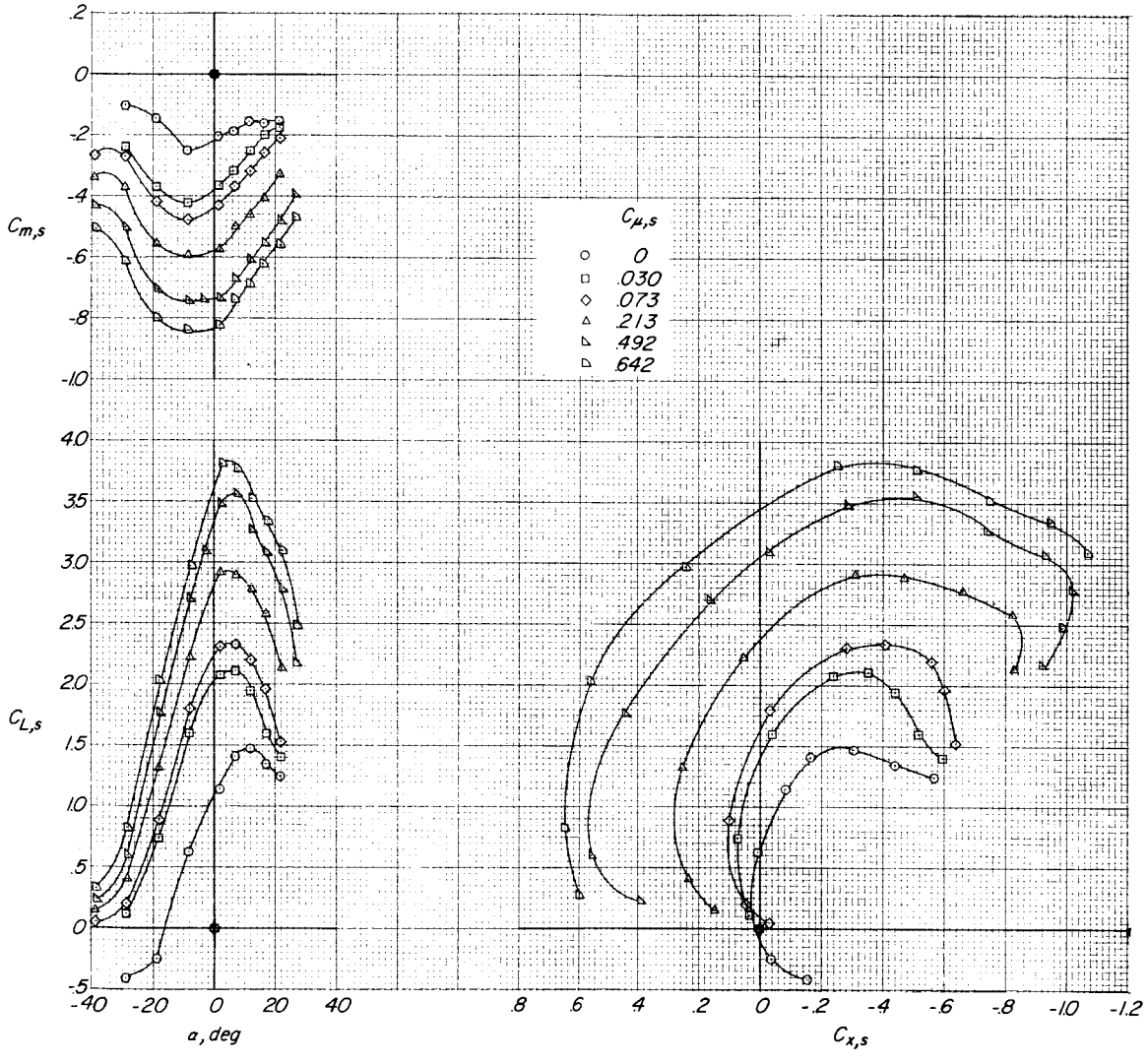

$C_{T,s} = 0.30$

(a) Continued.

Figure 9.- Continued.

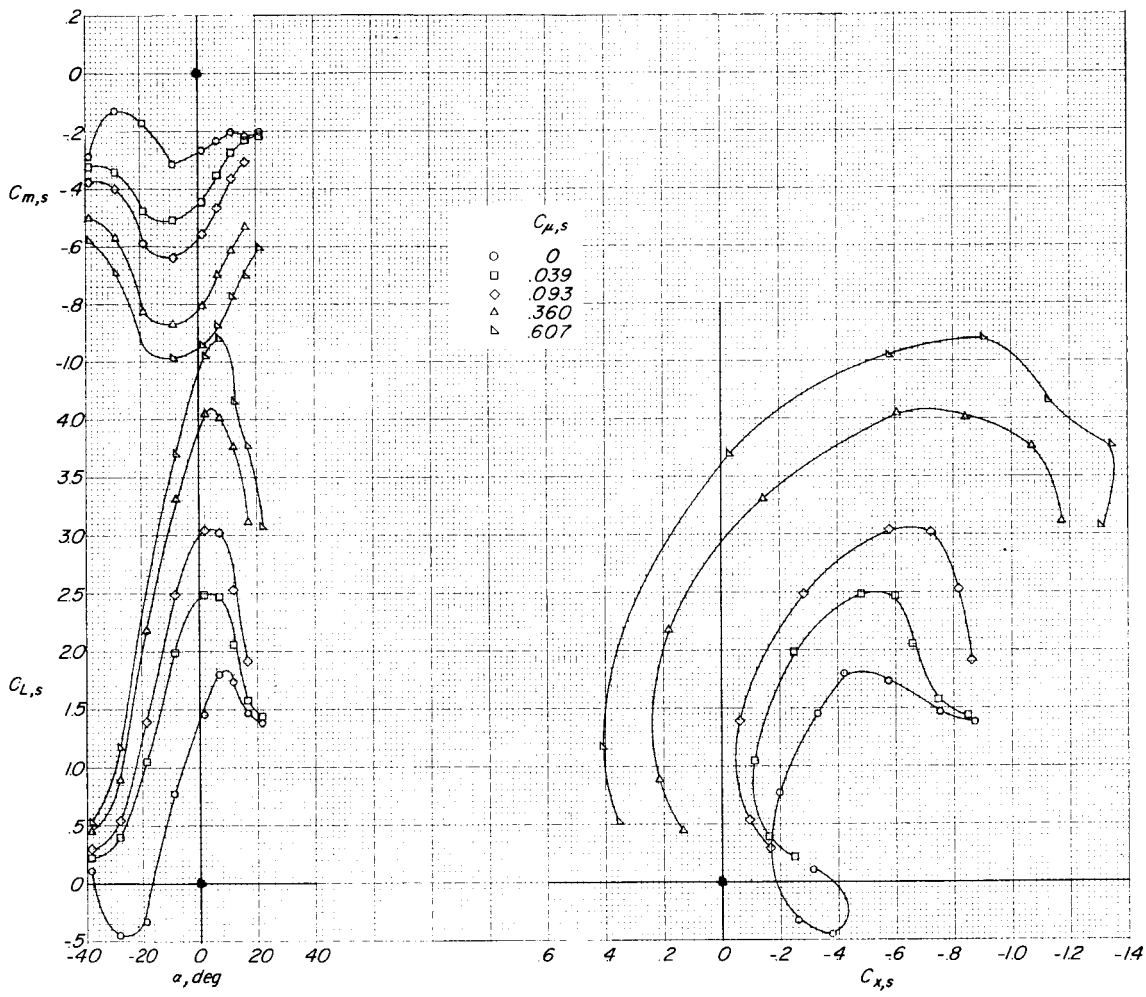

$C_{T,s} = 0$

(a) Concluded.

Figure 9.- Continued.

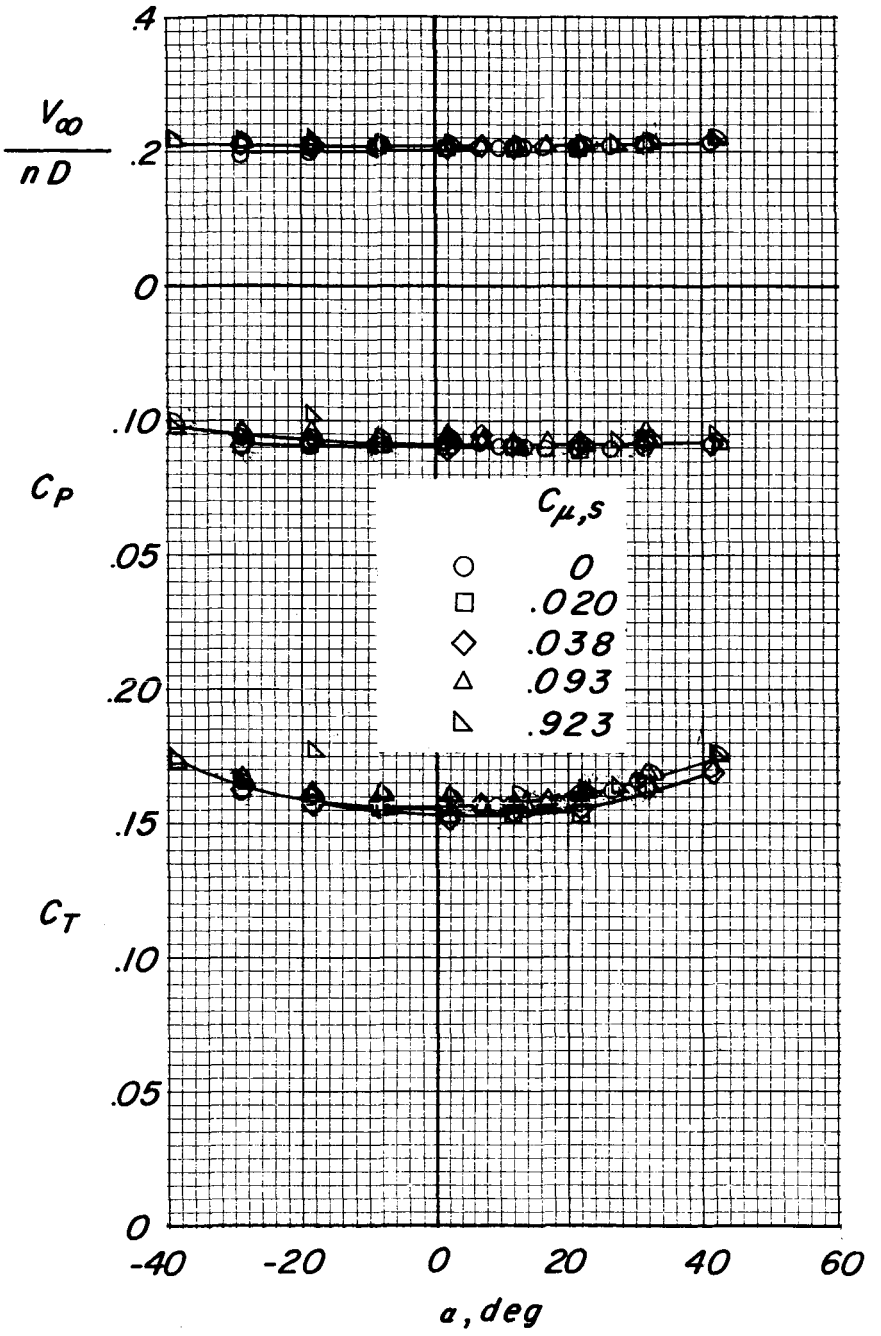

$C_{T,s} = 0.90$

(b) Propeller coefficients.

Figure 9.- Continued.

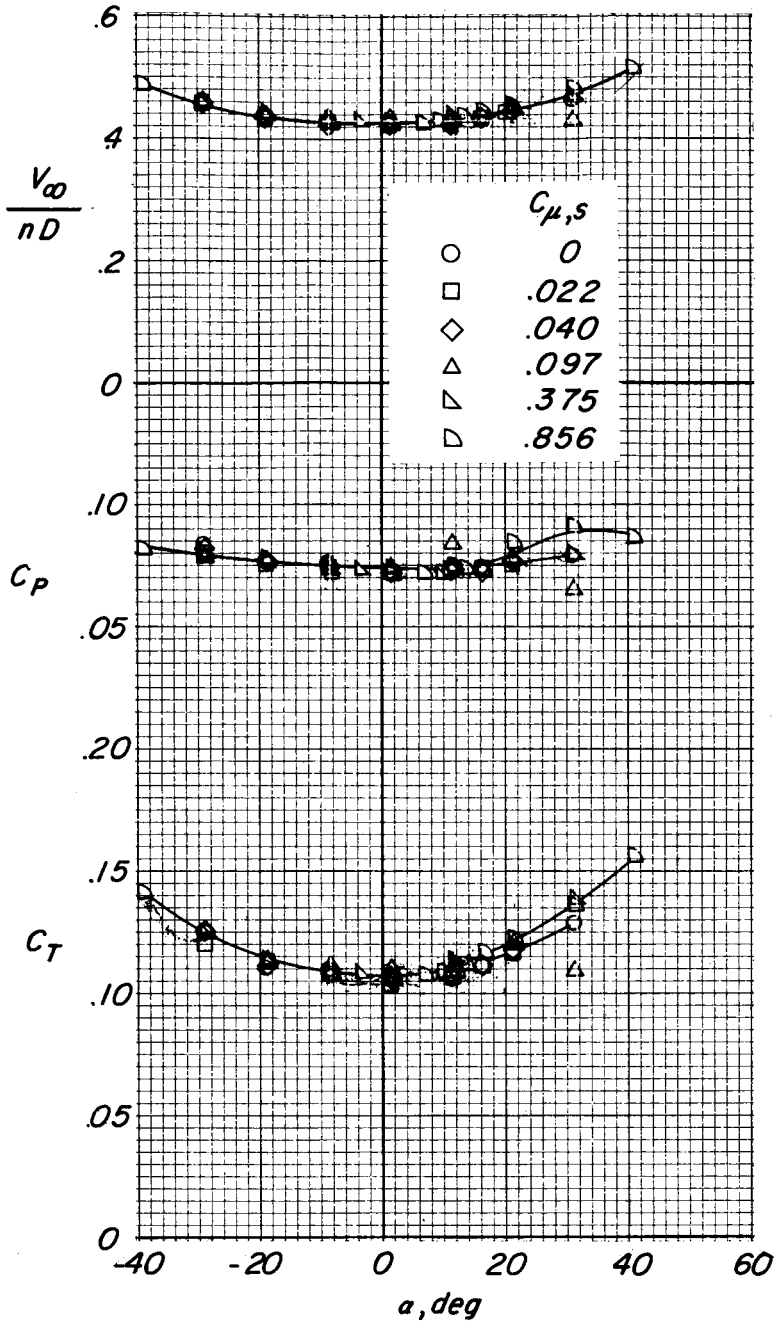

$C_{T,s} = 0.60$

(b) Continued.

Figure 9.- Continued.

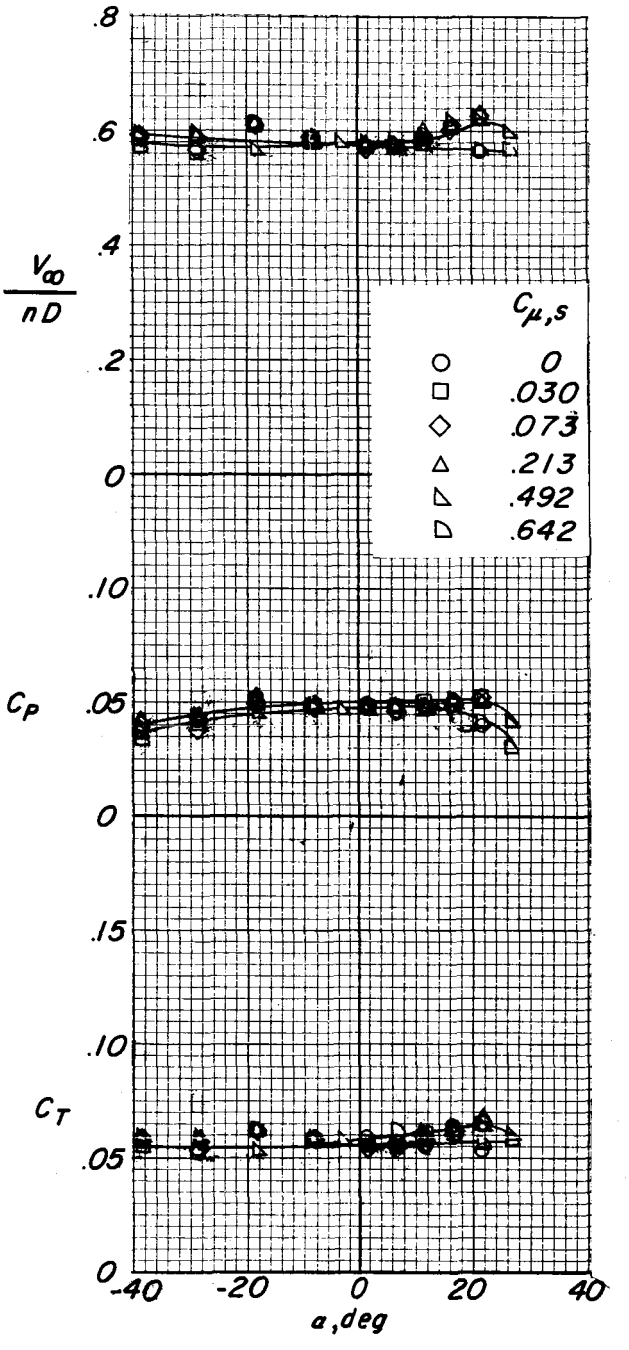

$C_{T,s} = 0.30$

(b) Concluded.

Figure 9.- Continued.

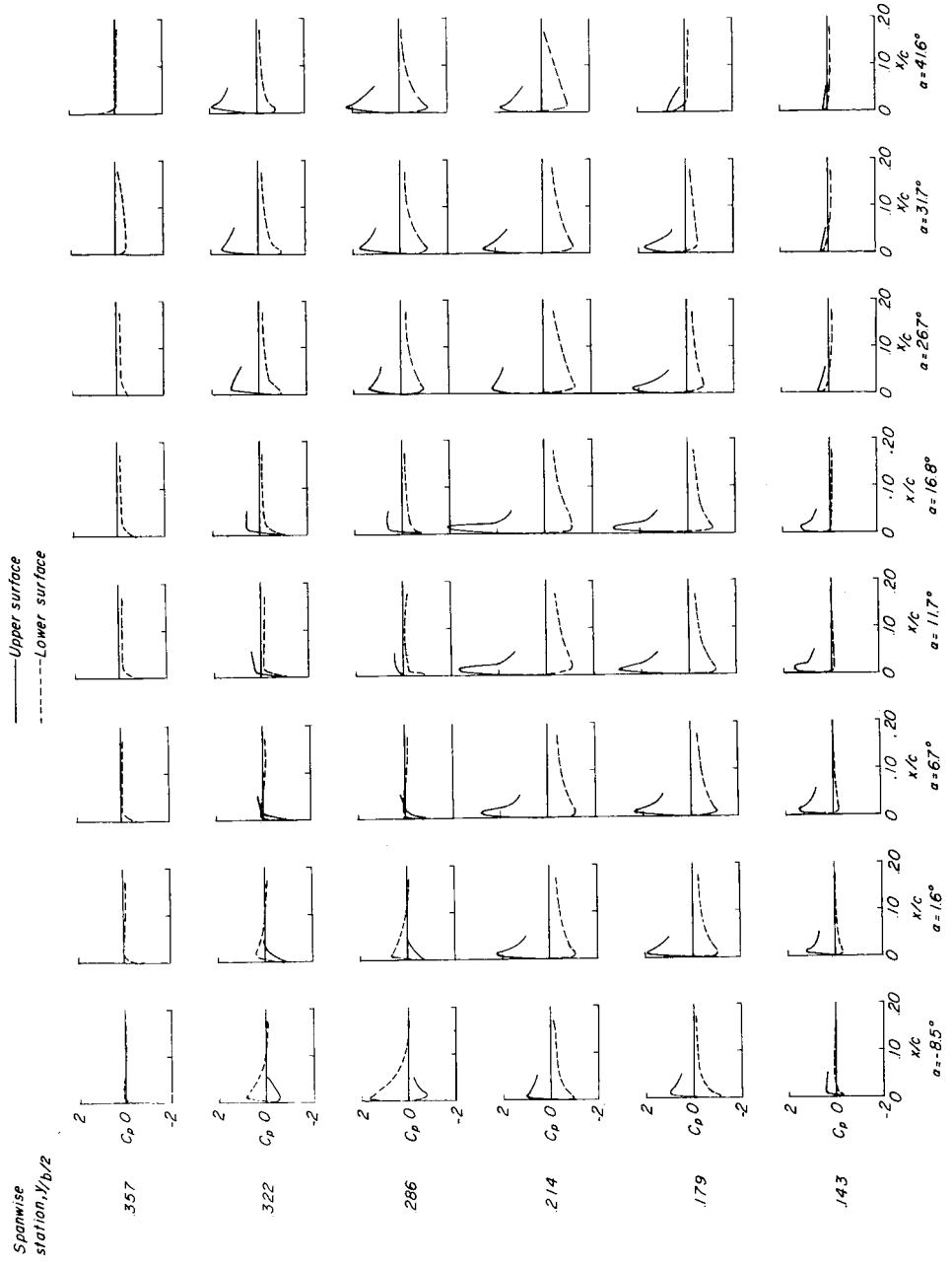

$C_{T,s} = 0.90$; $C_{\mu,s} = 0$

(c) Pressure coefficients.

Figure 9.- Continued.

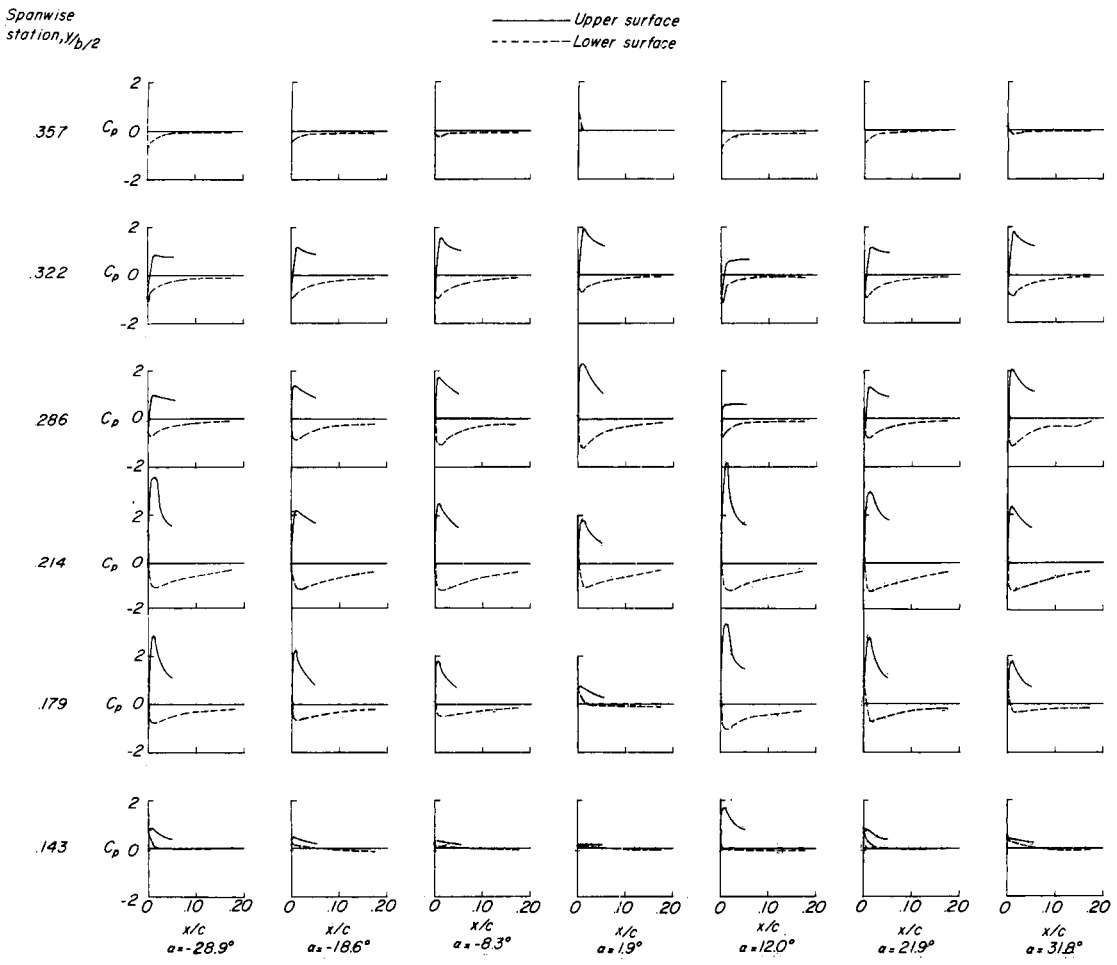

$C_{T,s} = 0.90$; $C_{\mu,s} = 0.020$

(c) Continued.

Figure 9.- Continued.

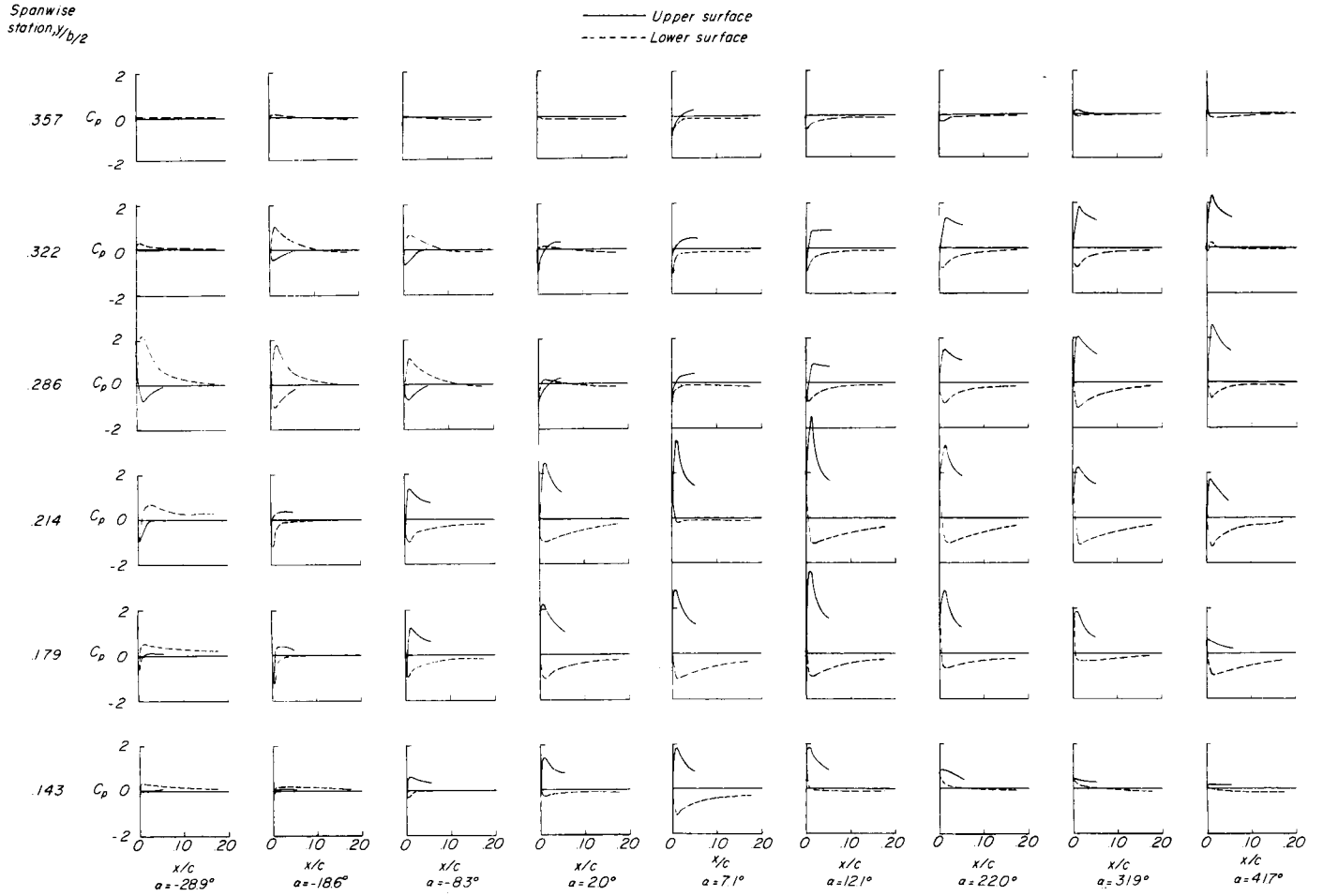

$C_{T,s} = 0.90$; $C_{\mu,s} = 0.038$

(c) Continued.

Figure 9.- Continued.

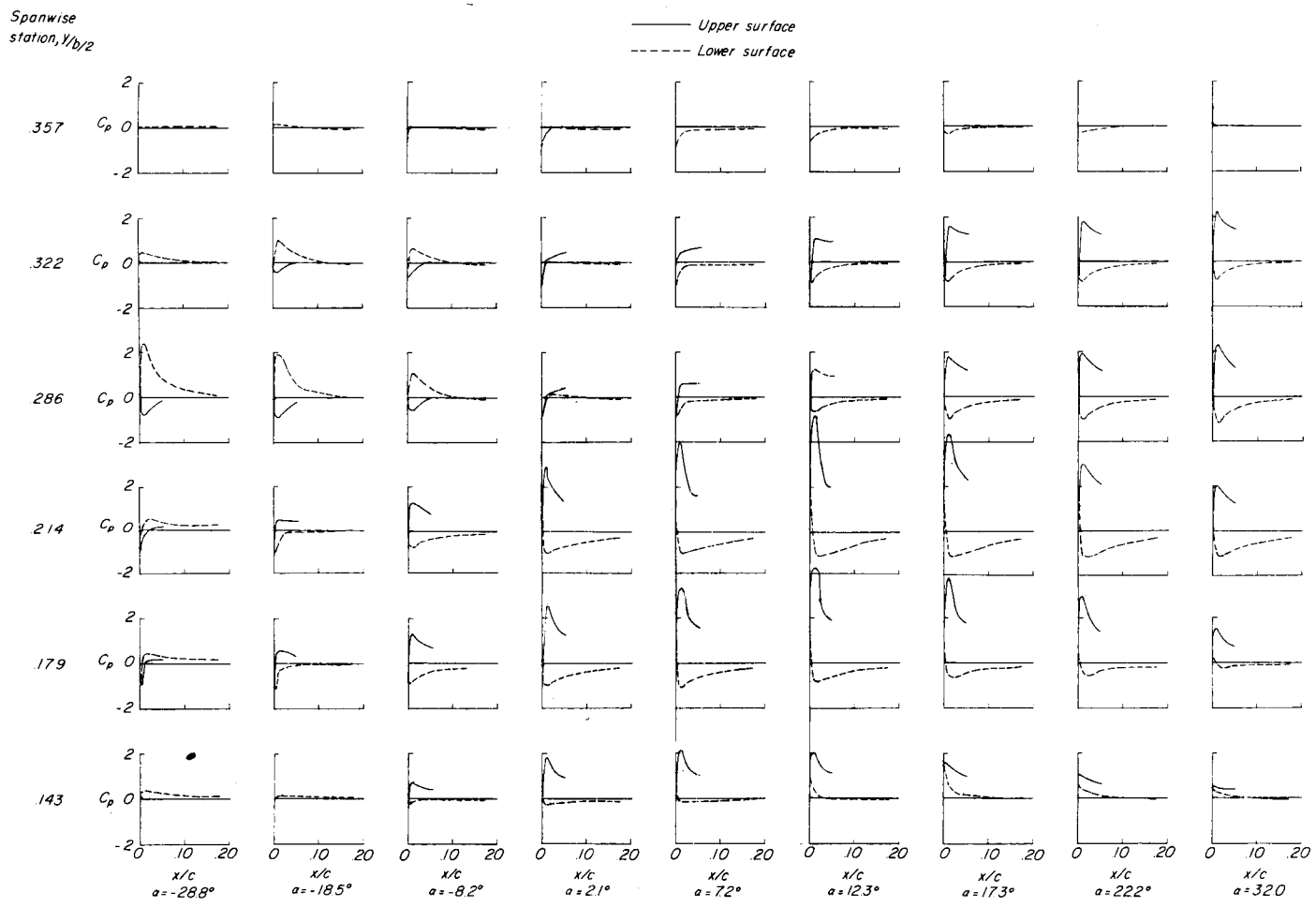

$C_{T,s} = 0.90$; $C_{\mu,s} = 0.093$

(c) Continued.

Figure 9.- Continued.

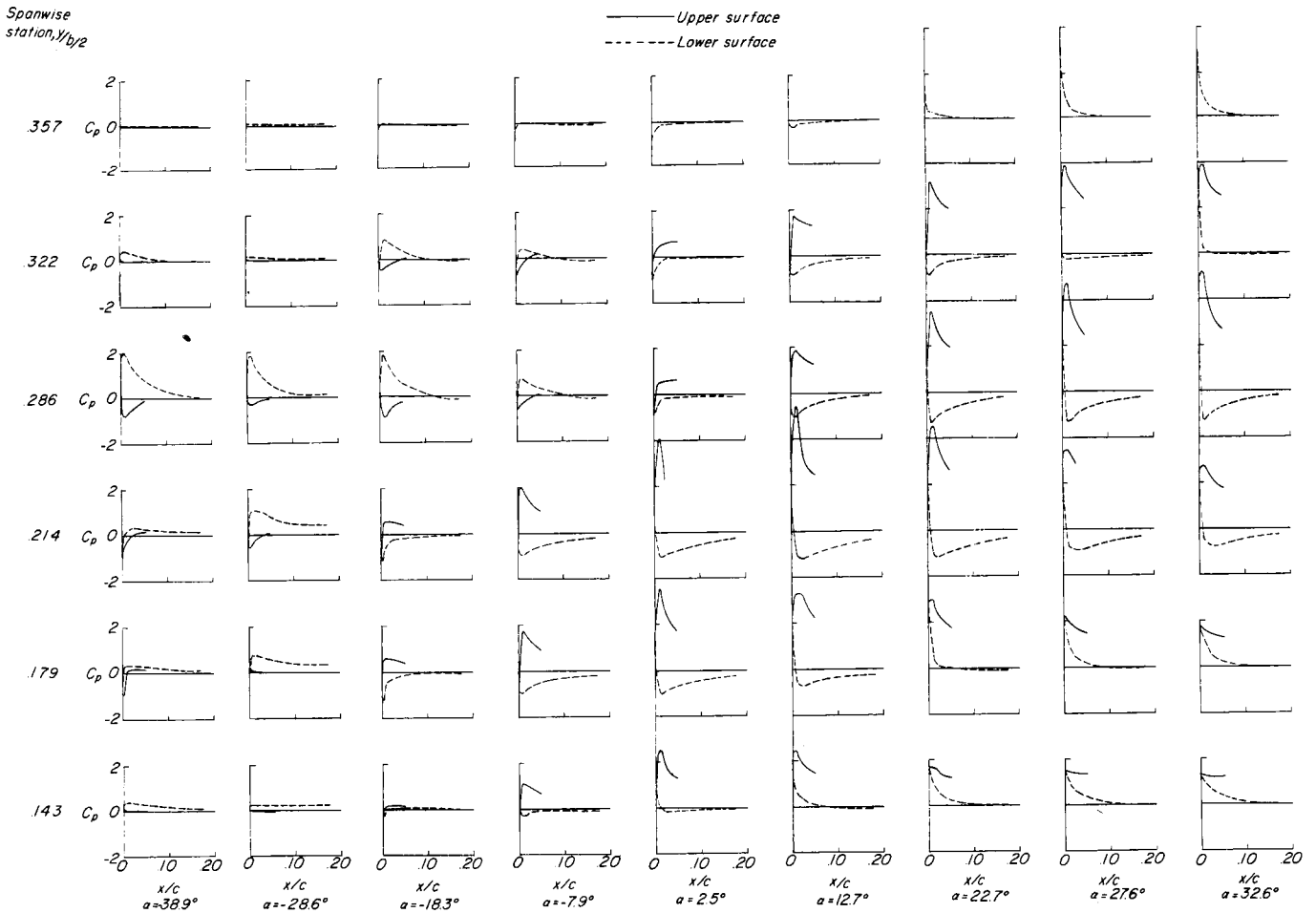

$C_{T,s} = 0.90$; $C_{\mu,s} = 0.428$

(c) Continued.

Figure 9.- Continued.

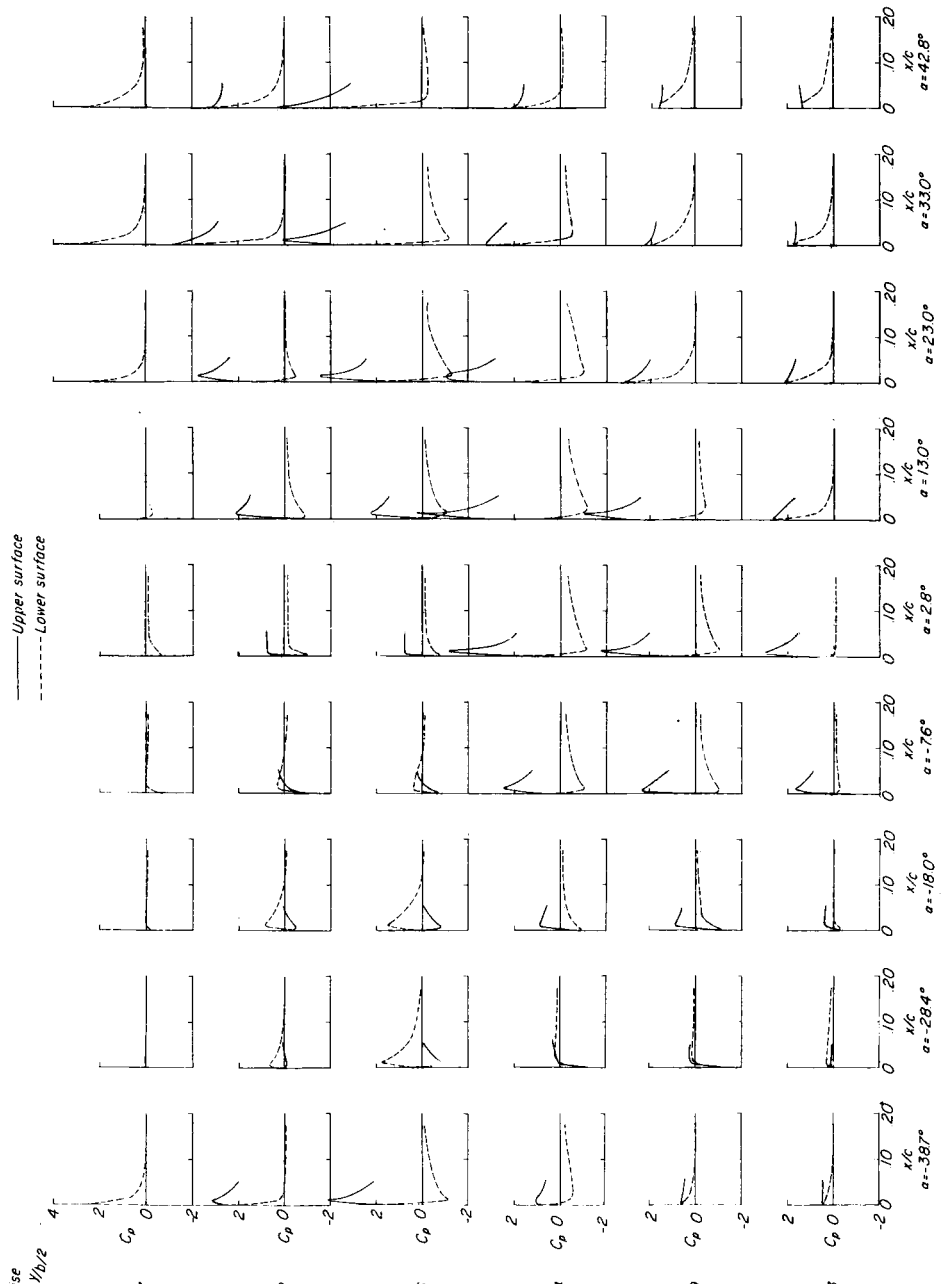

$C_{T,s} = 0.90$; $C_{\mu,s} = 0.923$

(c) Continued.

Figure 9.- Continued.

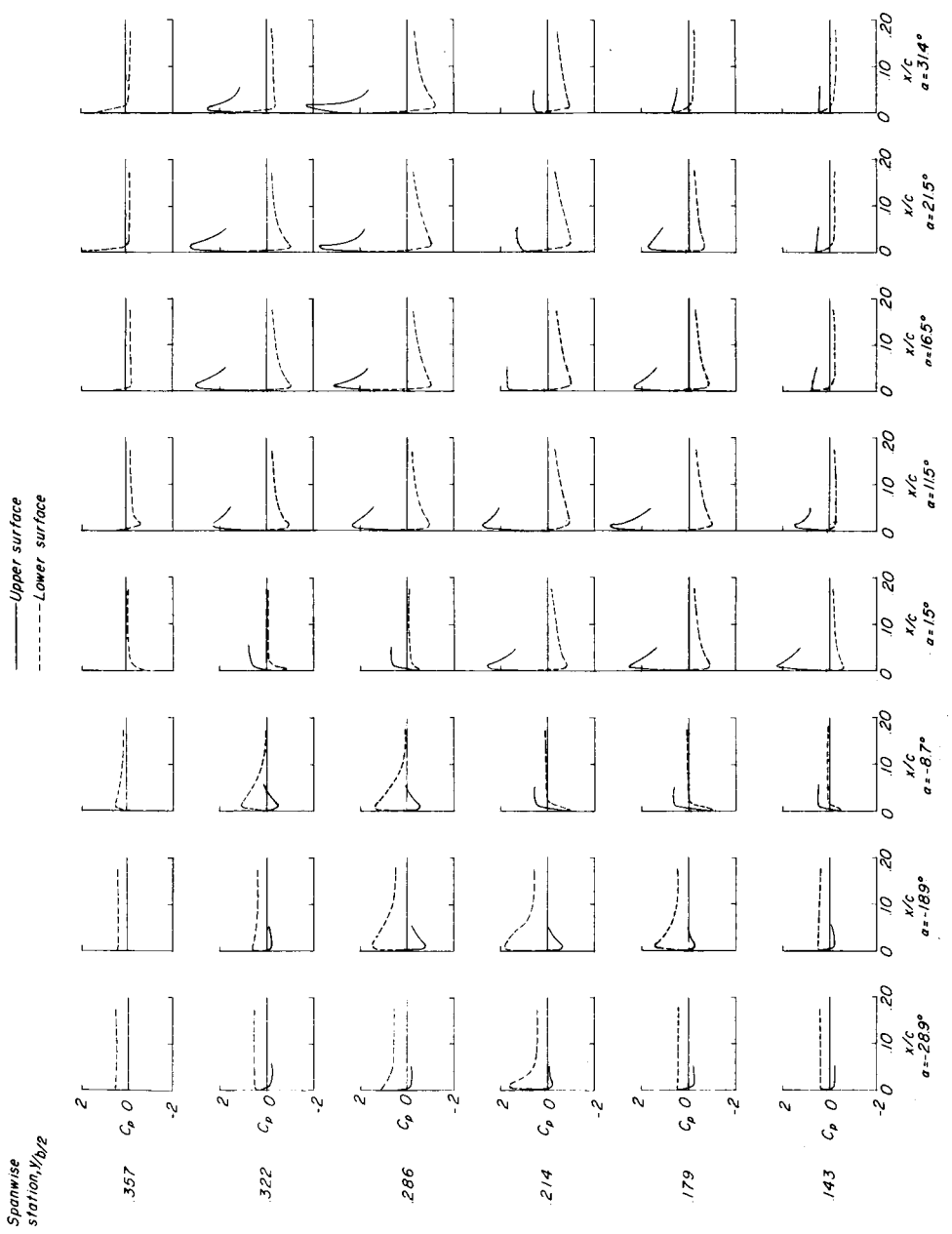

$C_{T,s} = 0.60$; $C_{\mu,s} = 0$

(c) Continued.

Figure 9.- Continued.

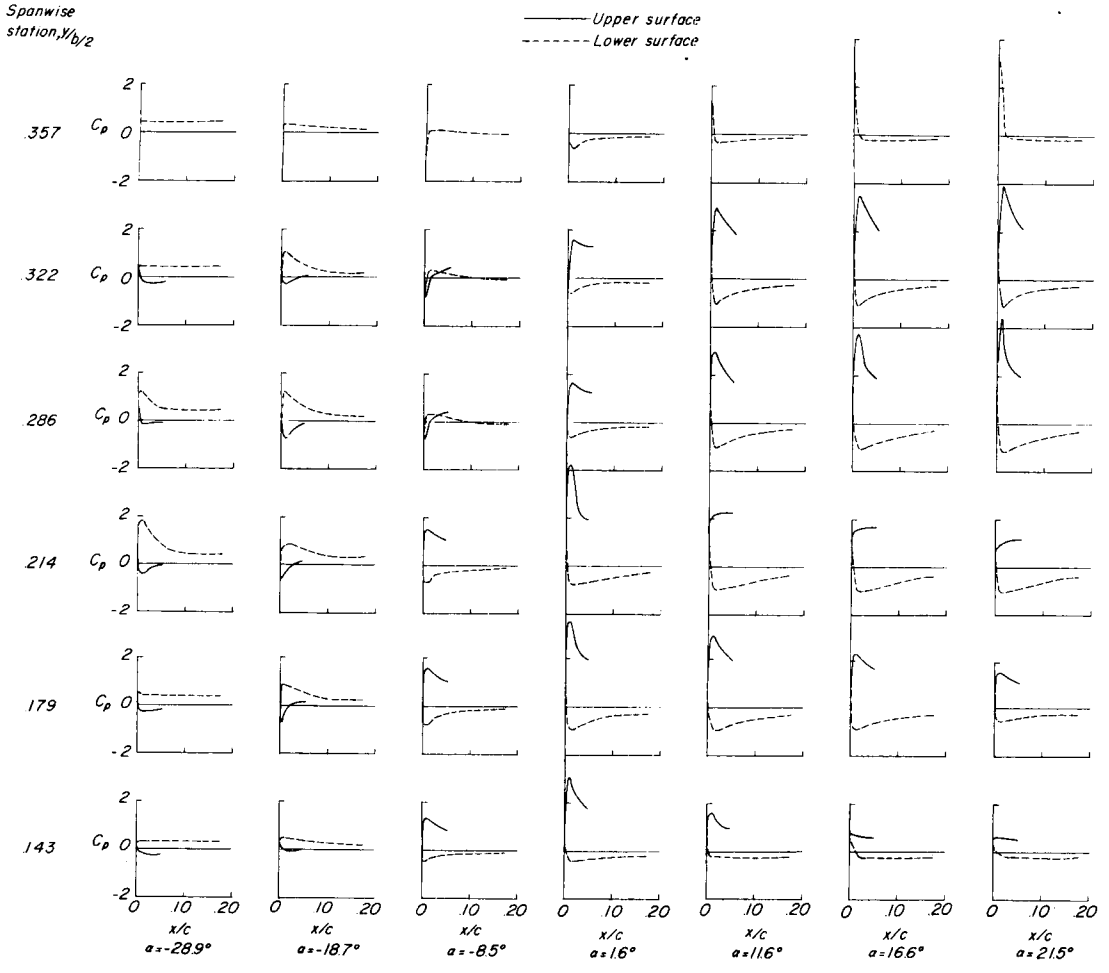

$C_{T,s} = 0.60$; $C_{\mu,s} = 0.022$

(c) Continued.

Figure 9.- Continued.

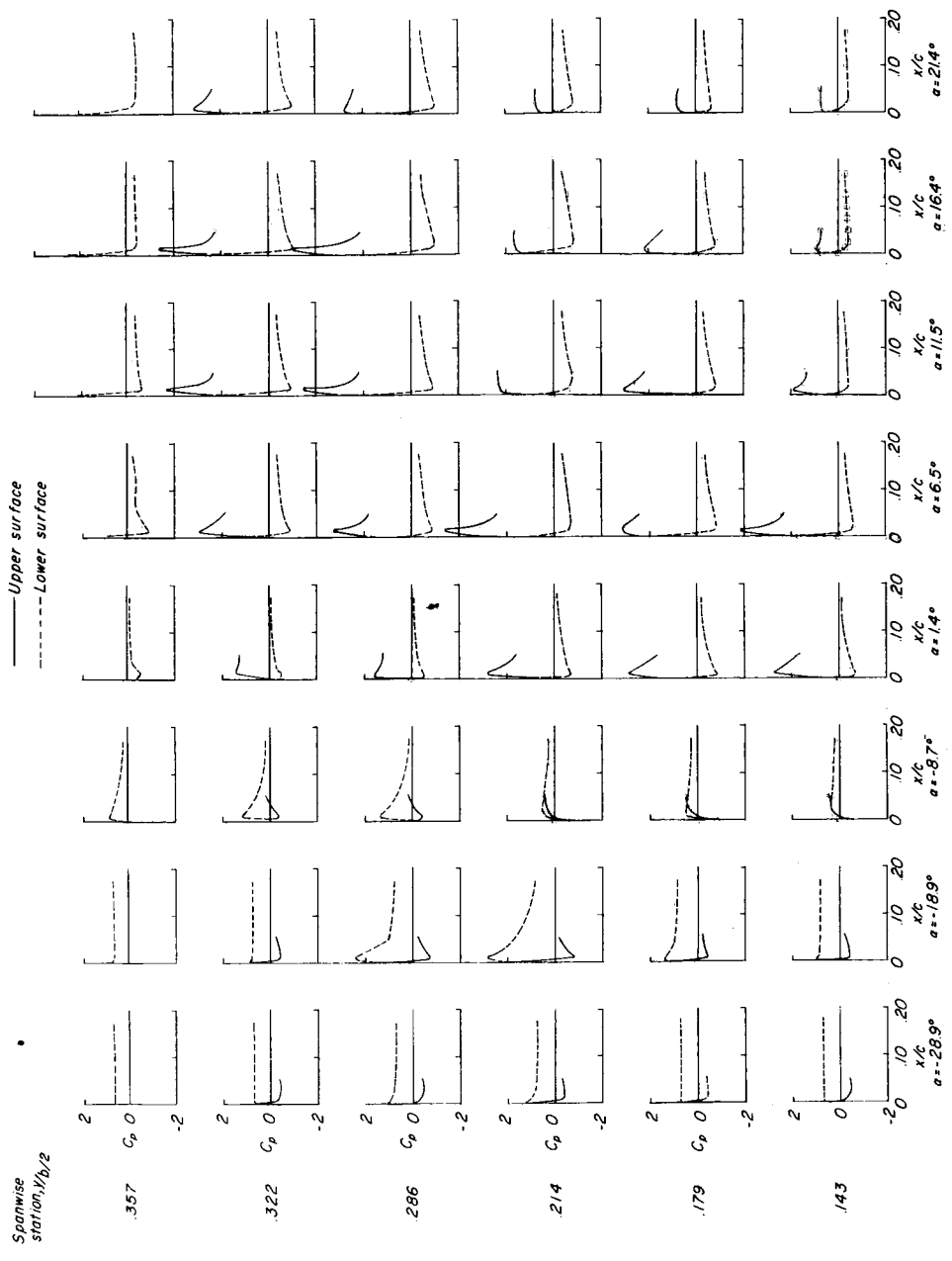

$C_{T,s} = 0.60$; $C_{\mu,s} = 0.040$

(c) Continued.

Figure 9.- Continued.

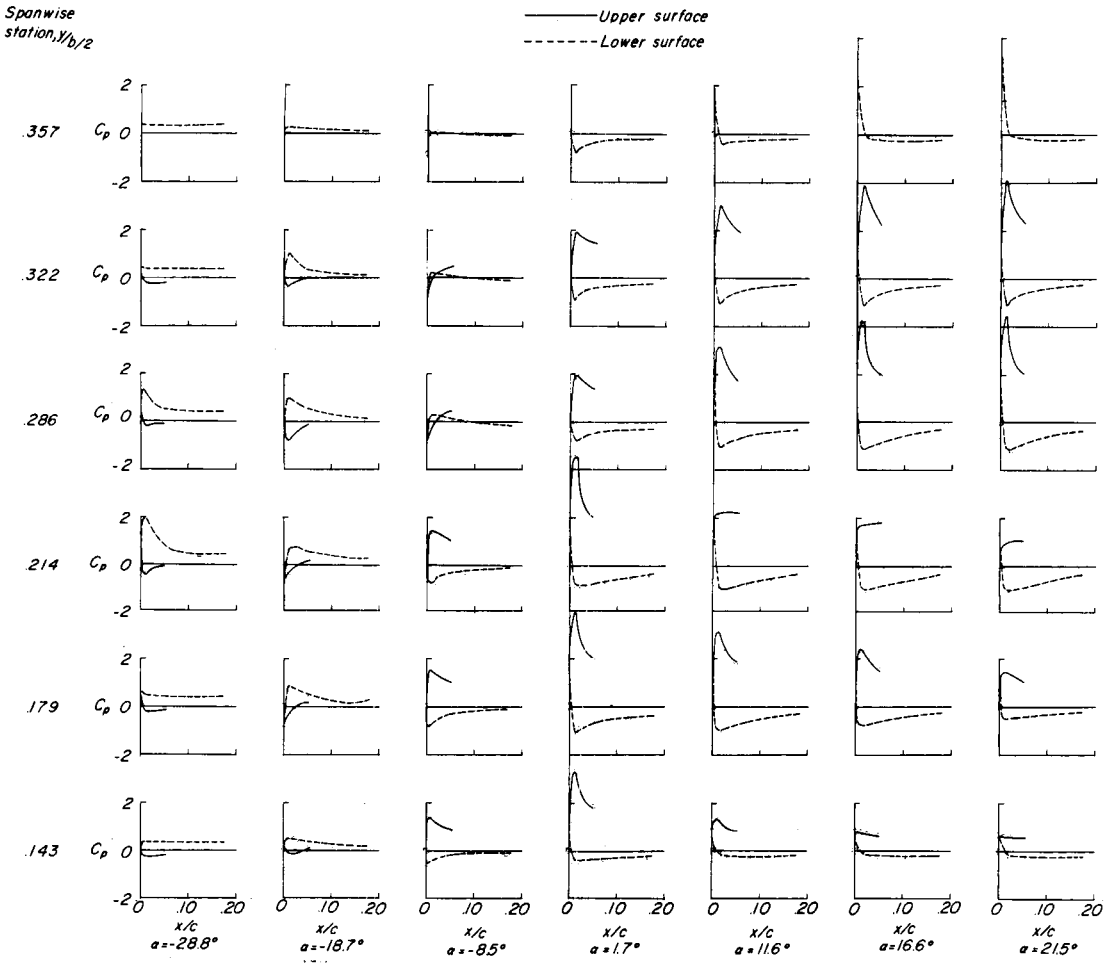

$C_{T,s} = 0.30$; $C_{\mu,s} = 0$

(c) Continued.

Figure 9.- Continued.

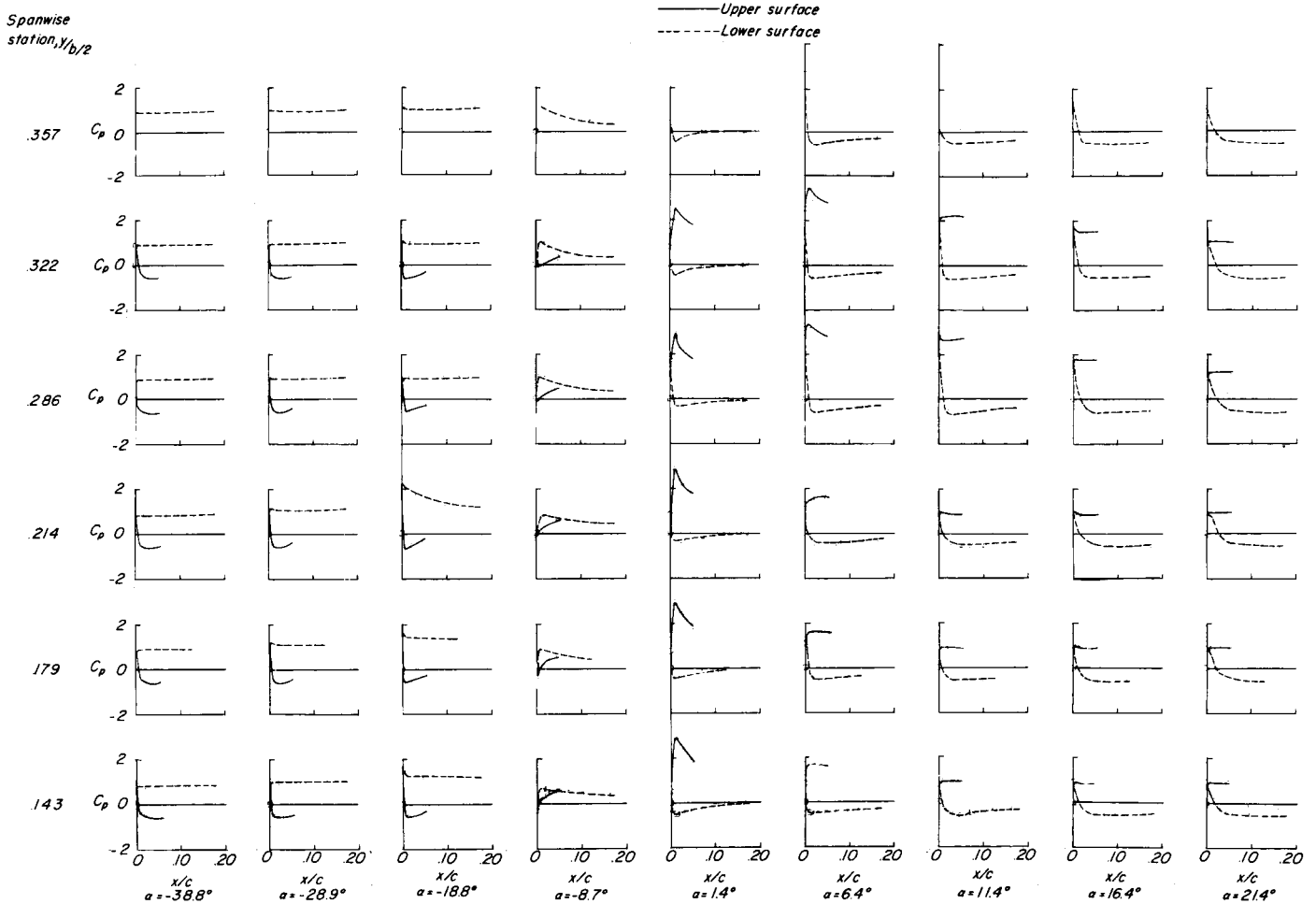

$C_{T,s} = 0$; $C_{\mu,s} = 0$

(c) Concluded.

Figure 9.- Concluded.

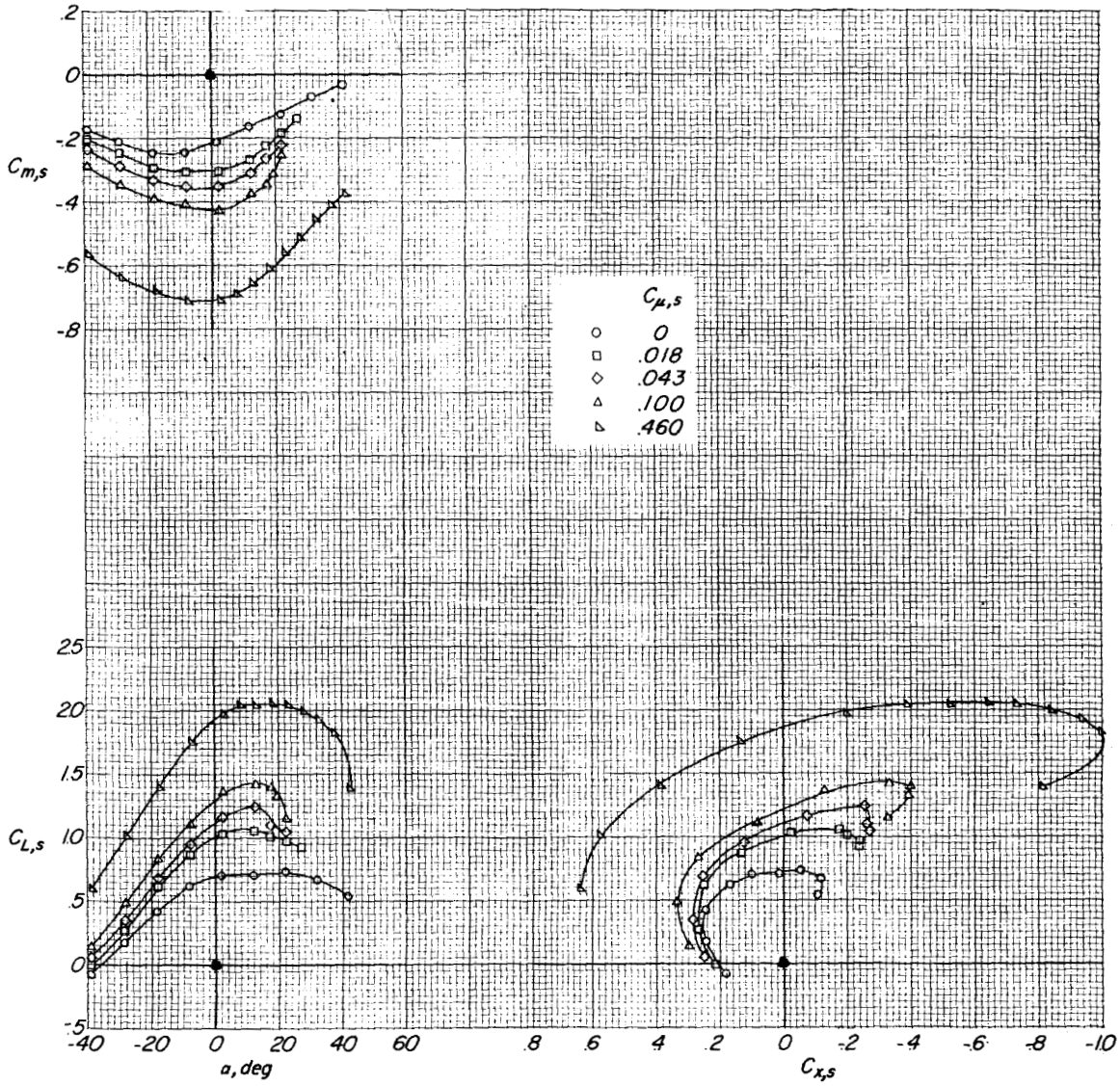

(a) Longitudinal characteristics.

Figure 10.- Effect of variations in momentum coefficient on the aerodynamic characteristics of model out of ground proximity. $\delta_f = 40^\circ$; $\delta_{T.E.} = 40^\circ$; $C_{T,s} = 0.90$.

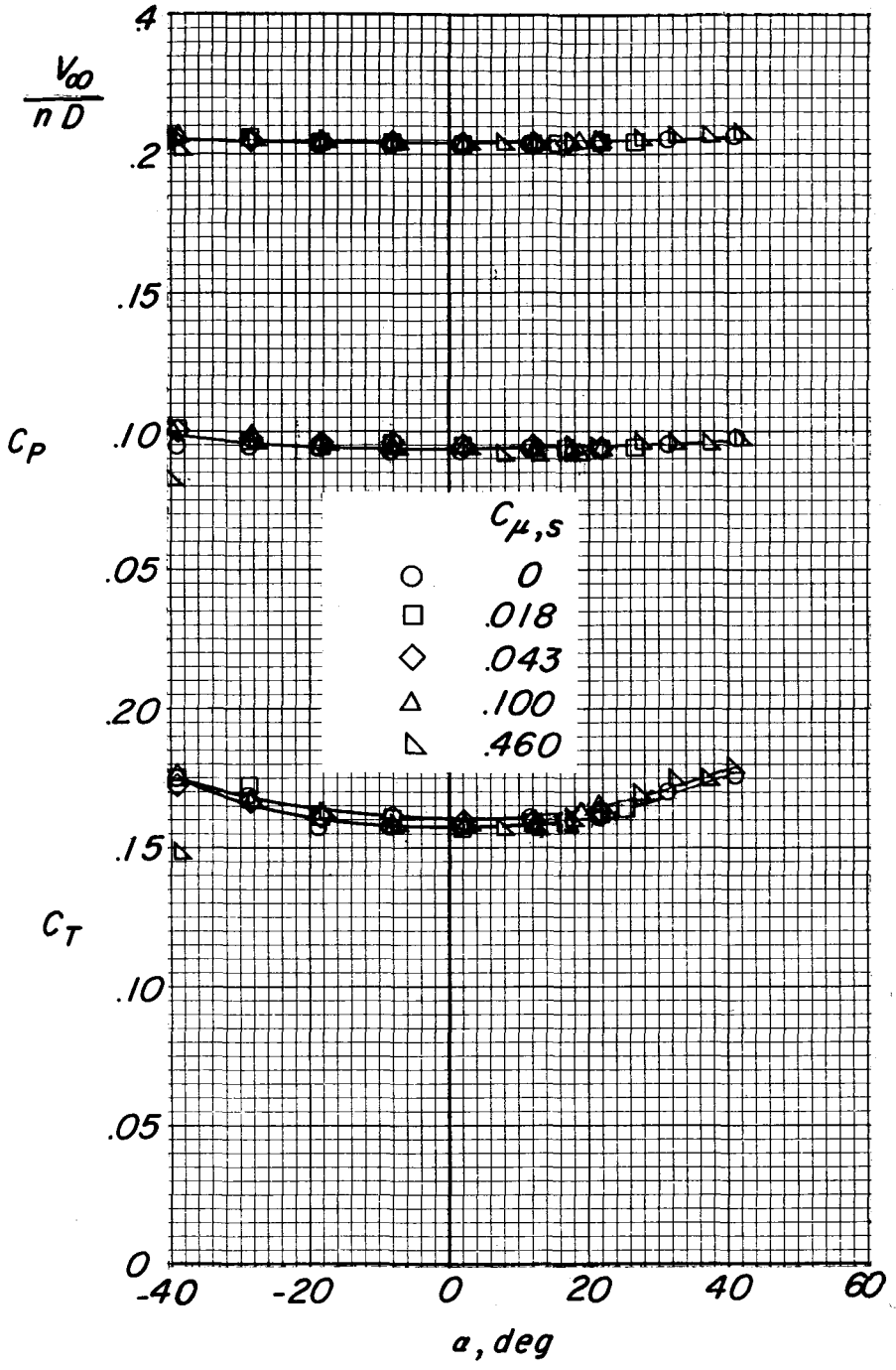

(b) Propeller coefficients.

Figure 10.- Concluded.

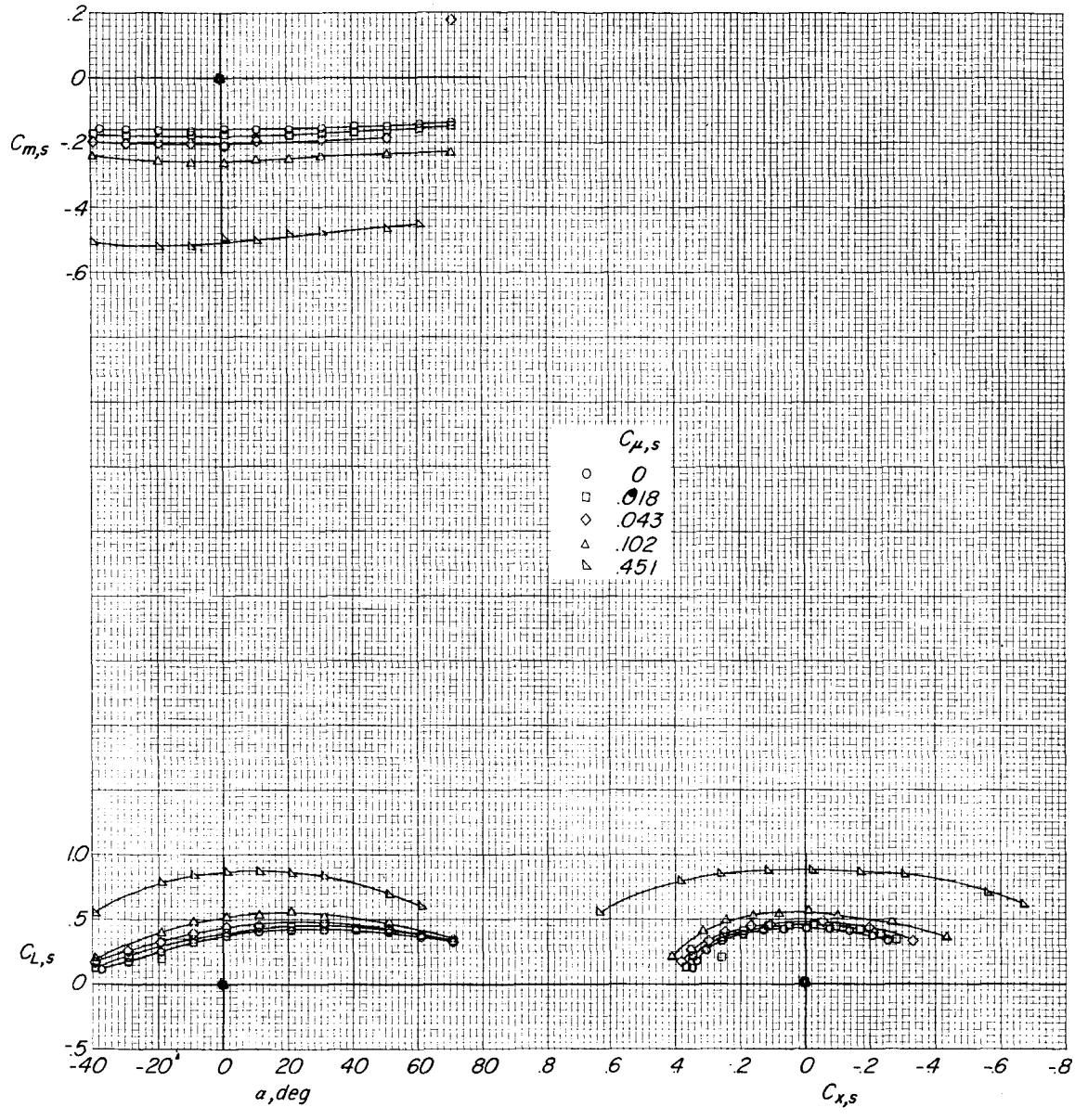

(a) $C_{T,s} = 1.0$.

Figure 11.- Effect of variations in thrust and momentum coefficients on the aerodynamic characteristics out of ground proximity. $\delta_f = 40^\circ$; $\delta_{T.E.} = 60^\circ$.

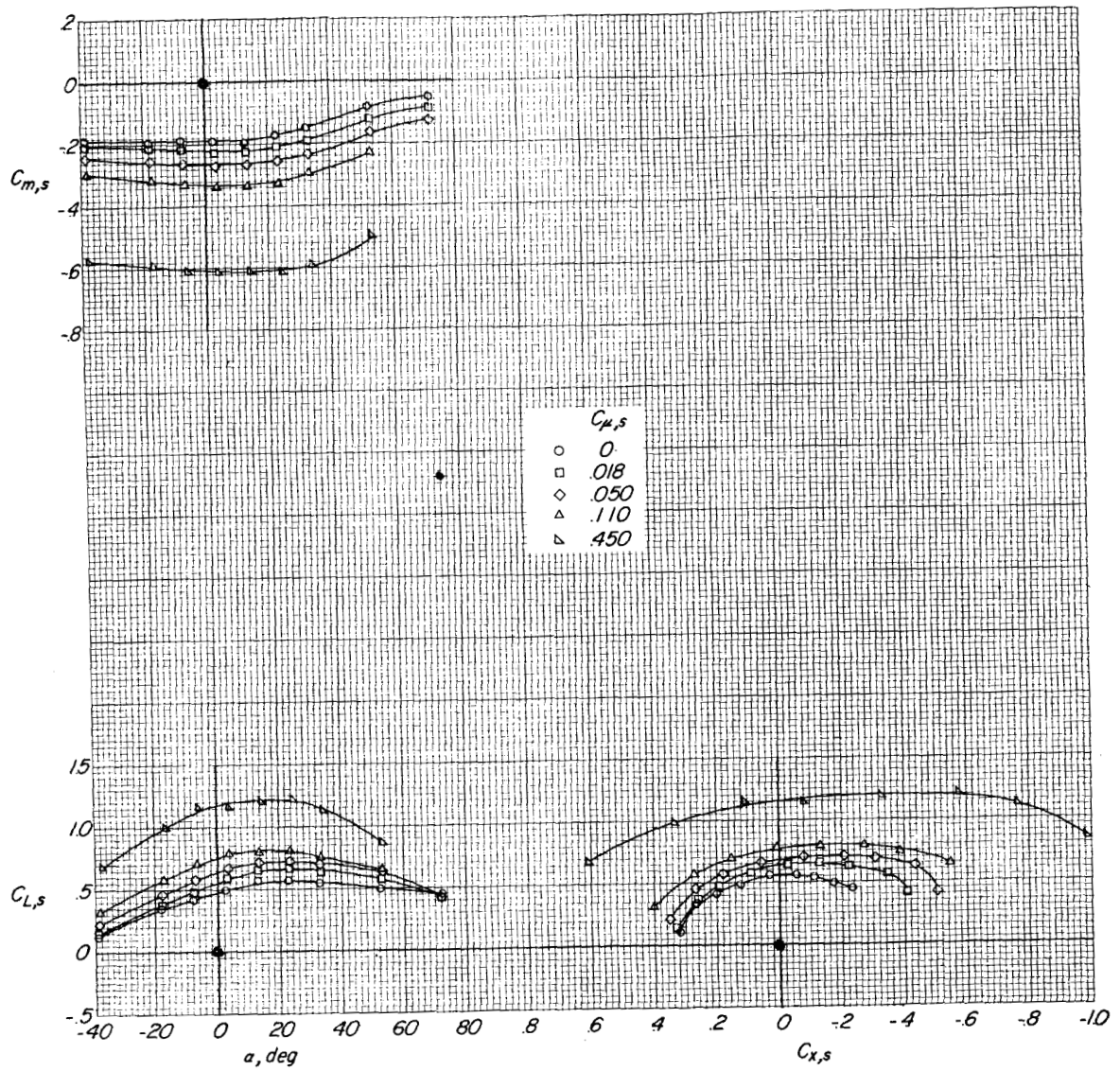

(b) $C_{T,s} = 0.98$.

Figure 11.- Continued.

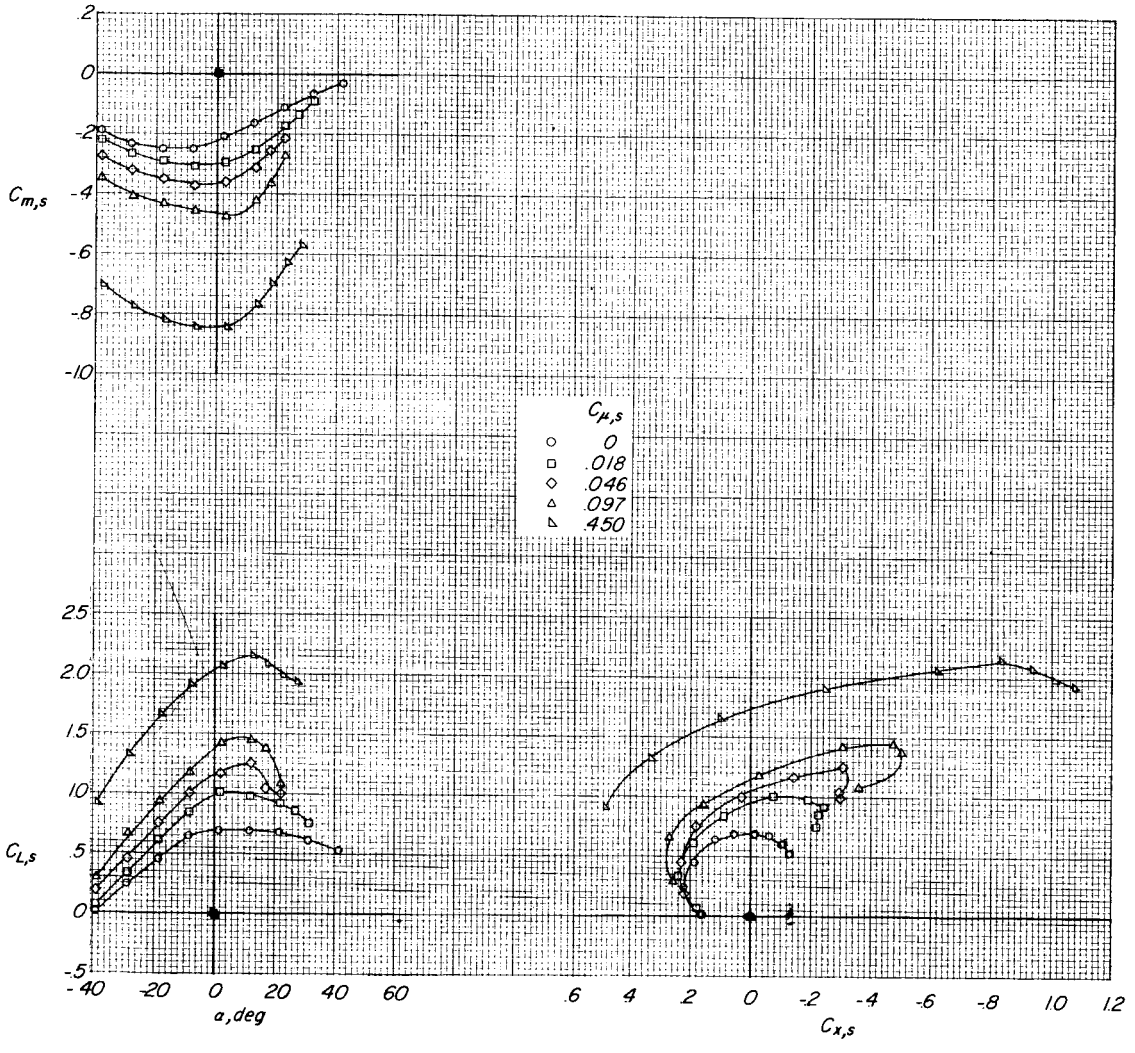

(c) $C_{T,s} = 0.90$.

Figure 11.- Continued.

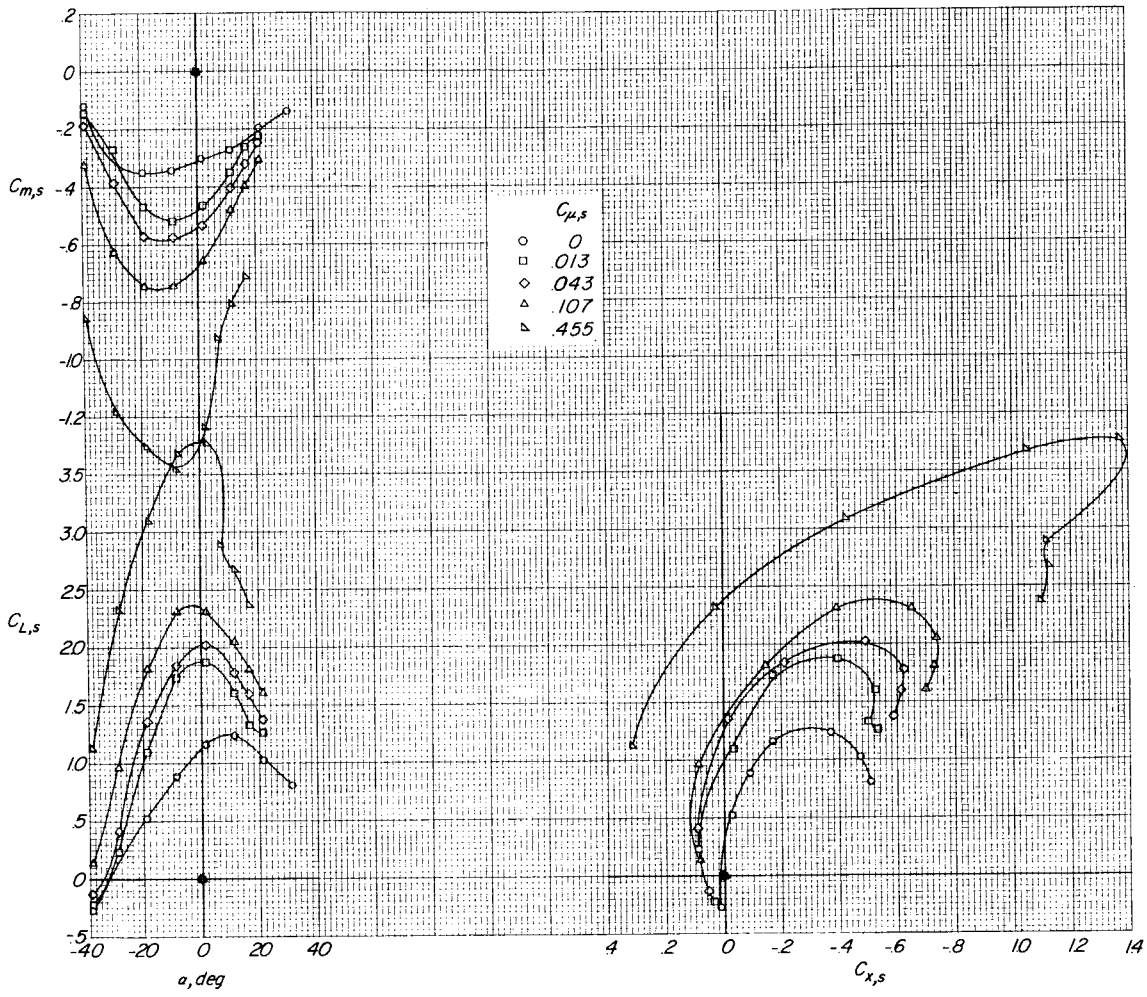

(d) $C_{T,s} = 0.60$.

Figure 11.- Continued.

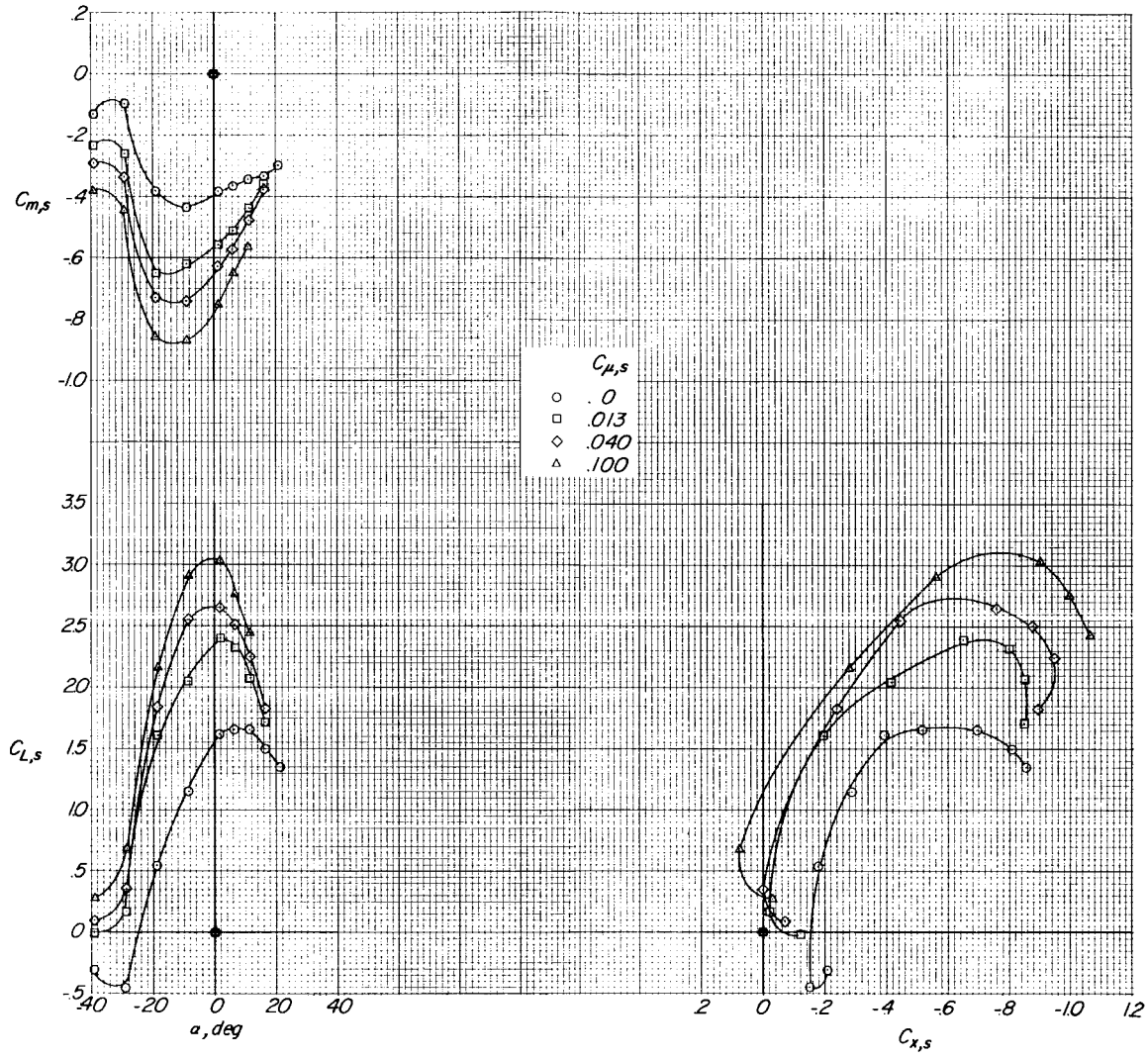

(e) $C_{T,s} = 0.30$.

Figure 11.- Continued.

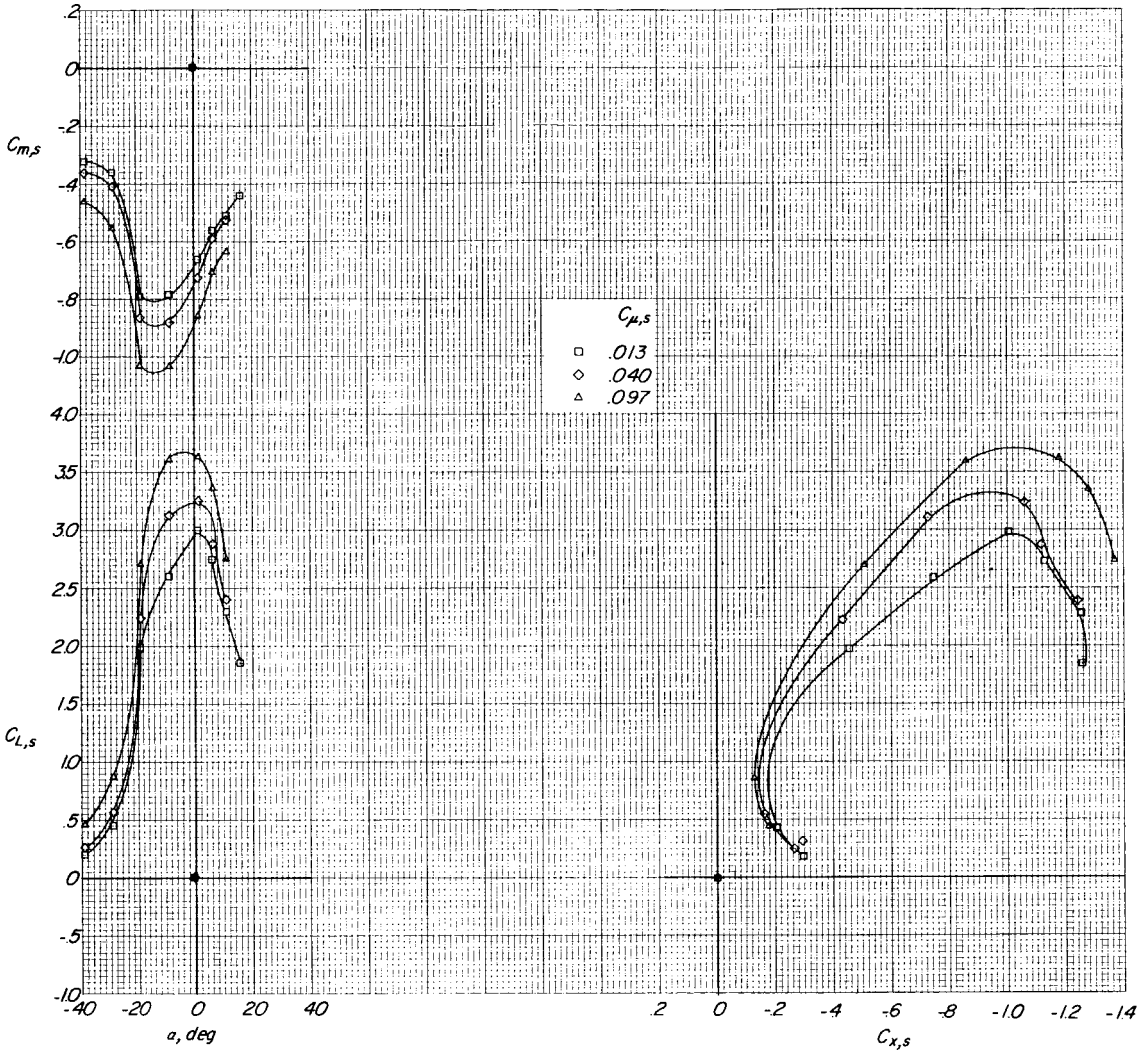

(f) $C_{T,s} = 0$.

Figure 11.- Concluded.

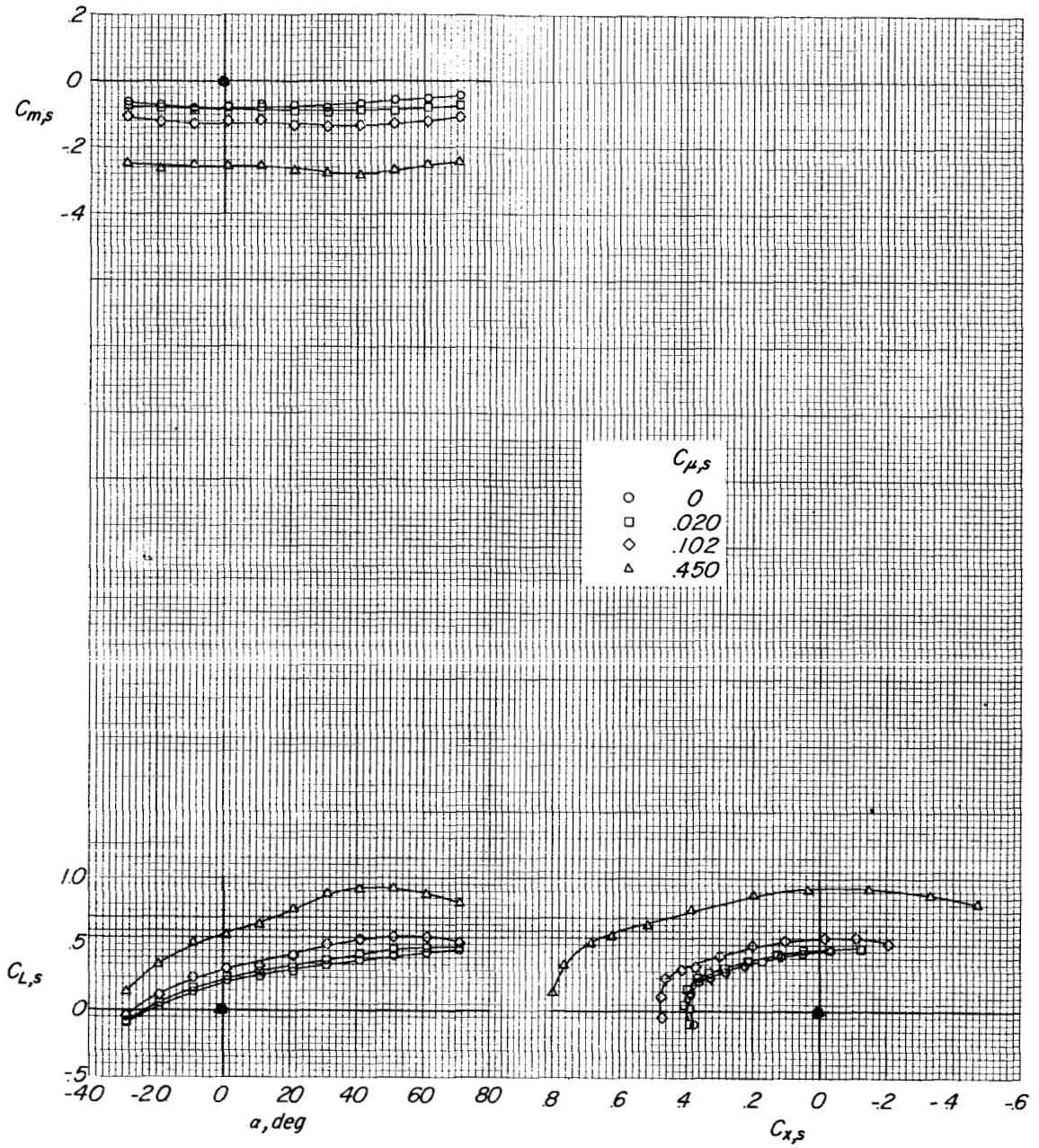

$C_{T,s} = 1.0$

(a) Longitudinal characteristics.

Figure 12.- Effects of variations in thrust and momentum coefficients on the aerodynamic characteristics of model within ground proximity. $\delta_f = 40^\circ$; h/D = 1.22.

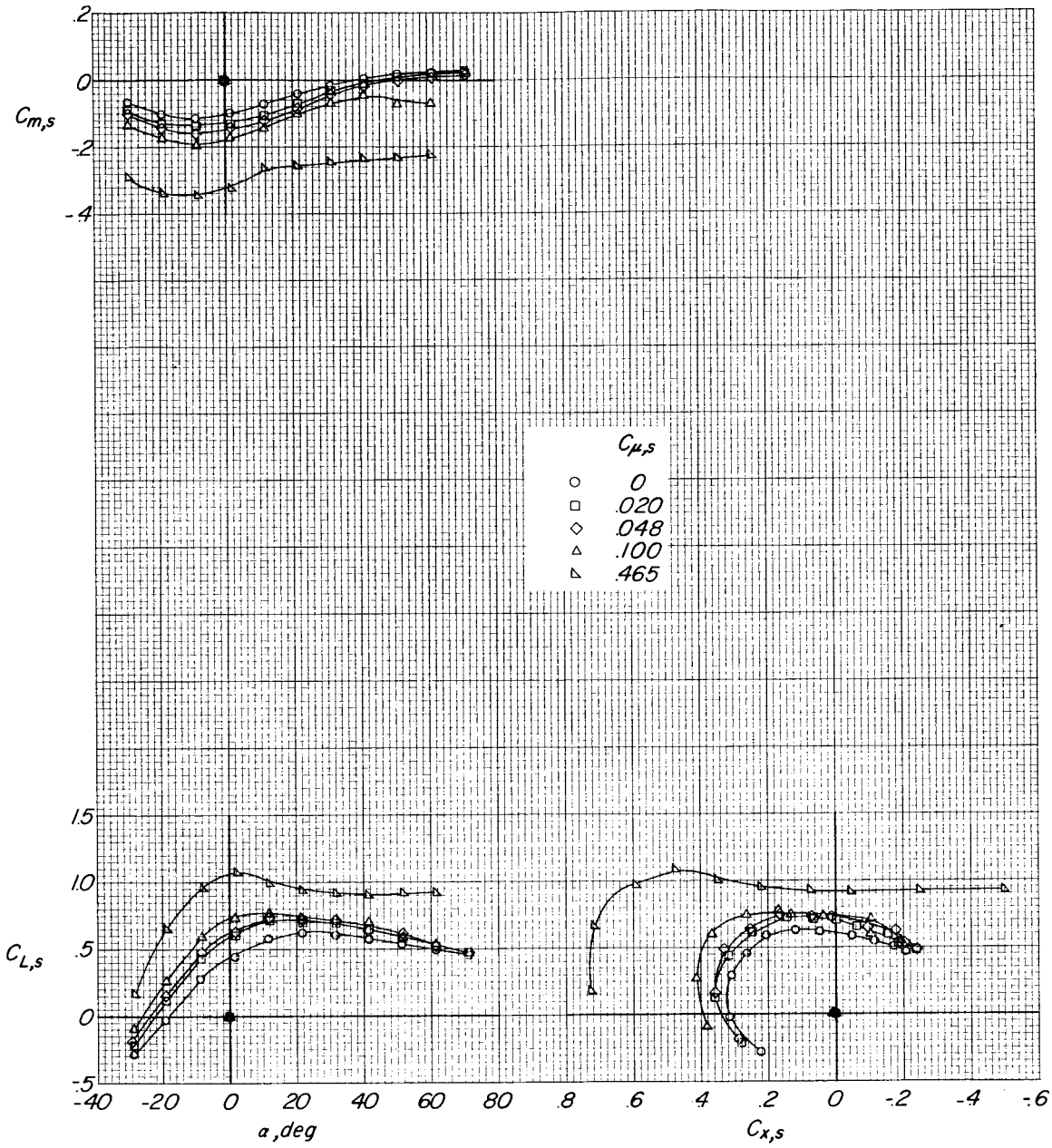

$C_{T,s} = 0.90$

(a) Continued.

Figure 12.- Continued.

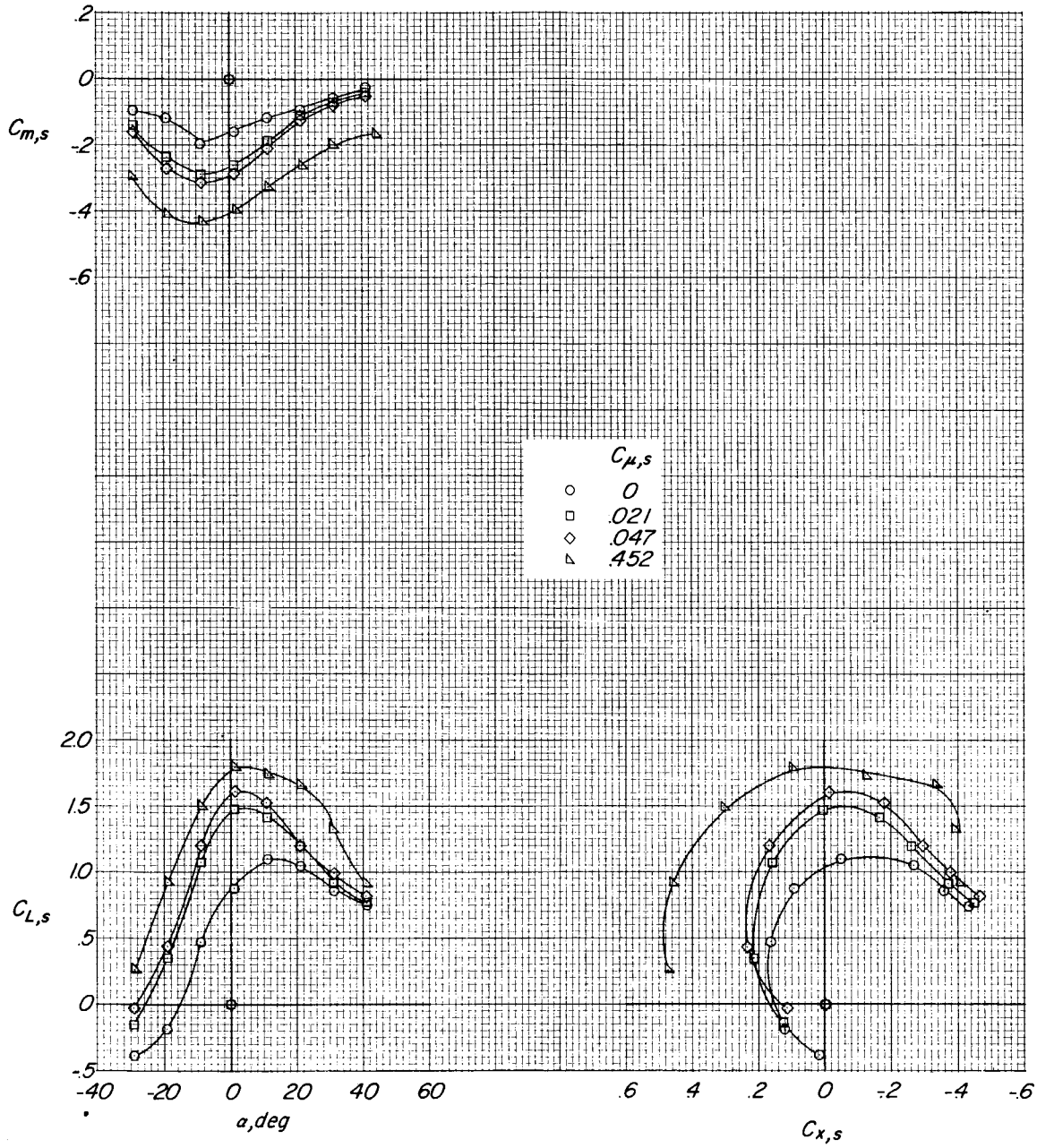

$C_{T,s} = 0.60$

(a) Concluded.

Figure 12.- Continued.

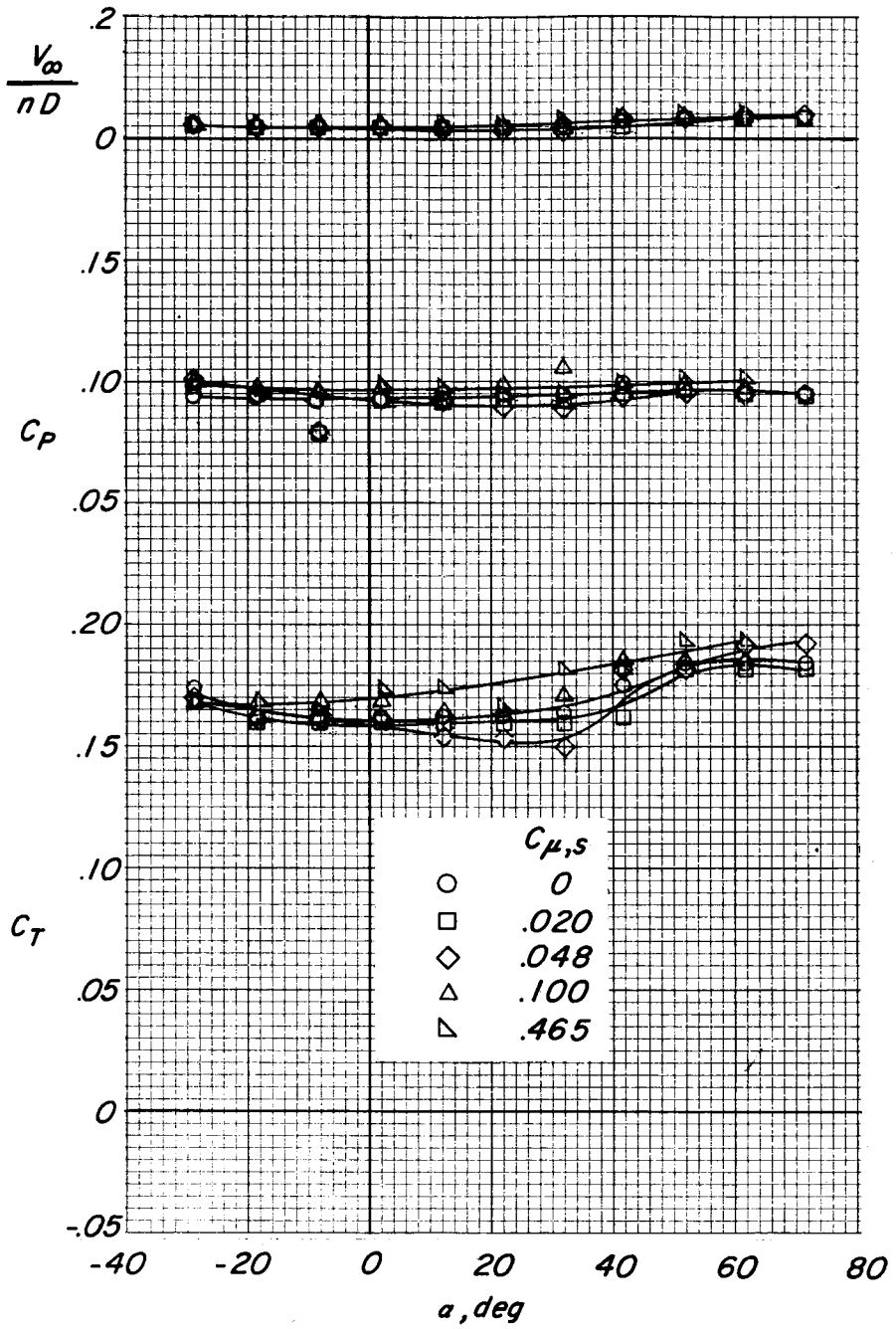

$C_{T,s} = 0.90$

(b) Propeller coefficients.

Figure 12.- Continued.

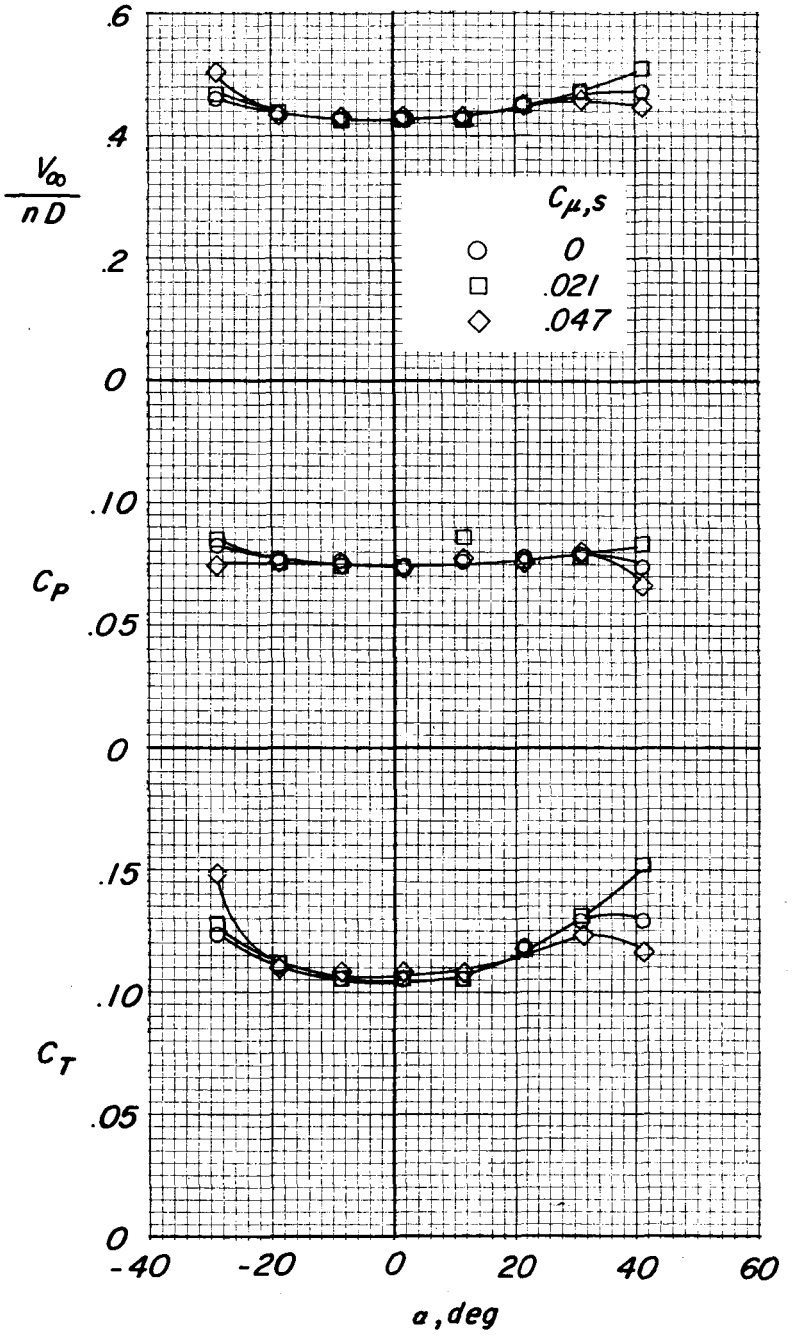

$C_{T,s}$ = 0.60

(b) Concluded.

Figure 12.- Continued.

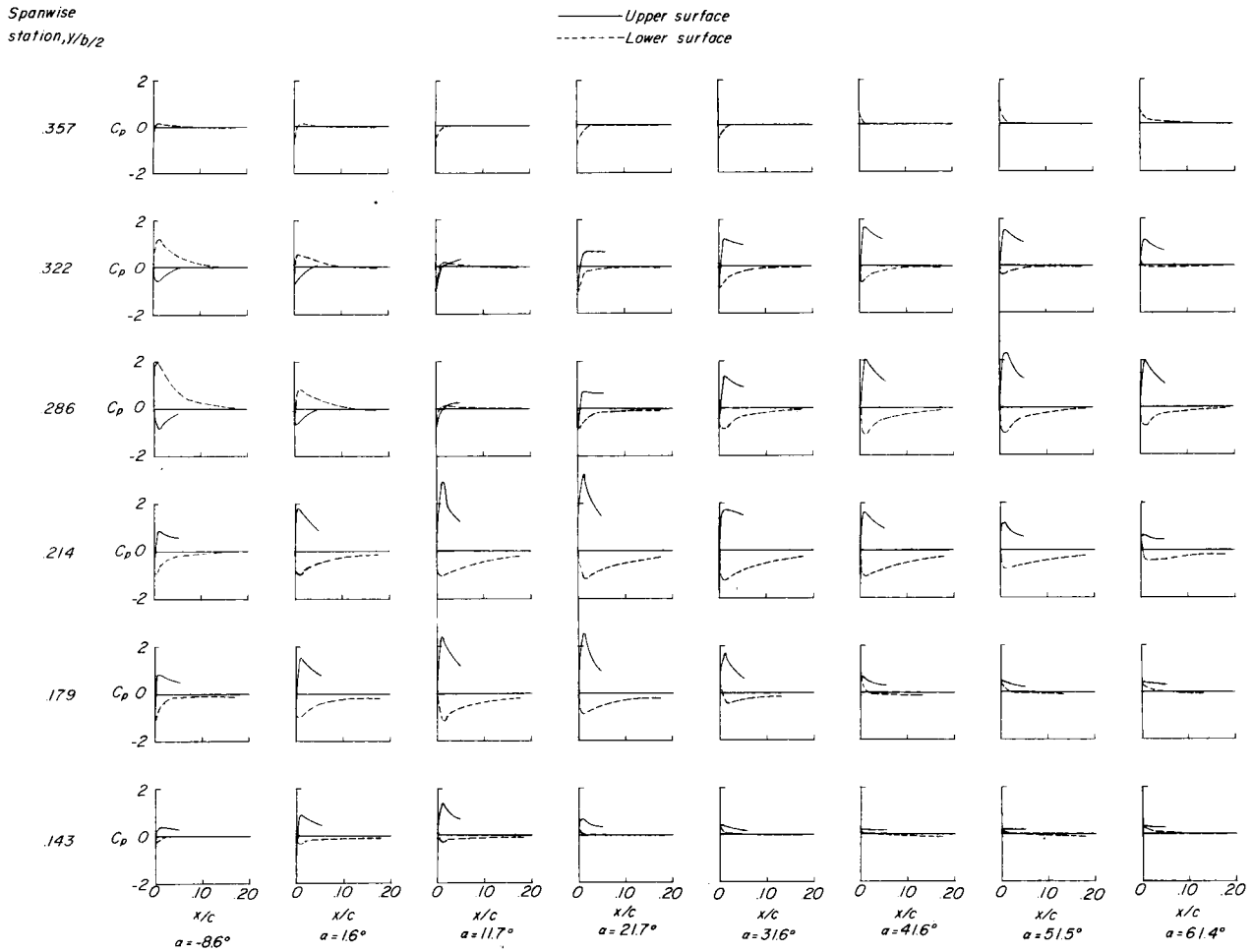

$C_{T,s} = 0.90$; $C_{\mu,s} = 0$

(c) Pressure coefficients.

Figure 12.- Continued.

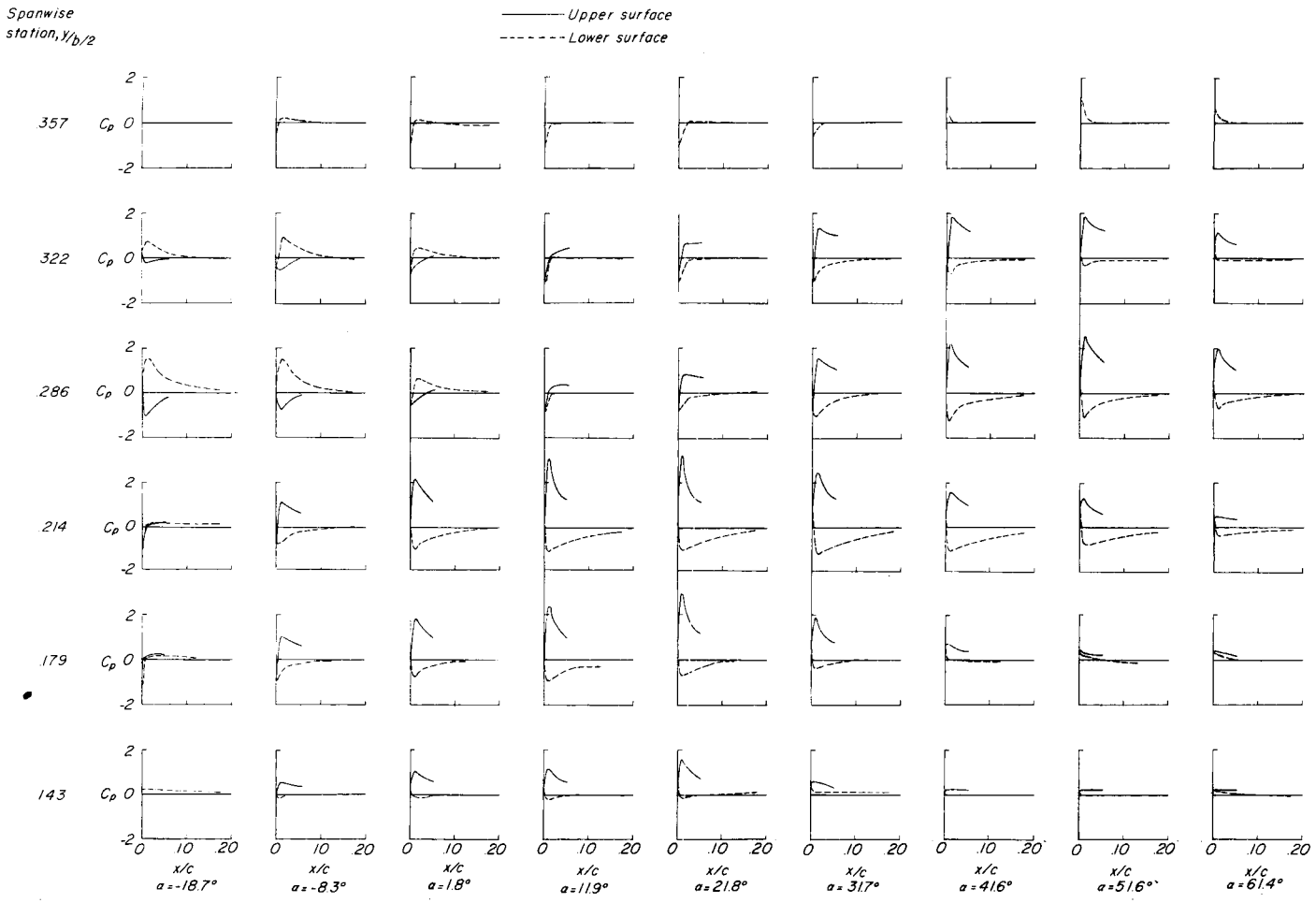

$C_{T,s} = 0.90$; $C_{\mu,s} = 0.048$

(c) Continued.

Figure 12.- Continued.

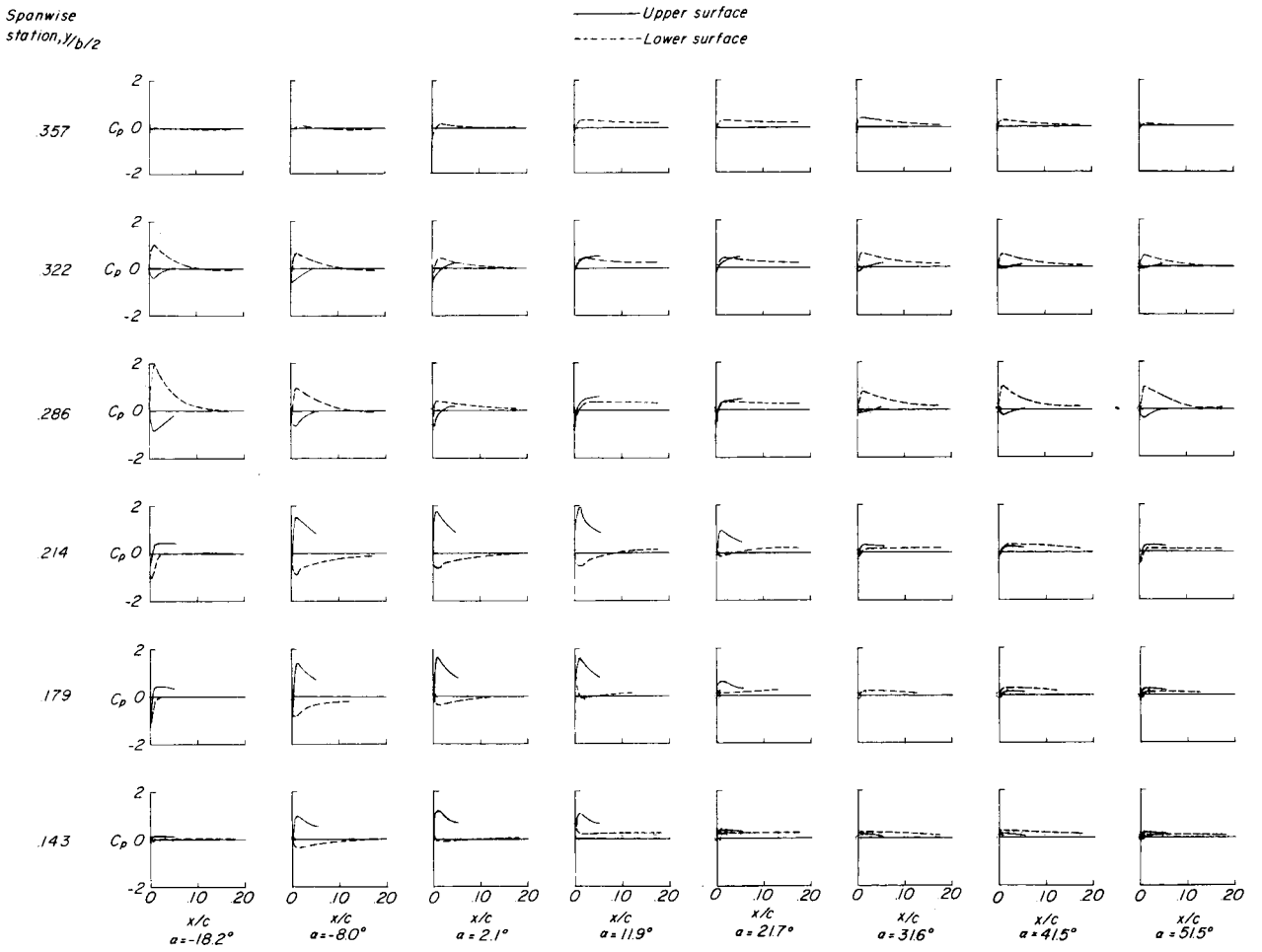

$C_{T,s} = 0.90$; $C_{\mu,s} = 0.465$

(c) Concluded.

Figure 12.- Concluded.

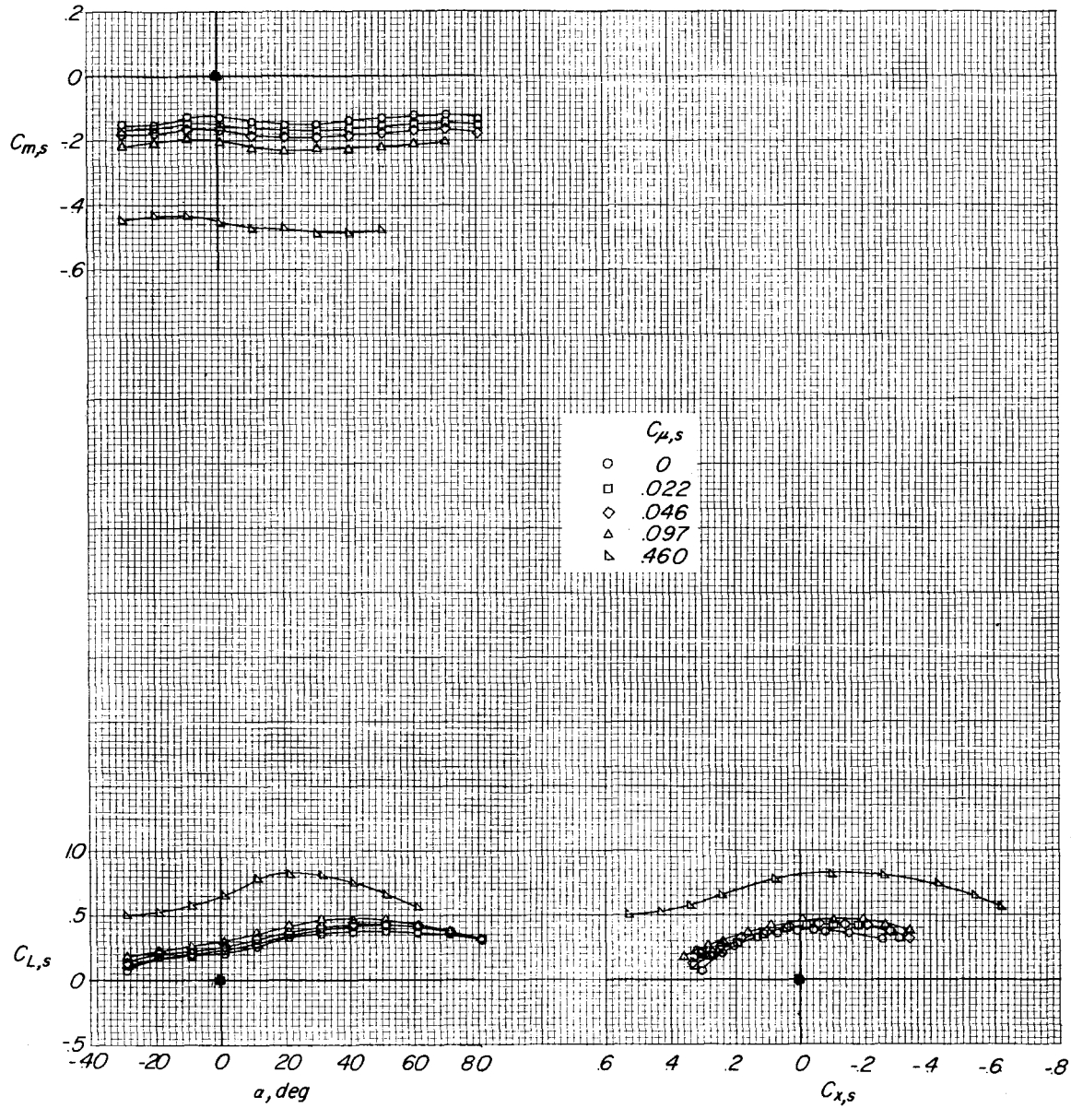

$C_{T,s} = 1.0$

(a) Longitudinal characteristics.

Figure 13.- Effects of variations in thrust and momentum coefficients on the aerodynamic characteristics of model within ground proximity. h/D = 1.22; $\delta_f = 40^\circ$; $\delta_{T.E.} = 60^\circ$.

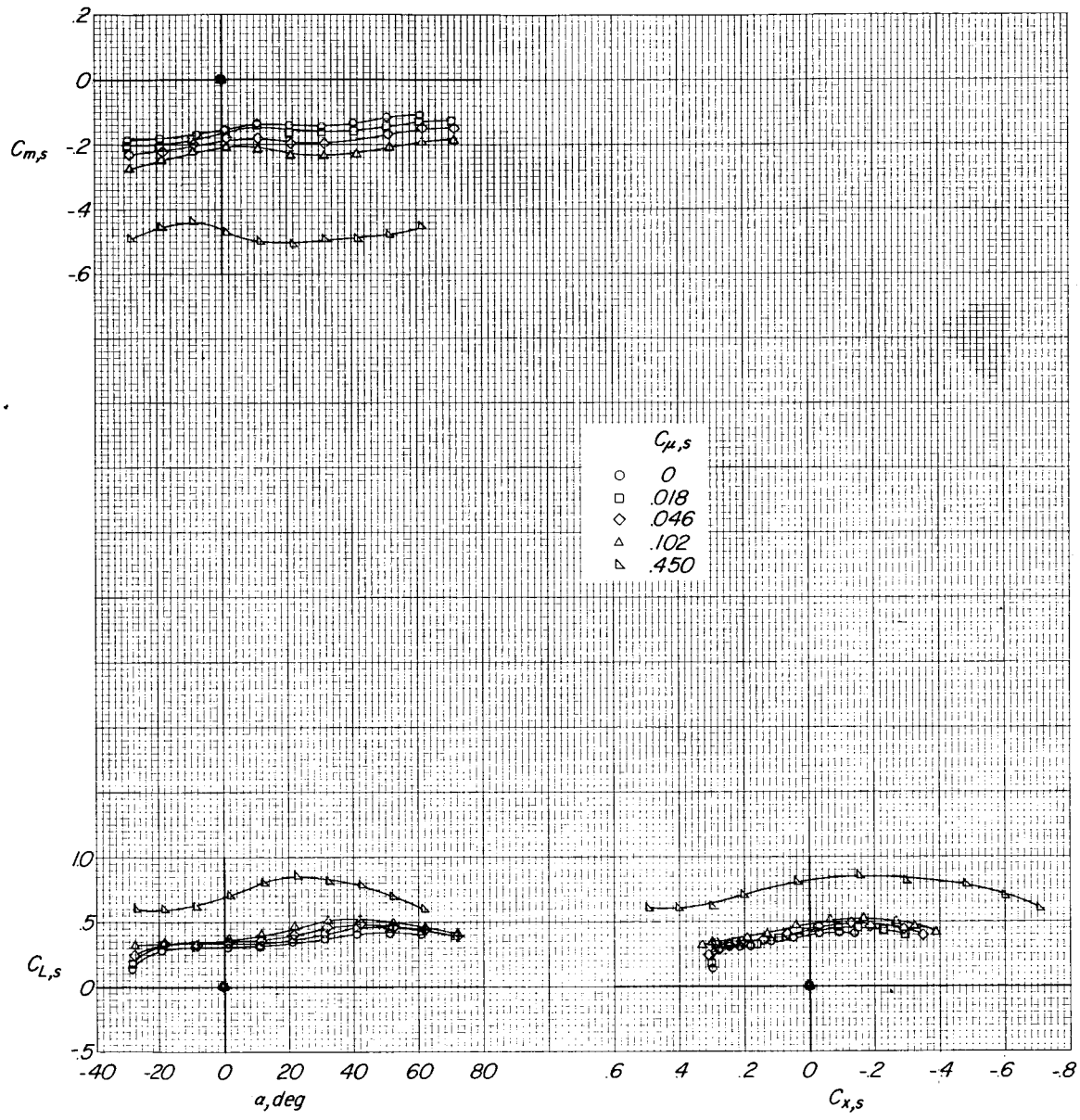

$C_{T,s} = 0.98$

(a) Continued.

Figure 13.- Continued.

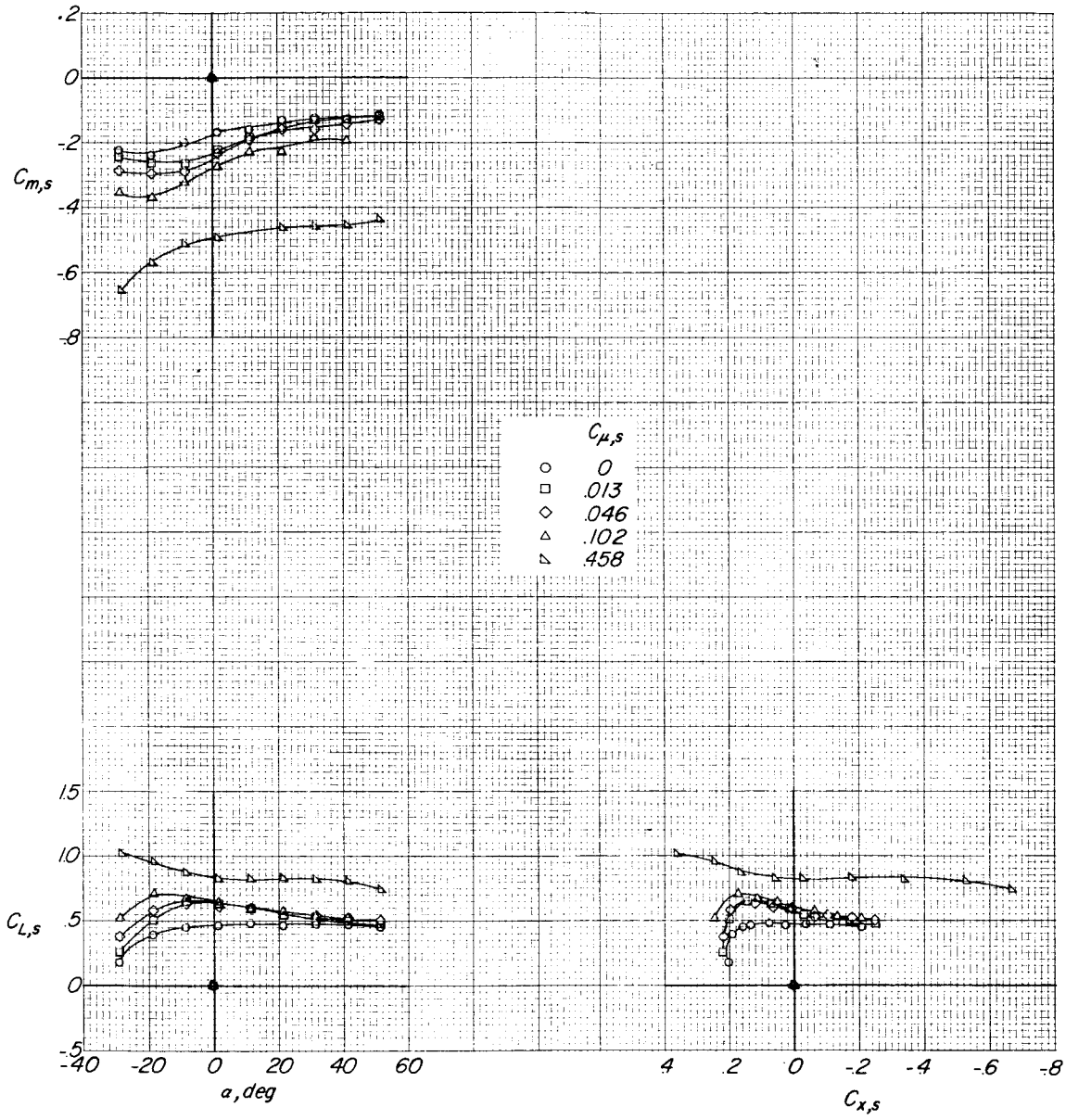

$C_{T,s} = 0.90$

(a) Continued.

Figure 13.- Continued.

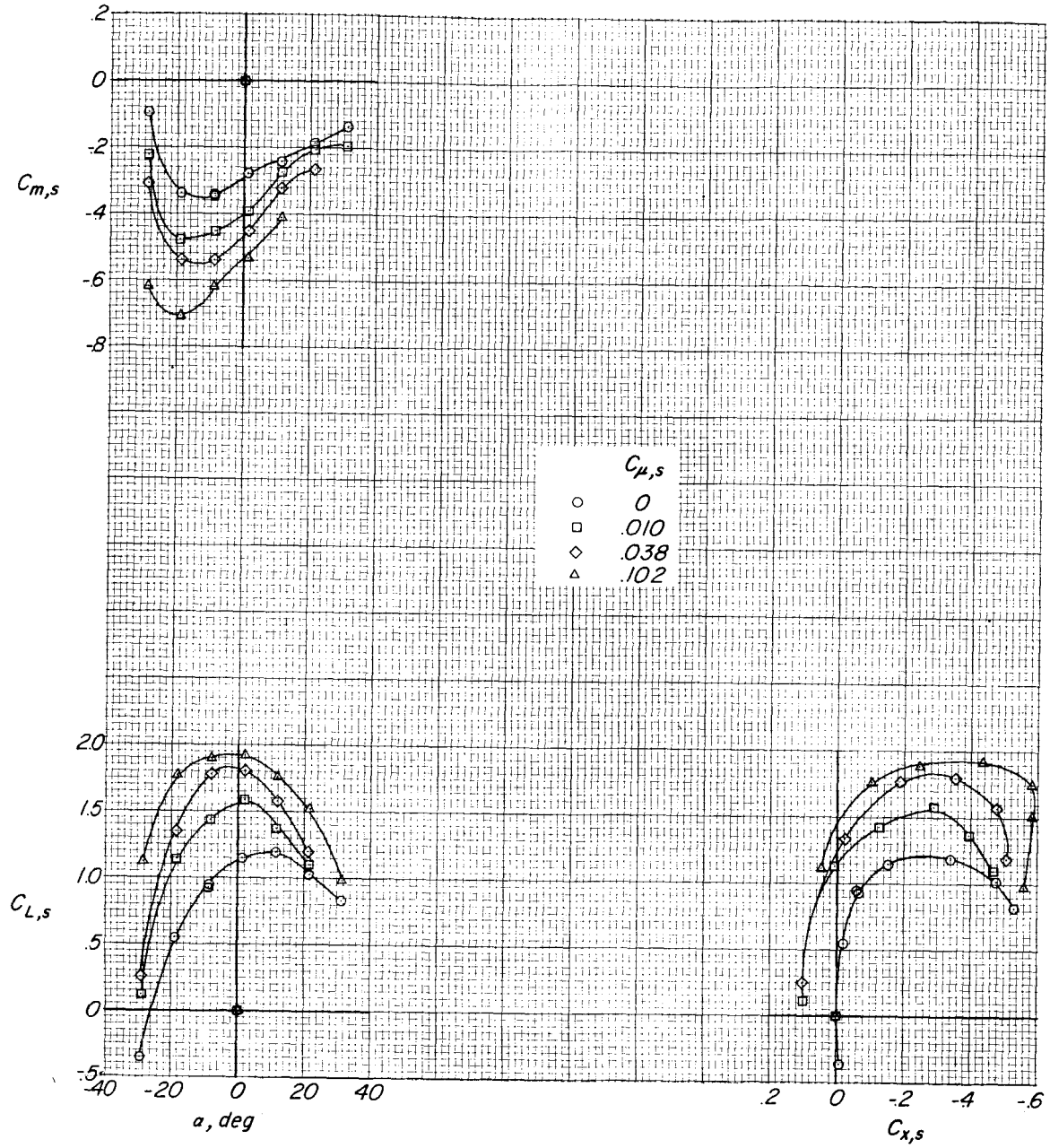

$C_{T,s} = 0.60$

(a) Concluded.

Figure 13.- Continued.

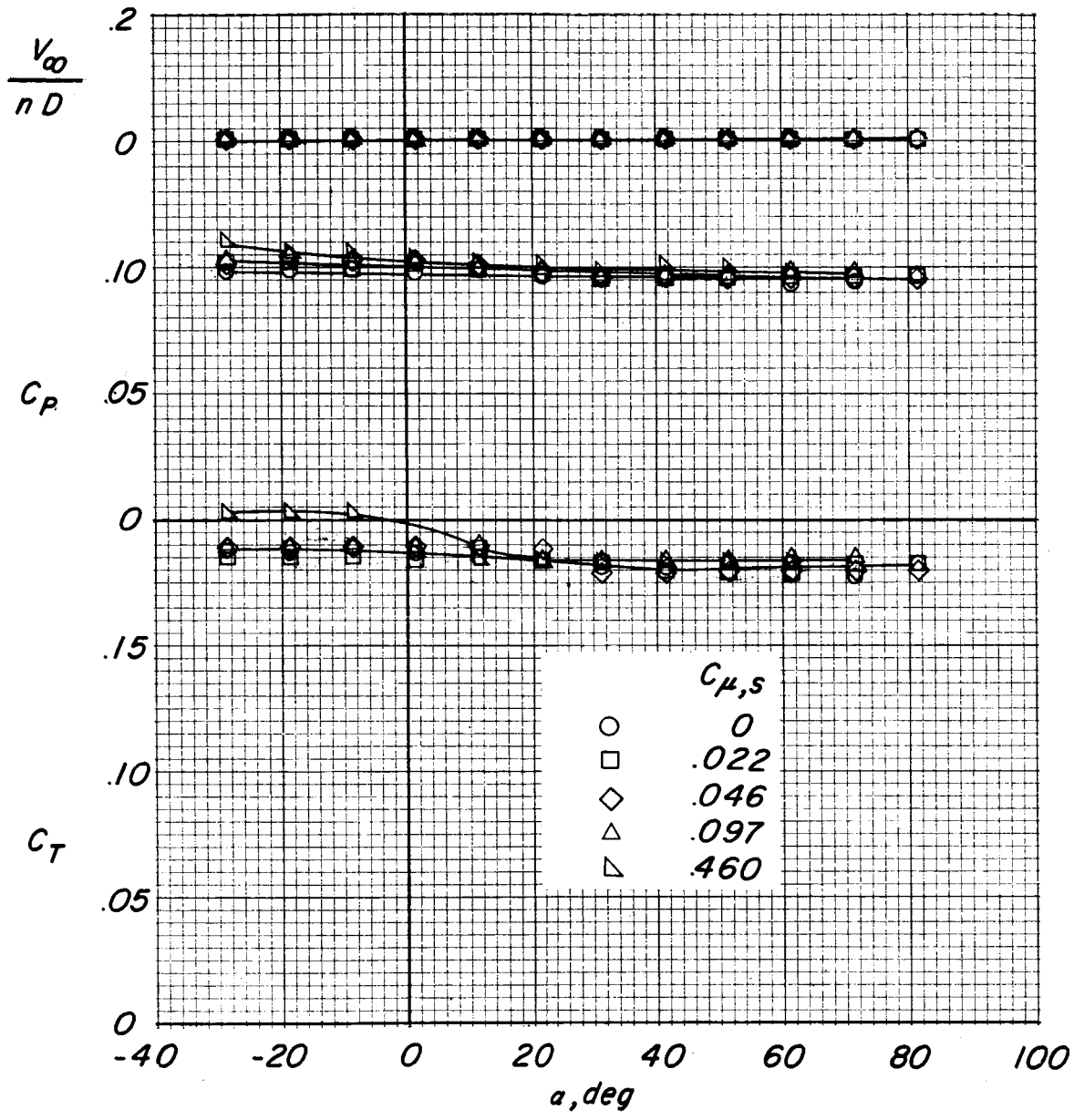

$C_{T,s} = 1.0$

(b) Propeller coefficients.

Figure 13.- Continued.

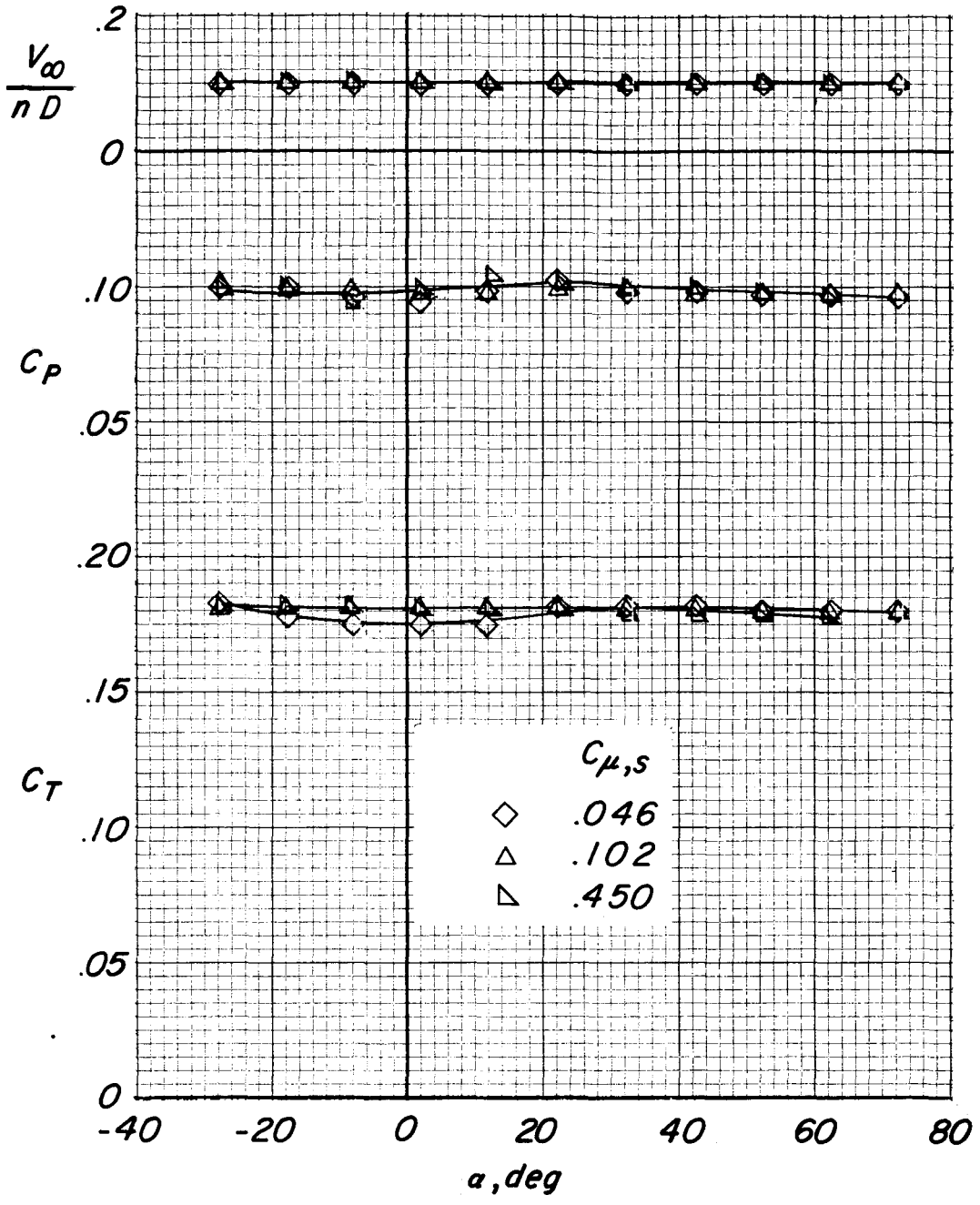

$C_{T,s} = 0.98$

(b) Continued.

Figure 13.- Continued.

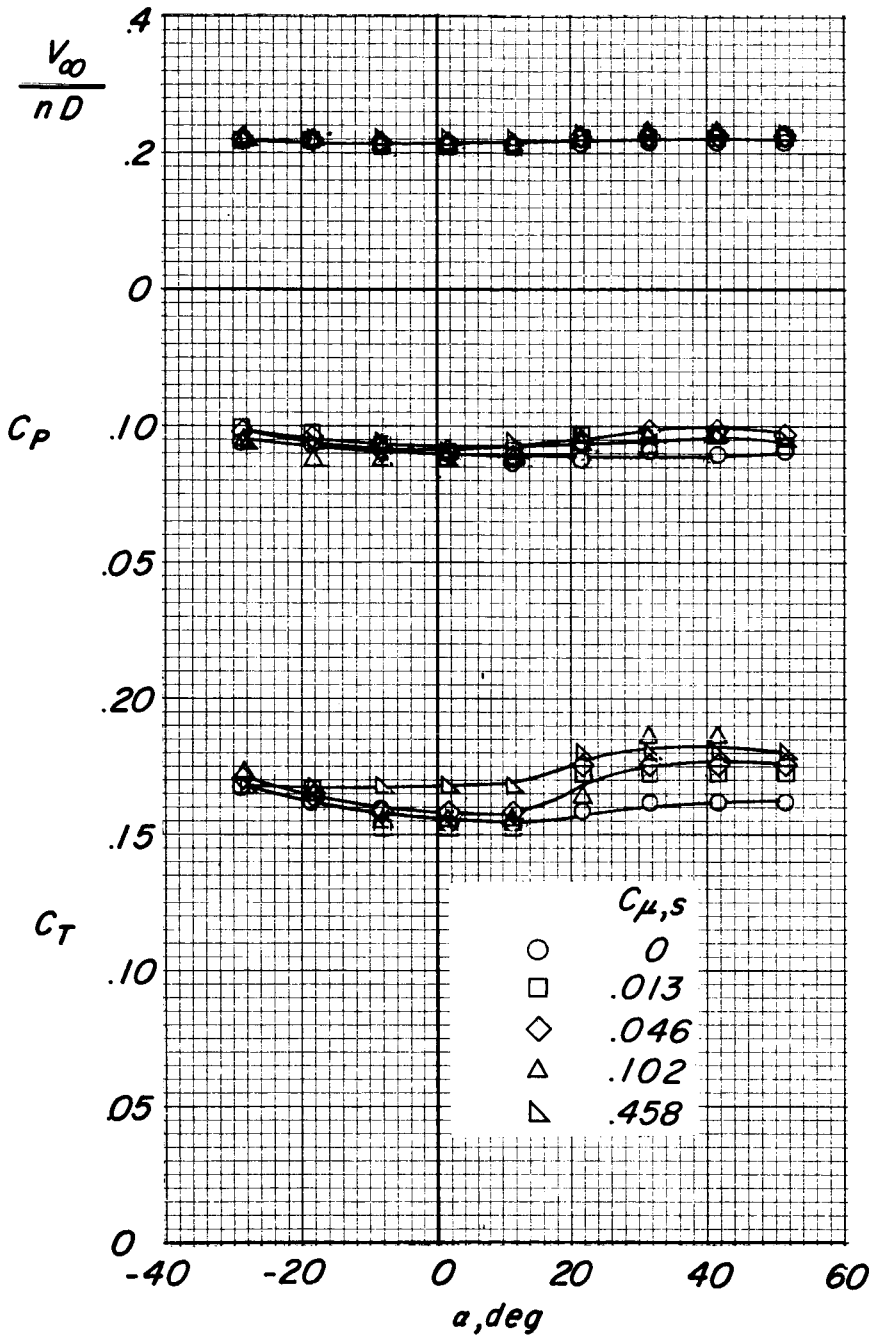

$C_{T,s} = 0.90$

(b) Continued.

Figure 13.- Continued.

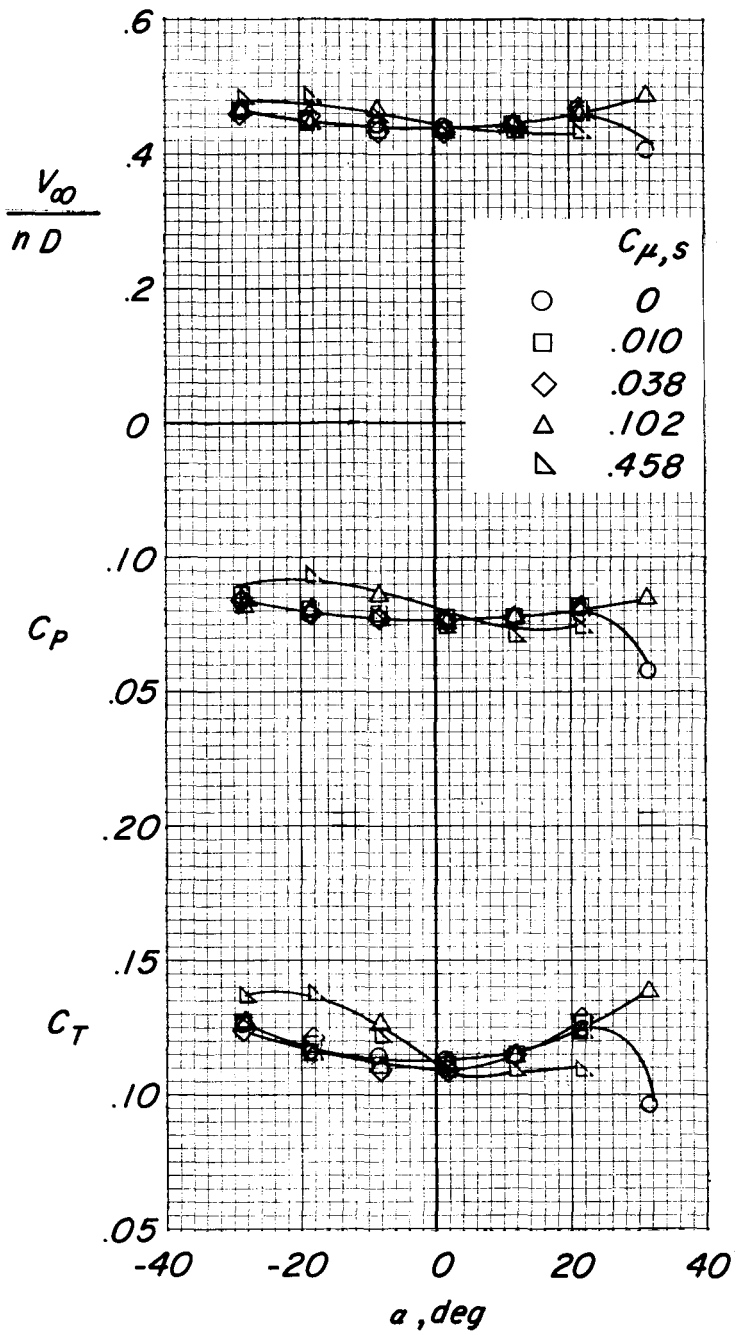

$C_{T,s}$ = 0.60

(b) Concluded.

Figure 13.- Concluded.

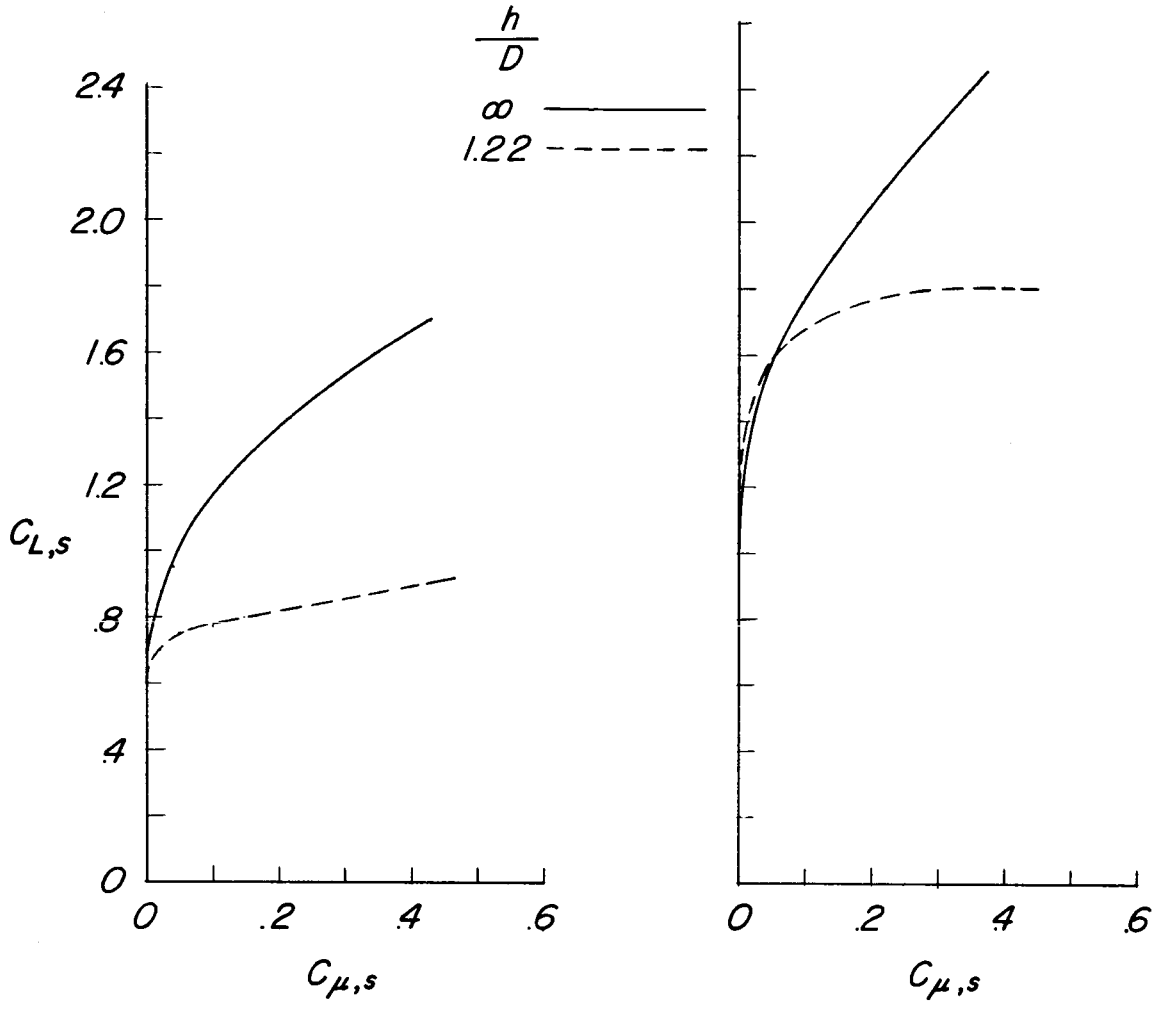

(a) $C_{T,s} = 0.90$.

(b) $C_{T,s} = 0.60$.

Figure 14.- Comparison of lift coefficients with model in and out of ground proximity with $\delta_f = 40^\circ$ and $C_{X,s} = 0$ (steady level flight). Basic data in figures 9 and 12.

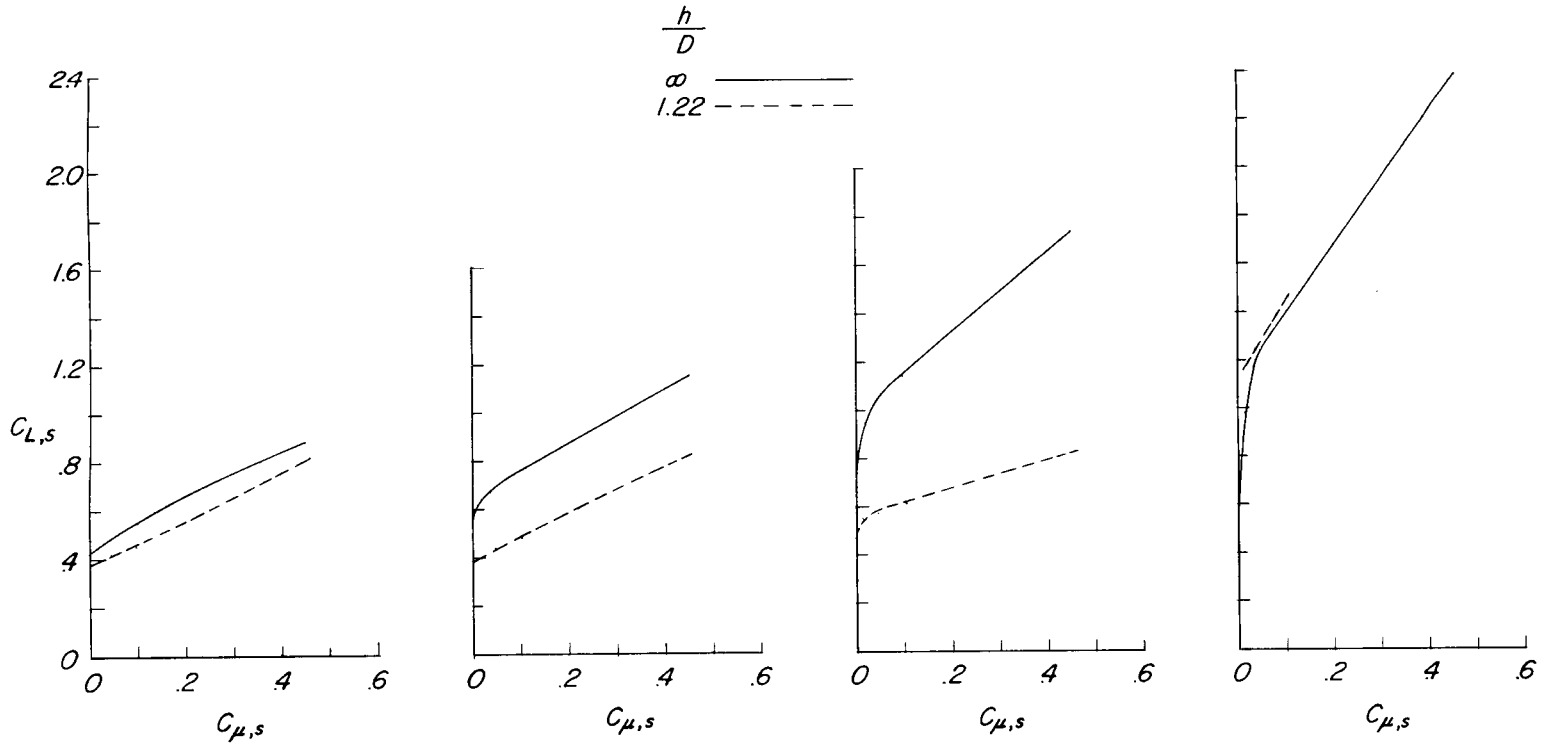

(a) $C_{T,s}$ = 1.0. (b) $C_{T,s}$ = 0.98. (c) $C_{T,s}$ = 0.90. (d) $C_{T,s}$ = 0.60.

Figure 15.- Comparison of lift coefficients with model in and out of ground proximity with $\delta_f = 40^\circ$, $\delta_{T.E.} = 60^\circ$, and $C_{X,s} = 0$ (steady level flight). Basic data in figures 11 and 13.